NASA TM-112648

Laser Shearographic Inspection for Debonds in Sprayed On Foam Insulation (SOFI)

March 1997

NASA TM-112648

Laser Shearographic Inspection for Debonds in Sprayed On Foam Insulation (SOFI)

F. W. Adams
NASA DL-ICD-A
John F. Kennedy Space Center
KSC, Florida

S. Simmons
I-INET, Inc.
John F. Kennedy Space Center
KSC, Florida

J. Hooker
I-NET, Inc.
John F. Kennedy Space Center
KSC, Florida

National Aeronautics and Space Administration
John F. Kennedy Space Center, Kennedy Space Center, Florida 32899-0001

March 1997

TABLE OF CONTENTS

Section	Title	Page
I	INTRODUCTION	1-1
1.1	Scope	1-1
1.2	Optical Nondestructive Testing Techniques and Limitations	1-1
1.2.1	Noncoherent Nondestructive Testing	1-1
1.2.2	Coherent Nondestructive Testing	1-2
1.2.2.1	Holography	1-2
1.2.2.2	Speckle Patterns	1-3
1.2.2.3	Electronic Speckle Pattern Interferometry (ESPI)	1-3
1.2.2.4	Shearing Interferometry	1-5
1.2.2.5	Summary	1-9
II	TEST METHODS, PROCEDURES, AND PARAMETERS	2-1
2.1	SOFI Test Panels	2-1
2.2	SOFI Test Panel Construction	2-1
2.3	SOFI Test Panel Inspection	2-2
2.4	Additional Testing	2-3
III	TEST RESULTS	3-1
3.1	Circular Debonds	3-1
3.2	Square Debonds	3-4
3.3	Seam Debonds	3-5
3.4	Testing with Vacuum Offset	3-13
3.5	Testing with 1 Degree Shear Vector Camera	3-17
3.6	Data Not Discussed	3-17
IV	PROBABILITY OF DETECTION ANALYSIS	4-1
4.1	Probability of Detection (POD) Analysis	4-1
4.2	Probability of Detection from Signal Response Data	4-1
V	POD CURVES BASED ON TEST RESULTS	5-1
5.1	Discussion of POD	5-1

TABLE OF CONTENTS (Cont)

Section	Title	Page
5.2	PODs For Circular Debonds	5-1
5.3	PODs for Square Debonds	5-12
5.4	PODs for Seam Debonds	5-12
5.5	Probability of False Detection	5-12
VI	CONCLUSIONS	6-1
APPENDIX A	UNAVERAGED DATA TAKEN DURING SHEAROGRAPHY TESTS	A-1
APPENDIX B	DEFECT LEGEND AND RAW DATA	B-1
APPENDIX C	LIST OF REFERENCES	C-1

LIST OF ILLUSTRATIONS

Figure	Title	Page
1-1	A Typical Configuration for ESPI	1-4
1-2	A Typical Configuration for Laser Shearography	1-6
1-3	Common Methods of Creating Image Shear in a Shearography System	1-7
1-4	An Example of a Shearogram	1-10
1-5	Deliberate Shearogram of a Debond in SOFI in the Shape of the Word "NASA" for Illustration Purposes Only	1-10
2-1	A Typical Shearogram of Debonds in SOFI	2-4
3-1	Average Detection Values of Circular Debonds vs SOFI Thickness and Defect Diameter - Full Panel View	3-2
3-2	Average Detection Values of Circular Debonds vs SOFI Thickness and Defect Diameter - Subareas	3-3
3-3	Detection Values vs Shear Vector in all Foam Thicknesses for 0.5-Inch Square Debond	3-6
3-4	Detection Values vs Shear Vector in all Foam Thicknesses for 1-Inch Square Debond	3-7
3-5	Detection Values vs Shear Vector in all Foam Thicknesses for 1.5-Inch Square Debond	3-8
3-6	Detection Values vs Shear Vector	3-9
3-7	Average Detection Values of Square Debonds vs SOFI Thickness and Defect Size - Full Panel View	3-10
3-8	Average Detection Values of Square Debonds vs SOFI Thickness and Defect Size - Subareas	3-11
3-9	Shearograms for a Seam Debond	3-12
3-10	Detection Values vs Shear Vector in all Foam Thicknesses for 0.75-Inch-by-3-Inch Seam Debond	3-14
3-11	Detection Values vs Shear Vector in all Foam Thicknesses for 0.75-Inch-by-10-Inch Seam Debond	3-15
3-12	Shearograms of a Horizontal Seam Debond With Different Orientations of Shear Vector	3-16
5-1	Probability of Detection of Circular Debonds in 0.5-Inch Thick SOFI (Full Panel View)	5-2
5-2	Probability of Detection of Circular Debonds in 0.75-Inch Thick SOFI (Full Panel View)	5-3
5-3	Probability of Detection of Circular Debonds in 1.0-Inch Thick SOFI (Full Panel View)	5-4

LIST OF ILLUSTRATIONS (Cont)

Figure	Title	Page
5-4	Probability of Detection of Circular Debonds in 1.25-Inch-Thick SOFI (Full Panel View)	5-5
5-5	Probability of Detection of Circular Debonds in 1.5-Inch-Thick SOFI (Full Panel View)	5-6
5-6	Probability of Detection of Circular Debonds in 0.5-Inch-Thick SOFI (Subareas)	5-7
5-7	Probability of Detection of Circular Debonds in 0.75-Inch-Thick SOFI (Subareas)	5-8
5-8	Probability of Detection of Circular Debonds in 1.0-Inch-Thick SOFI (Subareas)	5-9
5-9	Probability of Detection of Circular Debonds in 1.25-Inch-Thick SOFI (Subareas)	5-10
5-10	Probability of Detection of Circular Debonds in 1.5-Inch-Thick SOFI (Subareas)	5-11
5-11	Probability of Detection of Square Debonds in 0.5-Inch-Thick SOFI (Full Panel View)	5-14
5-12	Probability of Detection of Square Debonds in 0.75-Inch-Thick SOFI (Full Panel View)	5-15
5-13	Probability of Detection of Square Debonds in 1.0-Inch-Thick SOFI (Full Panel View)	5-16
5-14	Probability of Detection of Square Debonds in 1.25-Inch-Thick SOFI (Full Panel View)	5-17
5-15	Probability of Detection of Square Debonds in 1.5-Inch-Thick SOFI (Full Panel View)	5-18
5-16	Probability of Detection of Square Debonds in 0.5-Inch-Thick SOFI (Subareas)	5-19
5-17	Probability of Detection of Square Debonds in 0.75-Inch-Thick SOFI (Subareas)	5-20
5-18	Probability of Detection of Square Debonds in 1.0-Inch-Thick SOFI (Subareas)	5-21
5-19	Probability of Detection of Square Debonds in 1.25-Inch-Thick SOFI (Subareas)	5-22
5-20	Probability of Detection of Square Debonds in 1.5-Inch-Thick SOFI (Subareas)	5-23
5-21	Probability of Detection of 10-Inch Seam Debond as Function of Shear Vector and SOFI Thickness (Full Panel View)	5-24

LIST OF ILLUSTRATIONS (Cont)

Figure	Title	Page
5-22	Probability of Detection of 10-Inch Seam Debond as Function of Shear Vector and SOFI Thickness (Subarea)	5-25
5-23	Probability of Detection of 3-Inch Seam Debond as Function of Shear Vector and SOFI Thickness (Full Panel View)	5-26
5-24	Probability of Detection of 3-Inch Seam Debond as Function of Shear Vector and SOFI Thickness (Subarea)	5-27

ABBREVIATIONS AND ACRONYMS

CCD	charged coupled device
ESPI	Electric Speckle Pattern Interfermetry
ET	external tank
KSC	John F. Kennedy Space Center
mW	milliwatt (1×10^{-3} W)
NDT	nondestructive testing
POD	probability of detection
SOFI	Spray On Foam Insulation
VAB	Vehicle Assembly Building

SECTION I

INTRODUCTION

1.1 SCOPE

This document presents a consolidation and analysis of nondestructive testing (NDT) data taken on spray on foam insulation (SOFI) test panels utilizing laser shearography. The purpose of this investigation is to define test criteria for inspection of SOFI on the external tank (ET) using laser shearography, establish test parameters and begin the process of determining the probability of detection (POD) of flaws present in the inspected regions. Included in this report are:

- Detailed descriptions of the manufacture of the test panels and programmed debonds
- Test methods, procedures and parameters
- Test results
- Analytical description of probability of detection (POD) analysis
- POD curves based on test results
- Conclusions and recommendations for implementation of laser shearography on the Orbiter external tank

1.2 OPTICAL NONDESTRUCTIVE TESTING TECHNIQUES AND LIMITATION

The underlying principal of most optical NDT targeting subsurface defects is the comparison of optical information characterizing the surface of an object before and after the object is subjected to some form of stress. Localized deformations on the surface are typically indications of stress field disturbances within the object, and provide information that can be used to locate and possibly characterize the flaw.

Optical nondestructive testing generally falls into two categories: coherent and noncoherent techniques. Coherent NDT systems use laser light because of the ability of laser radiation to interfere with itself at a boundary. Noncoherent NDT systems may also utilize a laser; however, the laser is only a source of illumination and the spatial and temporal coherence of the radiation are not exploited. The choice of technique depends on the environment, surface characteristics and required resolution. Noncoherent techniques may yield submillimeter resolution with submicron resolutions possible with coherent NDT.

1.2.1 NONCOHERENT NONDESTRUCTIVE TESTING. Examples of noncoherent nondestructive testing are structured light and moiré interferometry. In a structured light system a known geometric pattern of illumination is projected onto a

surface to be inspected. Typical projection patterns are, but not limited to a line, a series of lines, or a square grid. Surface deformations and surface profile can be uniquely determined by analyzing the geometric distortion of the projected pattern caused by its intersection with the test object. Deviations of the deflection of the stressed surface from the expected natural response of the surface to the stress are indications of a flaw.

Moiré interferometry produces a fringe map characteristic of the surface being inspected and is referred to as a moiré interferogram. A moiré interferogram is produced when a grating (i.e., a series of light and dark bars with periodic spacing) is projected onto, and distorted by a surface as in the case of structured light. This distorted grating is then superimposed on to a reference grating identical to the one projected onto the object. The distorted grating and the reference grating interfere to produce the interferogram.

A moiré system can be configured such that the interferogram consists of a series of fringes which represent equal depth contour lines on the surface. However, as with all interferometric methods, nonuniqueness of the fringe order precludes the direct determination of the surface profile from a single interferogram. Where it is necessary to determine the unique surface profile, phase shifting methods are usually implemented to establish unique fringe order.

A moiré system does not require coherent light and thus the term moiré "interferometry" can be somewhat misleading. With respect to a moiré system, the word interferometry describes the interactions of the spatial phases of the distorted and reference gratings and not the interactions of the phases of the light waves themselves, as is the case in the coherent NDT techniques.

To analyze a surface, moiré interferograms are obtained in the stressed and unstressed conditions and compared. Deviations in the interferograms other than those expected by the natural response of the surface to the stress are indications of a flaw.

1.2.2 COHERENT NONDESTRUCTIVE TESTING. The ability of coherent light to interact with itself at a boundary is the basis of coherent NDT and the reason for its high, submicron resolution. Coherent NDT is accomplished by two techniques: holography and shearography.

1.2.2.1 Holography. Holography uses the phase relationship between a reference beam and a target beam (light scattered off of a test surface) to record surface deflections. When an object under inspection is subjected to some stressing mode, the surface deforms and causes the light scattered from that surface to change

phase relative to the reference beam. When the reference beam and target beam are recombined and the phase interactions are recorded via some medium (e.g., film plates or CCD's), the result is a fringe pattern or hologram.

The fringe pattern consists of a series of light and dark bands. The dark bands correspond to phase changes between the target and reference beams that are a half integer number of wavelengths while the light bands correspond to phase changes of integer numbers of wavelengths. Therefore, it is possible with holographic systems to measure surface displacements on the order of half a wavelength of the light being used. Holographically generated fringes represent true surface displacements as in the case of the moiré interferogram mentioned above. However, holography is typically many orders of magnitude more sensitive than moiré techniques.

Typical holographic methods include double exposure holography in which a holograph of a test object is exposed on a photographic medium before and after loading and electronic speckle interferometry (ESPI) which utilizes a phenomenon known as speckle. Because ESPI has made it out of the laboratory and in to field application a brief discussion of it follows beginning with the speckle pattern.

1.2.2.2 Speckle Patterns. Whenever an object is illuminated with a diverging laser beam, an observer viewing the object will notice the light to have a granular appearance. This granularity is referred to as speckle. The perceived speckle pattern, however, is not created at the surface, which is uniformly illuminated, but rather on the observer's optical detector, the retina. The optical receptor cells that make up the retina have a finite extent (i.e., they are not infinitely small) and, therefore, each cell receives light from more than a single geometric point on the surface being illuminated. Because laser radiation is coherent, the phase differences of the light form adjacent points on the surface reaching a single receptor cell causes constructive or destructive interference. The variation in this interference from one cell on the retina to the next is what is visualized as the seemingly random speckle pattern. The speckle pattern, however, is not random and actually represents a phase map of the surface being illuminated. If the retina is replaced with another detector constructed of small resolution elements, such as a CCD, the phase information constituting the speckle pattern may be exploited to render a set of very powerful NDT instruments[1].

1.2.2.3 Electronic Speckle Pattern Interferometry (ESPI). A typical layout for a ESPI system is shown in figure 1-1. Being a true holographic technique, the coherent radiation from the laser is separated into a reference and a target beam. The light scattered from the target is recombined with the reference beam via a beam splitter prior to illuminating the detector. The interaction between the target and reference beam at the detector causes interference which represents the speckle

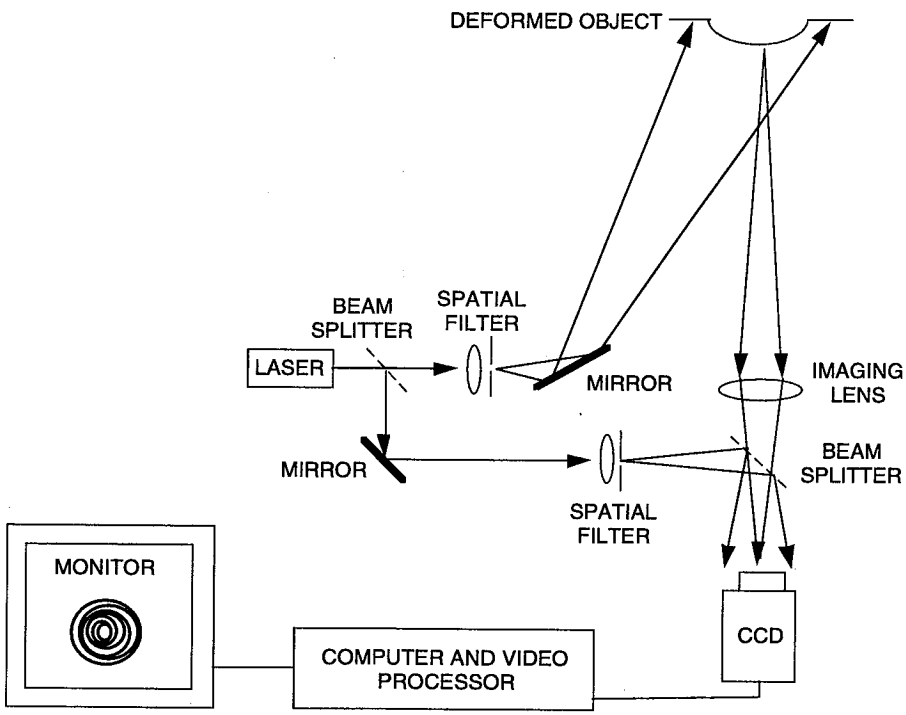

Figure 1-1. A Typical Configuration for ESPI

pattern at the surface. Out-of-plane surface deformations are detected by comparing the speckle patterns of the surface before and after applying some form and level of stress to the object. The initial image, against which all subsequent images will be compared, is refereed to as the reference image. The reference image is obtained by digitizing the output of the camera and storing the result in video or computer memory. The object is then subjected to various levels of stress, and subsequent speckle images are digitized and compared to the reference image by point-by-point image subtraction. This image subtraction can be done at video rates yielding a real-time display on a monitor of the out-of-plane surface deflections.

The output on the monitor is a fringe pattern consisting of a series of bright and dark bands representing equal depth contours of the surface. The bright bands correspond to surface deflections which are integer multiples of the wavelength in magnitude while the dark bands correspond to surface deflections which are half integer multiples of the wavelength in magnitude.

ESPI is a very powerful and sensitive NDT technique and has had some success in the field. However, ESPI does suffer from some serious limitations, most of which

are intrinsic to holographic systems—specifically, the use of separate reference and target beams.

First, ESPI requires a relatively complicated optical system consisting of many components which must be rigidly fixed and maintain precise alignment while operating in field environments. As is the case with all dual path interferometric systems, strict requirements are also placed on the coherence length of the laser being used. In order to achieve fringe patterns with high fringe visibility, the coherence length of the laser light must be longer than the entire optical path length of the system. This includes the length the beam must travel in the reference path of the system as well as the distance to and from the target surface. This coherence length restriction usually requires the laser being used to run in single mode. Fringe interpretation of holographically generated interferograms can also be difficult because of fringe patterns introduced by rigid-body motions as well as those created by localized surface deflections caused by defects.

The most limiting aspect of ESPI, however, is its sensitivity to vibrations. If the object under inspection, as well as any of the components of the instrument itself, move a distance which is on the order of the sensitivity of the instrument (i.e., half a wavelength), spurious fringe patterns will be formed. Therefore, vibration isolation equipment is usually required. This makes implementation of ESPI in typical field environments extremely difficult and limits the range of applications of this technique.

1.2.2.4 Shearing Interferometry. Many of the restrictions limiting the use of ESPI in the field can be relaxed to a great degree while still maintaining a high degree of out-of-plane resolution by implementing shearing interferometry[2]. A typical layout for a laser shearograph is shown in figure 1-2.

In shearography, the test object is illuminated with coherent laser radiation and the light scattered from the surface is collected and passed through some kind of shearing optic before the image is focused on the detector. The shearing optic splits the scene into two identical images and displaces the images in space relative to each other before they are focused on the detector. The result is that each resolution element of the detector receives energy form two distinctly different locations on the surface being imaged. Because this image shear has a magnitude and a direction it is often referred to a the shearing vector. There are many implementations of image shear such as linear/lateral shear, rotational shear, radial shear, inversion and folding. The most commonly used is lateral shear. Lateral shearing of an image may be realized in several ways, the most common of which are shown in figure 1-3.

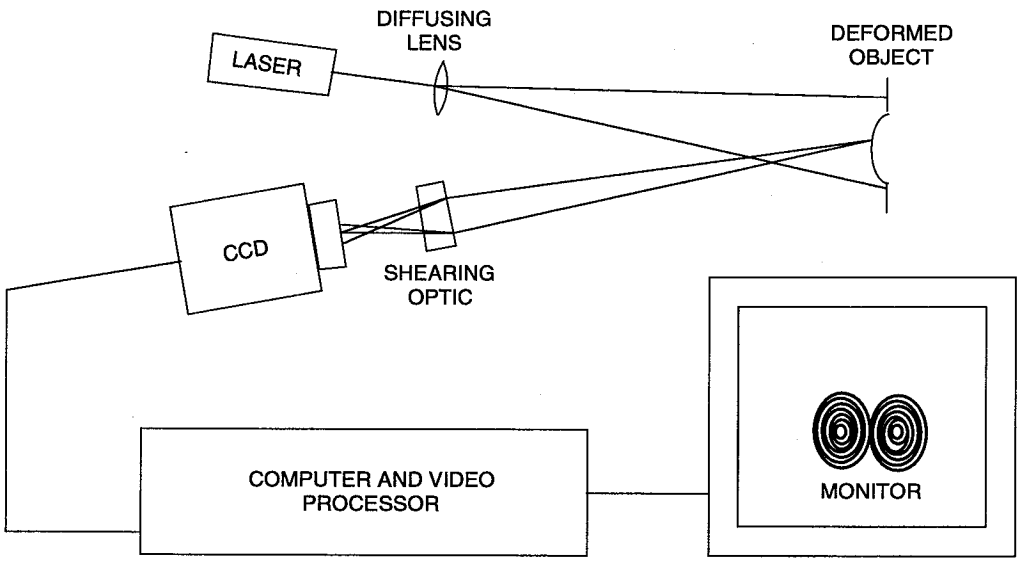

Figure 1-2. A Typical Configuration for Laser Shearography

The wedge prism method is not used to a great extent because proper placement of the prism within the optical system is critical to maintain good optical resolution characteristics and this may be difficult. The birefringent shearing optic is very convenient as it contains no moving parts, is very robust and compact for field use, and it is easily rotated to change the direction of the shear vector. However, the magnitude of the spatial separation between the two superimposed images cannot be dynamically changed because that is a function of the crystal dimensionality. Although not as robust or compact as the birefringent shearing optic the Michelson type optic is well suited for the field environment and adds the ability to dynamically change the magnitude as well as the direction of the shear vector. Magnitude changes are accomplished by tilting on of the mirrors in the system to shift one image relative to the other. Directional changes to the shear vector are made by rotating the entire Michelson system.

The laser shearograph used in this report utilized a birefringement shearing optic with a fixed shearing magnitude of 0.5 degrees; however, a camera with a 1-degree shearing optic was obtained for a short time and the results from each were compared[3,4]. This will be discussed in more detail later in this report.

When looking at the two figures representing a ESPI system and a shearographic, system several major differences are observed. First, the shearographic system has greatly simplified optical system. Second, the shearographic system does not utilize

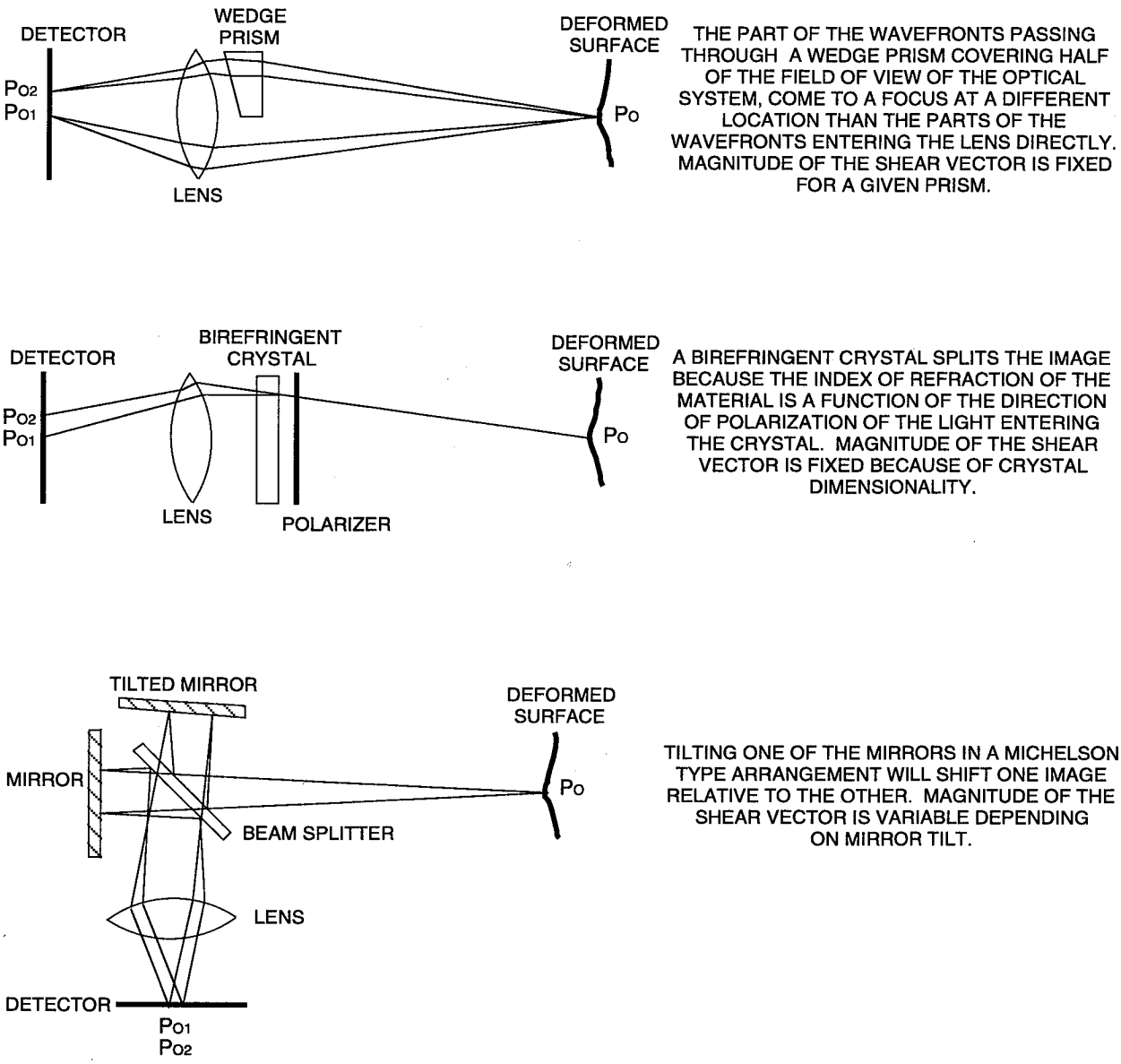

Figure 1-3. Common Methods of Creating Image Shear in a Shearography System

a reference beam. Because of this, a shearographic system may be referred to as a common path interferometric technique.

Common path interferometric systems have two distinct advantages over other systems utilizing phase interference as the detection mode. The light traveling to and from the surface encounters essentially the same environmental conditions (i.e.,

temperature, air movement, etc.). Therefore, thermal loading of a test object may be exploited because the effect of air currents between the test object and the detector, to some degree, tend to cancel out. Air motion may still be seen, but the effect is greatly reduced when compared to dual path interferometric techniques. Also, as with all common path interferometers, the demands of coherence length of the laser source are greatly mitigated, and there are no restrictions on the optical path length to the object to ensure coherence between the wavefronts forming the interferograms.

The final obvious difference is the presence of the shearing optic mentioned above. In shearography the light forming the image is split by the shearing optic and the two images are recombined on the detector laterally shifted by some distance. In this way the laser radiation illuminating the surface acts as its own reference. Each resolution element on the detector (from here on assumed to be a charged coupled device (CCD) camera) receives its speckle phase information from two distinct points on the surface whose separation is a function of the magnitude of the image shear.

When the object under inspection of a shearographic system vibrates or undergoes bulk motion the pair of points contributing to the speckle at a single resolution element on the CCD tend to move together. In this way the phase relationship at that element remains relatively constant and the shearographic system becomes largely insensitive to environmental vibrations and rigid-body motions.

When an object is being inspected with a shearographic system and a subsurface defect is present, stressing of the object will cause a localized surface deflection in the vicinity of the flaw. This local surface deflection will cause the two points that contribute to the speckle phase information at a resolution element on the detector to undergo an out-of-plane motion relative to each other. The relative motion between the paired points alters the phase relationship of the light reaching the element on the CCD and causes a change in the intensity response of that element. Because the difference in relative motion between the paired points is referenced to the magnitude of the image shear, the information contained in a shearogram is a scaled modular measure of the slope of the localized surface deflection along the direction of the image shear. Therefore, with shearography the fringe patterns represent regions of deformation gradient and not deformation amplitude as in the case of ESPI.

It should be noted here that the sensitivity of a shearographic system can be adjusted by changing the magnitude of the shear vector. However, while a larger image shear will increase the sensitivity of the system, it also causes the fringe patterns present in the shearogram to be less representative of the true first deriva-

tive of the out-of-plane surface deflections. True deformation gradient fringes are only realized at small shear vectors, and small shear vectors tend to produce very few resolvable fringes. This trade-off must be handled on a need-to-know basis. If the simple detection of flaws is the driving interest of an investigation, a relatively large shear vector would be appropriate. If the actual geometry of the surface deflection is to be inferred by the fringe pattern, say by phase-shifting techniques, as small a shear vector as possible which still yields a usable number of fringes should be used.

In practice a shearographic system operates similar to an ESPI system. A sheared reference image of the surface containing speckle information is acquired, digitized and stored in computer memory prior to applying stress. Subsequent sheared images of the object under varying degrees of stress are subtracted point-by-point from the reference image at video rates, and the results are displayed on a monitor. The output on the monitor presents a fringe pattern in the area of localized surface deflections and black where there is no local out-of-plane motion or uniform bulk motion. A typical shearogram is shown in figure 1-4. A special shearogram of a debond in the shape of the word "NASA" is shown in figure 1-5.

With the availability and reliability of small, high-power diode lasers which operate in a range of wavelengths suitable for use with silicon-based CCD cameras (visible to near infrared), laser sheargraphy heads can be made small and compact. For example, a diode laser, shearing optic and CCD camera can all be integrated within a self-contained vacuum hood small enough to reach areas of difficult access. The ability to reach and inspect areas of awkward or difficult access is essential for any NDT tool to be considered useful.

1.2.2.5 Summary. In brief summary, a comparison of holography and shearography will show that holography is inherently more sensitive and can detect smaller deformations; however, it is extremely sensitive to ambient vibrations and rigid-body motions and, therefore, must typical be carried out on a vibration isolation platform. Shearography is theoretically less sensitive because it measures displacement gradients instead of true surface deflections, but it is significantly more immune to vibrations and bulk motions. As a result, holography is usually the method of choice for small objects which are easily isolated from vibration. Shearography is the method of choice for larger object such as aerospace structures and where these inspections must take place in the field and often in difficult access ares. For this reason laser shearography appears to be the most appropriate method to inspect the orbiter ET SOFI for debonds and voids.

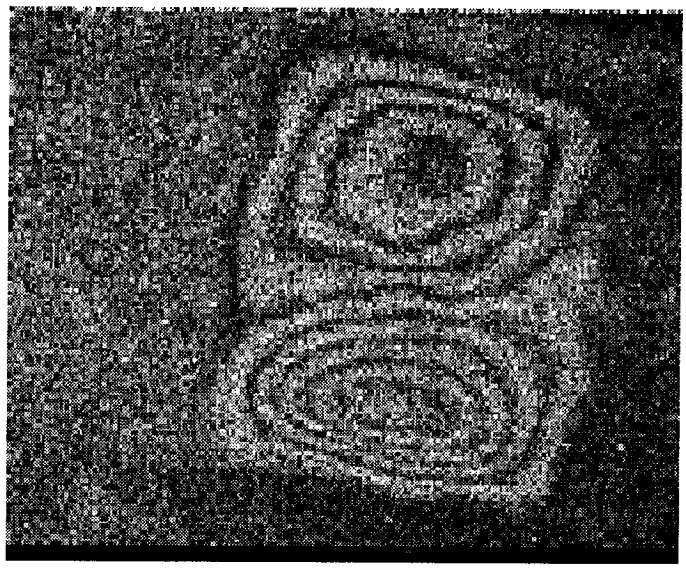

Figure 1-4. An Example of a Shearogram.
(This data was taken from a test panel constructed of K5NA ablative material used on the solid rocket motors.)

Figure 1-5. Deliberate Shearogram of a Debond in SOFI in the Shape of the Word "NASA" for Illustration Purposes Only

SECTION II

TEST METHODS, PROCEDURES, AND PARAMETERS

2.1 SOFI TEST PANELS

Three test panels were fabricated for this investigation. It was desirable to have a larger set of panels to increase the data set; however, due to time and availability constraints, the test specimens were limited to three. Every effort was made to maximize the information content of each panel.

2.2 SOFI TEST PANEL CONSTRUCTION

Each test panel was constructed from a 24-inch square aluminum substrate with a nominal thickness of 0.125 inch. The substrate was prepared with a two-part epoxy primer by Martin Marietta Corporation[5]. Prior to applying the programmed debonds, the primer was prepared to a "water-break-free" surface by cleaning with distilled water and a freon wash.

The programmed debonds were prepared by the Teflon sandwich method in which two thin sheets of Teflon are cut to the desired shape, placed face-to-face and covered with a thin layer of tape to maintain debond integrity. The debonds were placed close enough to each other on the test panels to maximize the number of debonds per panel, but not so close as to interfere with each other during testing.

Programmed debonds consisted of symmetric and asymmetric geometries. Circular and square debonds were created ranging from 0.5 inch to 2 inches in 0.25-inch increments. There are also seam/strip debonds and "L" shaped debonds to determine the dependency of detectability on shear vector orientation. Also incorporated in the test panels are annular debonds and groups of debonds placed in close proximity to determine the ability of the system to spatially discriminate flaws which may be separate but closely spaced. A resolution debond was constructed from a triangle approximately 12 inches in height with a 4-inch base. This debond was used to help determine the detectability threshold for SOFI depth verses lateral flaw extent.

The test panels were sprayed with standard SOFI equipment used at KSC to a nominal thickness of 3 inches. Subsequently, the panels were planed off to a thickness of 1.5 inches.

2.3 SOFI TEST PANEL INSPECTION

Each panel was inspected with two fields of view with four orientations of the shear vector in each view. The first view consisted of the entire 24-inch square panel. Using this field of view the entire panel was inspected using a vertical shear vector, a shear vector 45 degrees off of vertical, a horizontal shear vector and a shear vector 135 degrees off of vertical. The field of view was then reduced to an area which subdivided the test panel in to nine subareas with some overlap between adjacent subareas. Each of the nine subareas were then inspected, again, with the four shear vector orientations. This process was carried out for each of the three test panels at a fixed SOFI thickness.

Because of the material properties of SOFI, vacuum stressing was considered to be the optimum stressing mode and was used to inspect all of the SOFI test panels. To facilitate this, a vacuum chamber was manufactured from Plexiglas. The vacuum chamber measured 25x26 inches. The side walls were made from 1/2-inch thick Plexiglas and the top and bottom of the chamber were made from 3/4-inch Plexiglas to minimize deflection during the vacuum drop. Vacuum was applied to the chamber from the vacuum device provided by Laser Technology, Inc. with the laser shearography system. The chamber was also connected to a vacuum gauge so pressure drops could be monitored.

Two to three inspectors were present during all testing and the panels were tested in random order. In order to impose a quantitative value on visual data, a scale was developed for use in grading the detection of the flaws. The grades were assigned with a value of 1 to 10 and the following criteria were used:

1. A perceived nonuniform disturbance in the image when observed under dynamic stress (Metaphysical Detection).
2. A nonuniform disturbance in the image observed under static stress.
3. An apparent separation of two areas (derivative) under dynamic stress warrant future investigation (possible detection).
4. A surface deflection sufficient to cause single phase step resulting in uniformly bright doublet with no secondary fringes. Considered to be a detection of a flaw.
5. A surface deflection sufficient to cause the formation of a double bullseye; i.e., one complete set of fringes. (light/dark pair)
6. A surface deflection sufficient to cause the formation of two sets of fringes.
7. A surface deflection sufficient to cause the formation of three sets of fringes.
8. A surface deflection sufficient to cause the formation of four sets of fringes.

9. A surface deflection sufficient to cause the formation of five sets of fringes.
10. A surface deflection sufficient to cause the formation of six or more sets of fringes.

For the purposes of flaw identification, a grade of 4 or higher is considered to be a detection. A grade of 3 would be cause for additional testing; e.g., by zooming in on an area of grade 3 the image is enhanced and the area may then be upgraded to 4 if it meets the criteria.

When the inspection of all panels at a fixed foam thickness was completed, the SOFI was then reduced by 0.25 inch and the entire test procedure was repeated. This process continued until the SOFI was reduced to a thickness of 0.5 inch. The nominal thickness of the SOFI on the external tank is 1 inch and as such extra data was taken at that thickness. This is discussed in more detail below.

2.4 ADDITIONAL TESTING

Data at all thicknesses and views were typically taken at 1 inch of water vacuum. Full panel views were performed at a nominal laser power of 500 mW and subarea testing was performed at 100 mW. Additional testing at the nominal foam thickness of 1 inch included vacuums of 1, 5, 10, and 15 inches of water in the full panel views and 1 and 10 inches of water in the small area testing. No detectability enhancement was observed for the higher vacuum levels in the SOFI. A possible reason for this phenomenon will be discussed further in section III. For field inspections on SOFI, a vacuum hood containing a shearography camera and laser source would typically be used. The vacuum hood is attached to the inspection surface by pulling just enough vacuum to hold it in place. At that point the reference image is obtained and the vacuum is increased slightly to cause a surface deformation in the area of a debond. Therefore, additional testing at the nominal foam thickness of 1 inch included vacuum offsets of 1, 5, 10, and 15 inches of water in the full panel views and 1 and 10 inches of water in the small area testing. Also, at the 1-inch SOFI, thickness tests were performed using a shearography camera with a 1-degree shear vector instead of the 0.5-degree shear vector which was supplied with KSC's laser shearograph. These results will be discussed later. Figure 2-1 shows a typical shearogram showing debonded areas in 1 inch of SOFI at a vacuum of 1 inch of water. The debond in the upper left corner is a 1-inch square, the debond in the upper right corner is a 1.5-inch circle, and the debond in the lower right corner is a 2-inch circle. There is a 0.5-inch debond present in the lower left corner but it is not quite visible in this image.

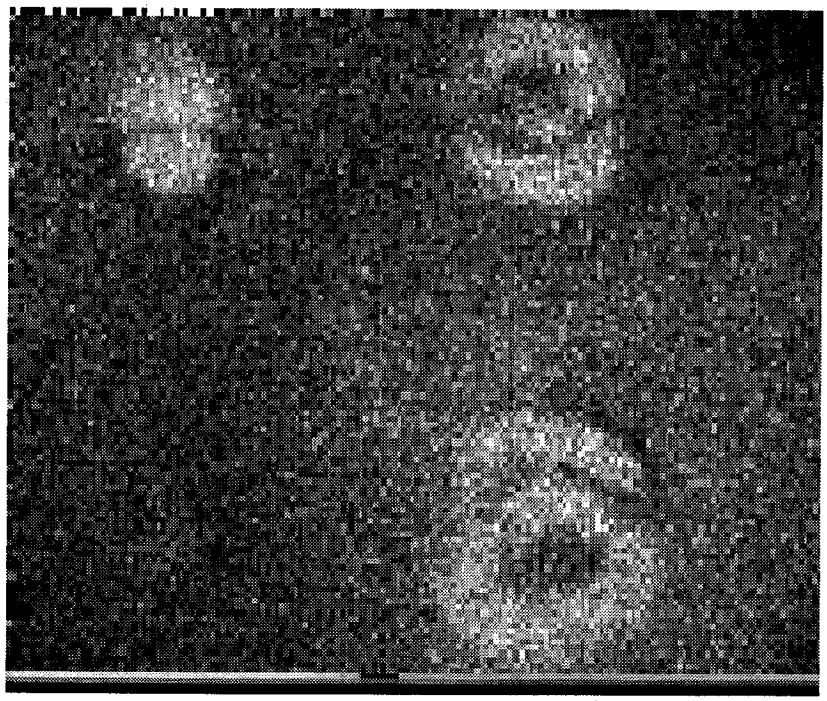

Figure 2-1. A Typical Shearogram of Debonds in SOFI

SECTION III

TEST RESULTS

3.1 CIRCULAR DEBONDS

Because of their symmetry, the circular debonds provide the easiest shearograms to interpret. They also provide the largest and most consistent data set due to their invariance under shear vector rotation (i.e., except for the elongation of the shearographic indication along the direction of the shear vector, the shearograms look very similar).

As mentioned earlier each test panel was inspected with two fields of view: a view which looked at the entire 24-inch square panel and a view which subdivided the panel into 9 subareas with some overlap. Shown in figure 3-1 are the average detection values of circular debonds plotted as a function of SOFI thickness and defect diameter for the field of view consisting of the entire test panel. (**Note:** see appendix A for plots of the unaveraged values.) This data consists of measurements made at all shear vector orientations, SOFI thicknesses, and vacuum drops of 1 inch of water. Because the defect grading system used integer values for rating detection, with 3 being a possible detection and 4 being considered a true detection, when the data is averaged the values between 3 and 4 must be accounted for. Therefore, in presenting the data in averaged form a detection value **greater** than 3 is considered a detection. Also, a conservative estimate of error of $\pm$ 1 detection value is imposed based on the standard deviation of the data and the discrepancies between inspectors grading of defects.

From figure 3-1 it is seen that the 0.5 inch diameter defect was not detected at any SOFI thickness in the full panel view and 1 inch of water vacuum drop. As would be expected, however, the larger the defect the thicker the SOFI in which it was detected. Every defect larger than 0.5 inches met the detection criteria at all SOFI thicknesses. Figure 3-2 shows the same defects, SOFI thicknesses and vacuum drop but with the smaller field of view. By zooming in to reduce the field of view, the effective resolution of the shearographic system is increased. This effect is clearly seen in this figure by the detection of the 0.5- and 0.75-inch defects not present in figure 3-1, as well as the greater detection values for all the other defects. There are also two other important aspects of detecting debonds in SOFI by shearography that are apparent in this figure.

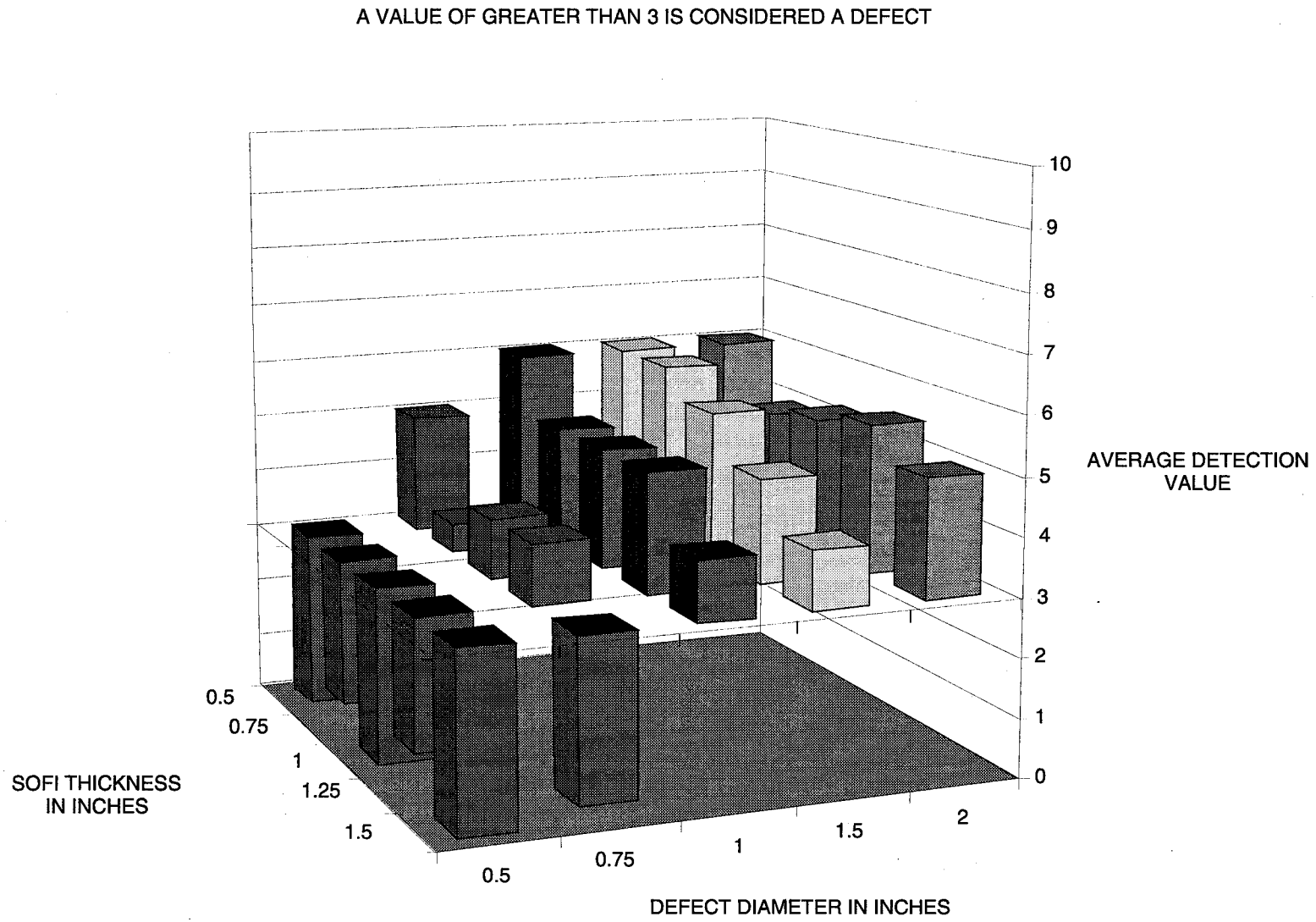

Figure 3-1. Average Detection Values of Circular Debonds vs. SOFI Thickness and Defect Diameter – Full Panel View

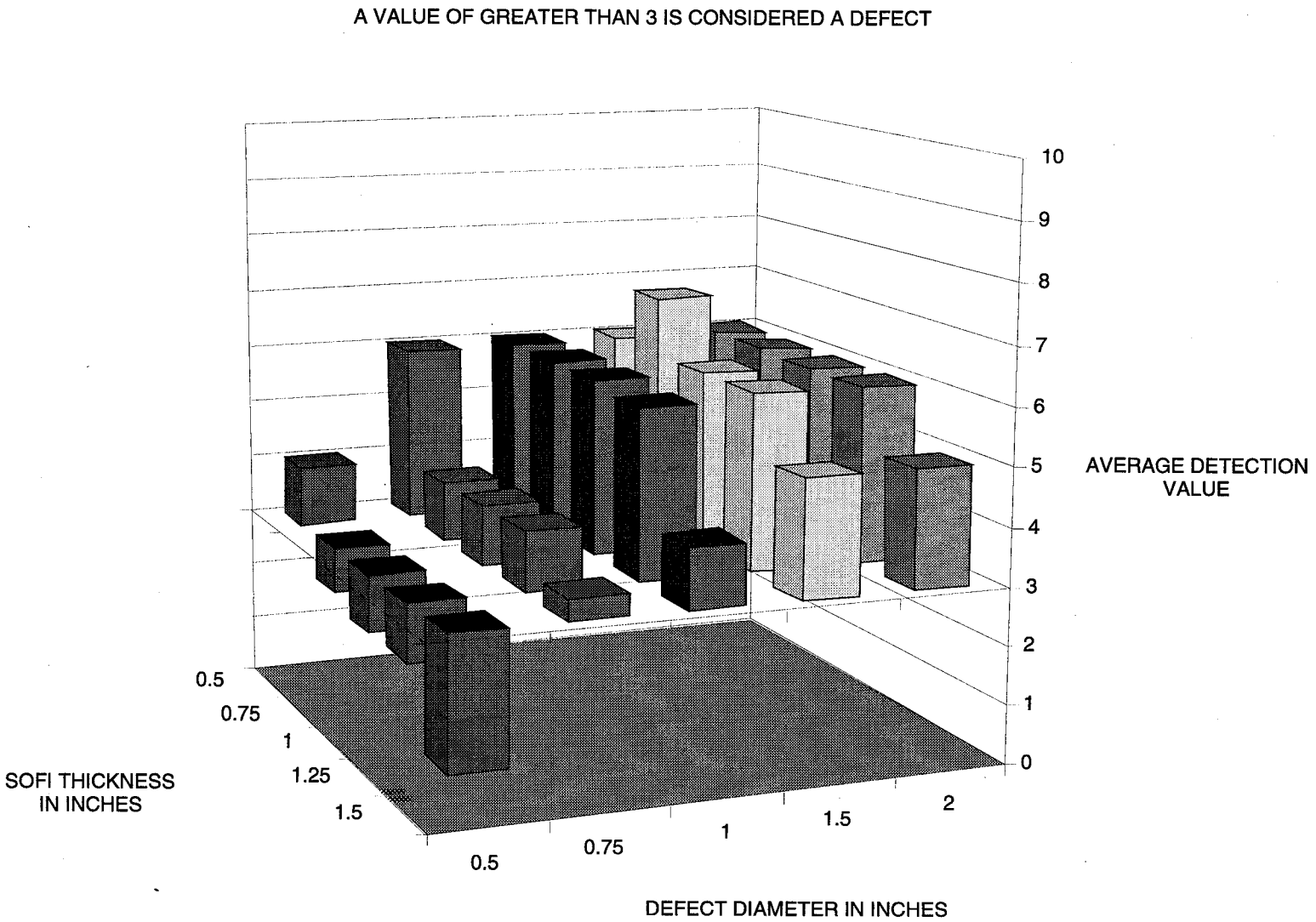

Figure 3-2. Average Detection Values of Circular Debonds vs. SOFI Thickness and Defect Diameter – Subareas

First, by moving from left to right along a line of equal SOFI thickness in figure 3-2, it is clear that the growth in detection value as a function of defect size is not constant. Because of the material properties of SOFI (and all materials where surface deflections are being measured) such as elasticity and Poisson ratio, smaller defects require more force to achieve the same surface deflection as that of a larger defect. Because it is surface deflection that is detected by shearography, this limits the detectability of small defects with small vacuums. This now begs the question: why not just increase the vacuum until the smaller defects are detected? There are two reasons. First, field inspections of the ET SOFI will likely be conducted by use of a vacuum hood which will be placed on the surface of the SOFI. Pulling too large a vacuum could result in damage to the SOFI. Second, there is a physical limitation imposed by material characteristics of SOFI which establishes a threshold of a vacuum.

SOFI is a relatively soft closed-cell material and each cell contains a small volume of air. When vacuum stressing is applied to SOFI, the entire surface under inspection expands. Therefore, there is a race between the deformation of the surface due to a debond and that due to the individual expansions of the cells. At low pressure drops the surface deflection caused by the expansion of the larger volume of air present at a debond wins out. However, as the vacuum increases, the deformations caused by the closed cells grow to a point where the image decorrelates and the defect can no longer be distinguished. Throughout the testing of the panels it became clear that, in SOFI, if a defect was not detected with a pressure differential of 1 inch of water, it was not likely to be detected at all.

Another important factor can be seen from figure 3-2 by looking at the detection values along a line of constant defect diameter. For a fixed pressure differential, in this case 1 inch of water, larger defects grow more quickly to a maximum detection value as a function of SOFI thickness than do smaller defects. Further, increasing the vacuum level after these maximums have been reached does not usually increase the detection value but, instead, causes decorrelation of the image and the defect can no longer be seen.

3.2 SQUARE DEBONDS

Square debonds obviously do not possess the same degree of symmetry as do circular debonds. Therefore, when investigating the ability of a shearographic system to detect debonds having a square, or approximately square geometry, the dependence of detection as a function of shear vector must be considered. This is true for all defects which do not possess complete symmetry about the viewing axis of the shearographic system. This statement implies that in field inspections on flight

hardware, every area tested must be inspected with multiple shear vector orientations. The extreme importance of inspecting with multiple shear vector orientations will be clearly seen when the data on seam debonds is presented below. (**Note:** seam debonds are one of the most common debonds found on the ET.)

Figures 3-3 through 3-6 show the results for the square programmed debonds. Each figure represents a single square debond and plots detection value as a function of SOFI thickness and shear vector orientation. This data is not averaged because the possible functional dependency of detection value on shear vector is shown and therefore, the detection threshold is taken to be 4. As seen before in the circular defect data, a conservative estimate of error in the detection value is ± 1.

By going to any of the figures 3-3 through 3-6 and moving along a line of constant foam thickness, it is seen that for the square debonds there is no significant amount of change in the detection value as a function of shear vector orientation. The overall detection values for the square debonds are, however, higher than those of the corresponding circular debonds. This is not surprising because a square debond 1 inch on a side has a larger surface area than a circular debond 1 inch in diameter. Also, the higher stresses associated with the coroners of a square debond may propagate to the surface and enhance surface deflections.

Since there is no strong dependency of detection values as a function of shear vector orientation for the square debonds figures 3-7 and 3-8 are provided for consistency. Figures 3-7 and 3-8 represent the average of all the data for the square debonds in the full panel and subarea views respectively. As with figures 3-1 and 3-2, the detection threshold is 3 and the estimated error in detection value is ± 1.

By comparing figures 3-1 and 3-2 with figures 3-7 and 3-8, it is seen that circular and square debonds exhibit many of the same characteristics. Both exhibit a non-linear growth in detection value as a function of defect size as well as the leveling off of detection values as SOFI thickness decreases.

3.3 SEAM DEBONDS

As discussed earlier, laser shearography detects the gradient of the out-of-plane displacement of a surface along the direction of the shear vector. This can pose a problem in the case of defects which possesses a high degree of asymmetry as in the case of a seam debond.

Consider a long and narrow, substrate level, horizontal seam debond under some thickness of SOFI (or any other material). When some stressing mechanism is

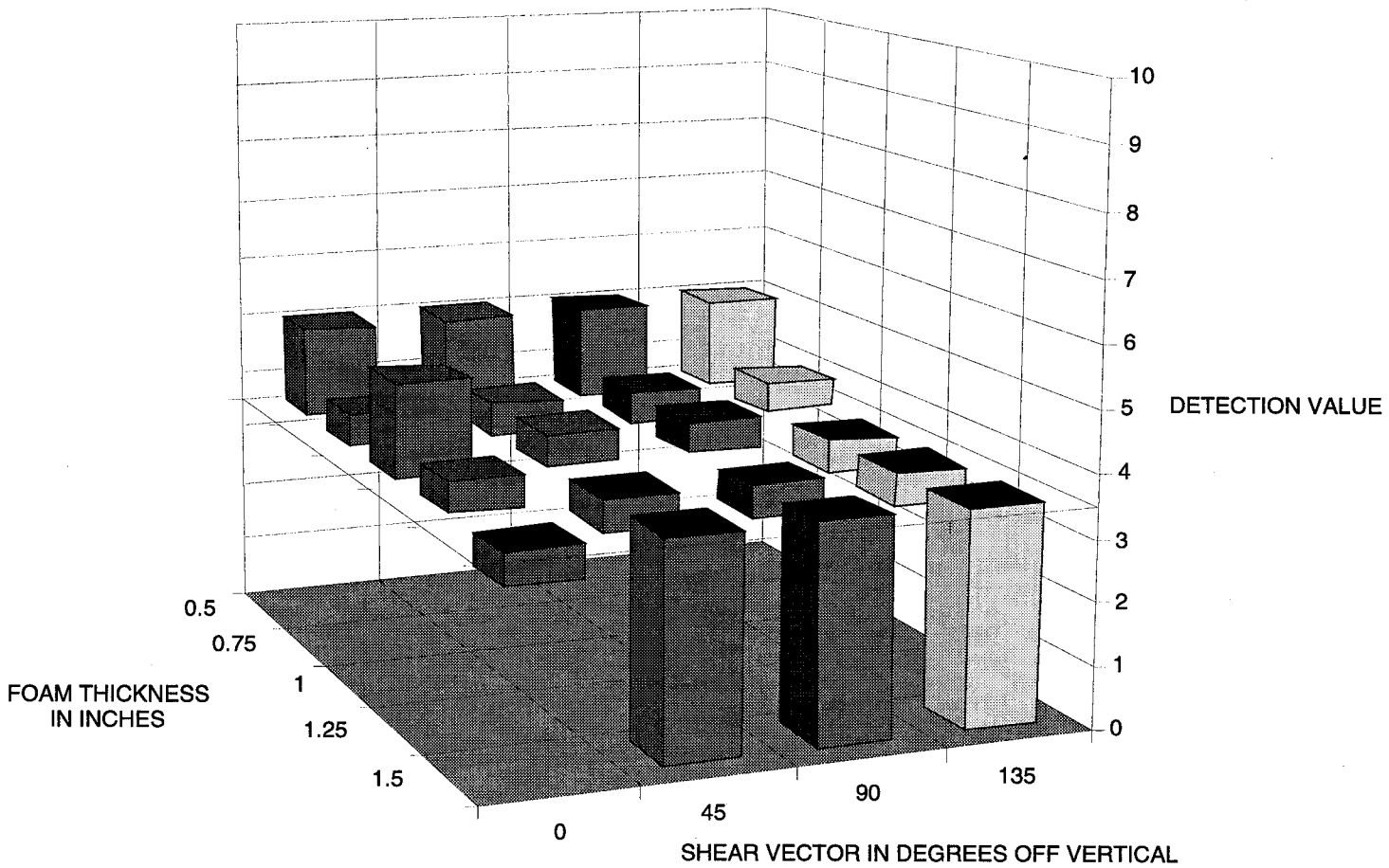

Figure 3-3. Detection Values vs. Shear Vector in all Foam Thicknesses for 0.5-Inch Square Debond

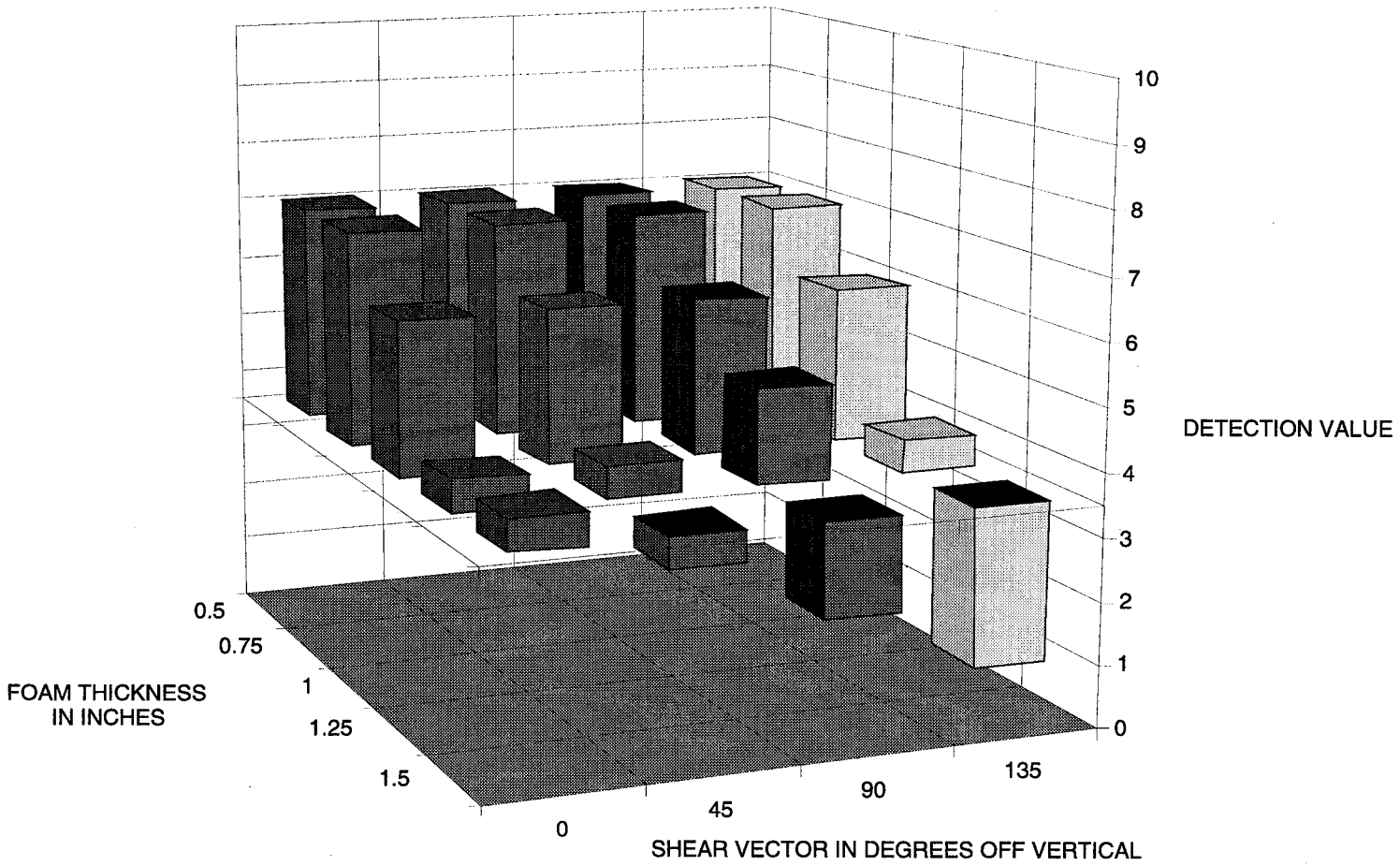

Figure 3-4. Detection Values vs. Shear Vector in all Foam Thicknesses for 1-Inch Square Debond

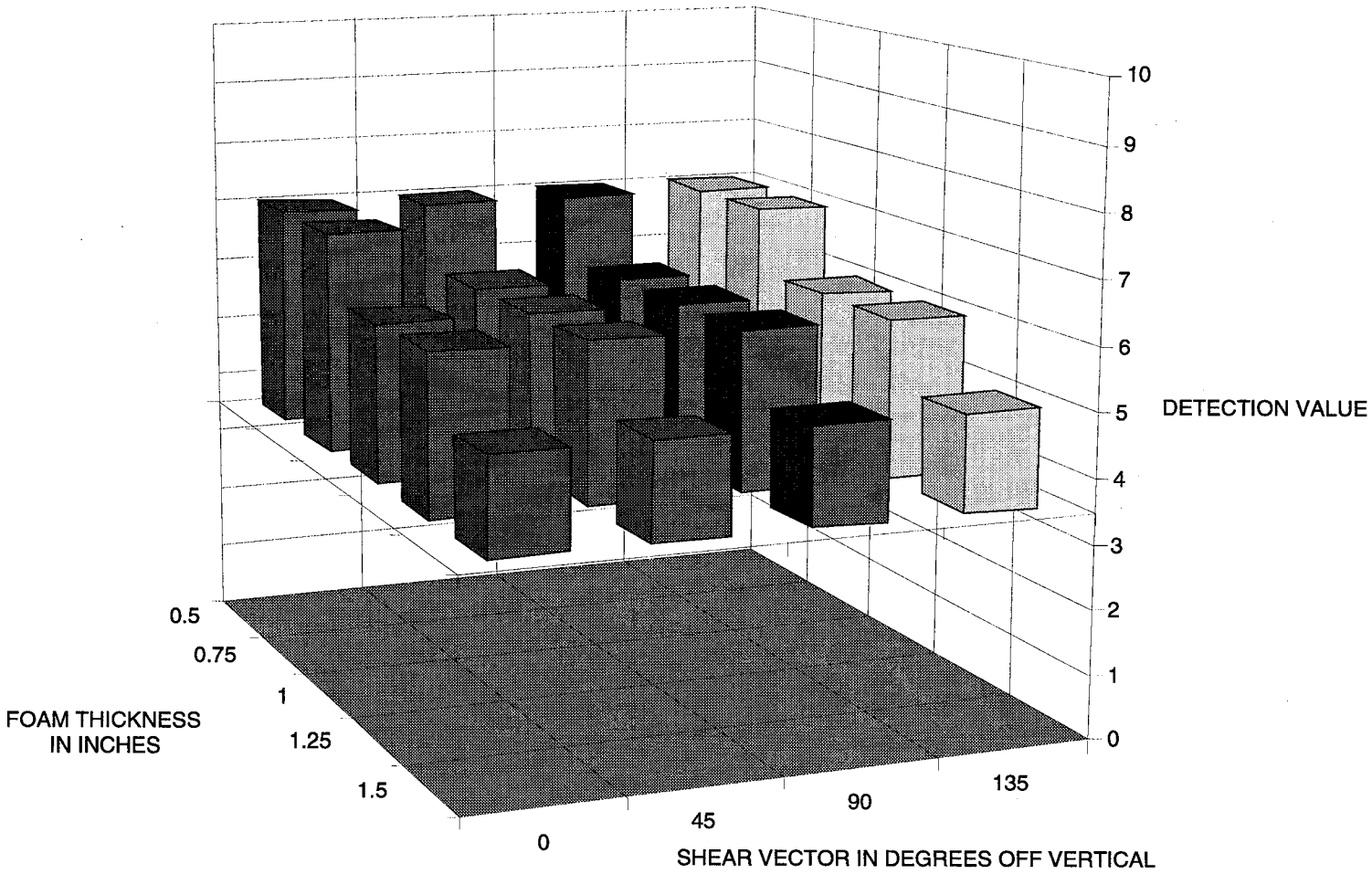

Figure 3-5. Detection Values vs. Shear Vector in all Foam Thicknesses for 1.5-Inch Square Debond

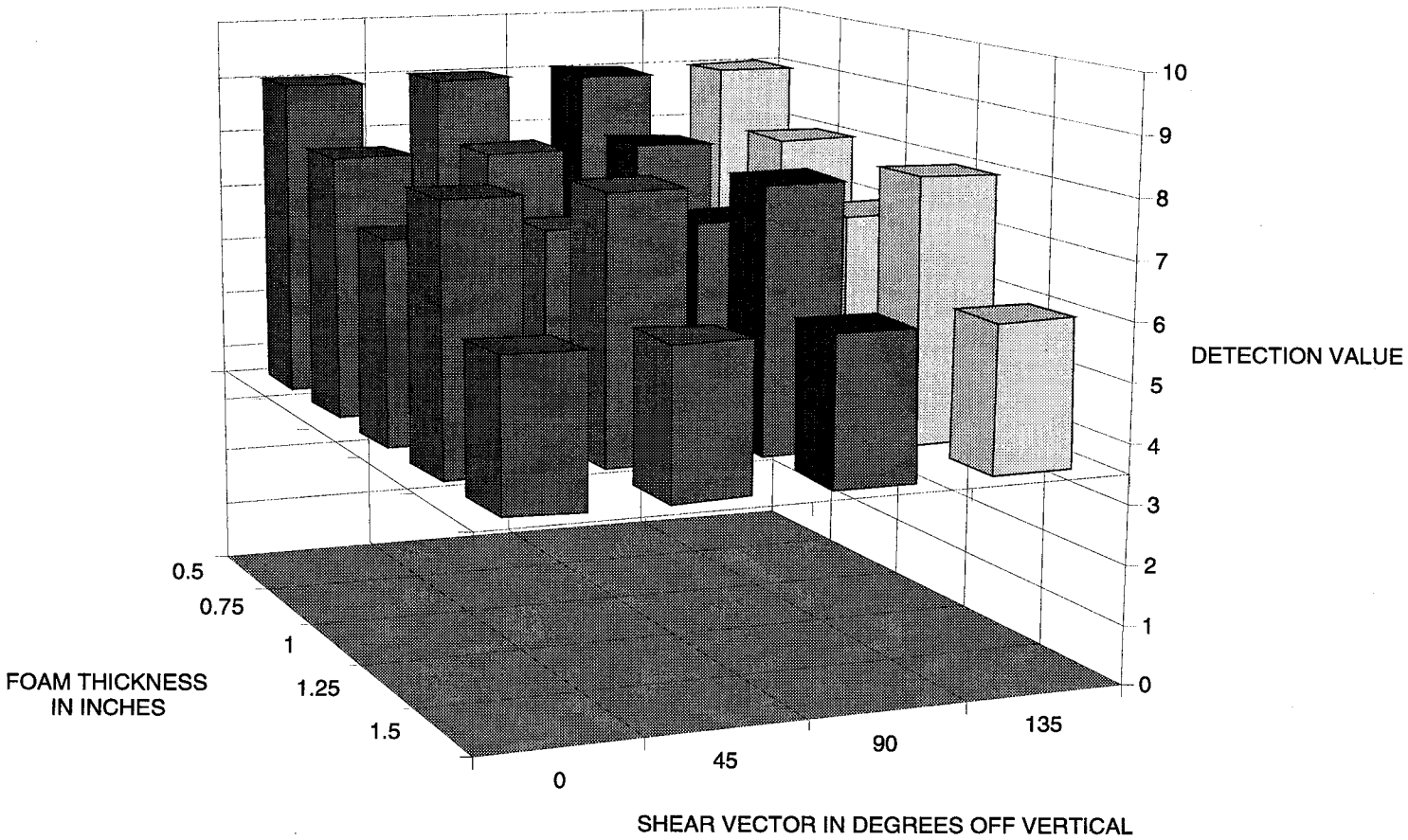

Figure 3-6. Detection Values vs. Shear Vector in all Foam Thicknesses for 2-Inch Square Debond

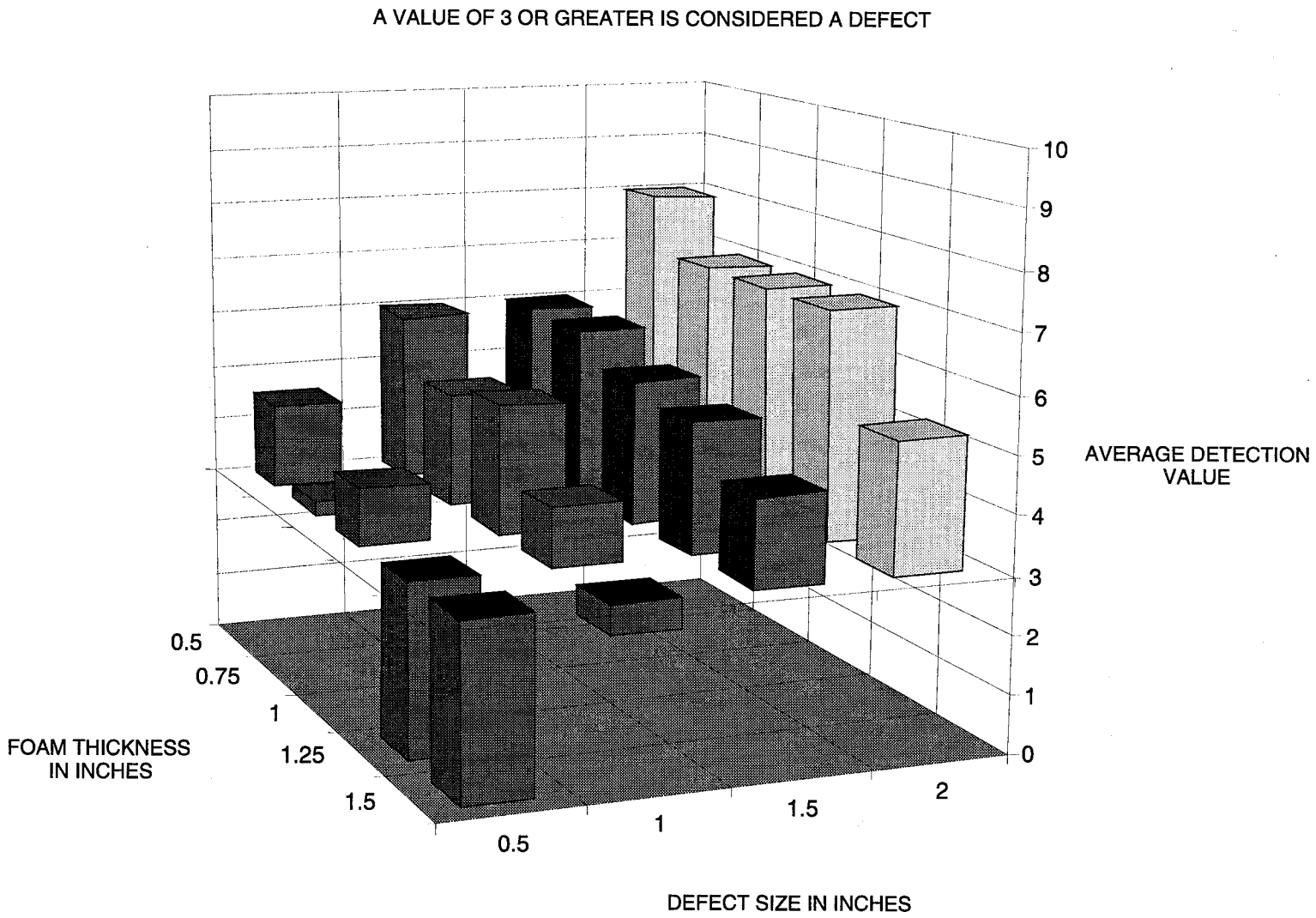

Figure 3-7. Average Detection Values of Square Debonds vs. SOFI Thickness and Defect Size – Full Panel View

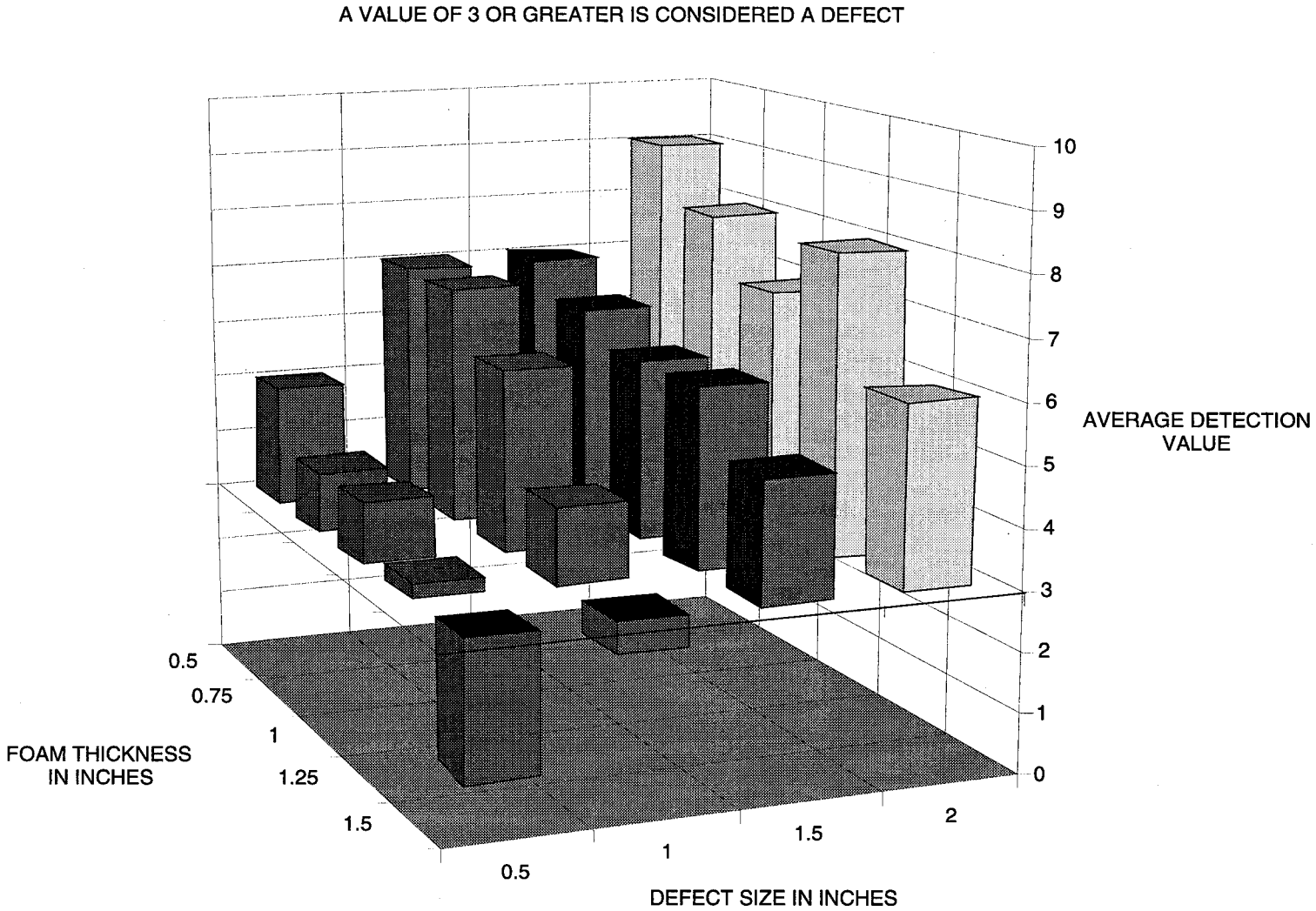

Figure 3-8. Average Detection Values of Square Debonds vs. SOFI Thickness and Defect Size – Subareas

applied, in this case vacuum stressing, the debond manifests itself as a surface deformation the outline of which will approximate the shape of the debond to a degree depending on the thickness and characteristics of the material. When this surface deformation is viewed with the shear vector in the vertical position (perpendicular to the long dimension of the seam debond) the gradient is imaged for every point along the length of the deformation. The result is a shearogram consisting of a classic shearographic double bullseye extending the length of the surface deformation. (This is illustrated in figure 3-9).

When the surface deformation is viewed with the shear vector parallel to the debond the result is much different. Surface gradients are localized at the end points of the seam debond. Therefore, two shearographic indications are created at the end points, but in the middle area of the surface deformation where the gradient is nearly zero, no indication is formed. This situation is shown in figure 3-9. This phenomenon results in a greatly reduced visual indication of the debond, and if the seam is long enough, can result in misinterpreting the indication as two separate debonds or not identifying the seam debond at all.

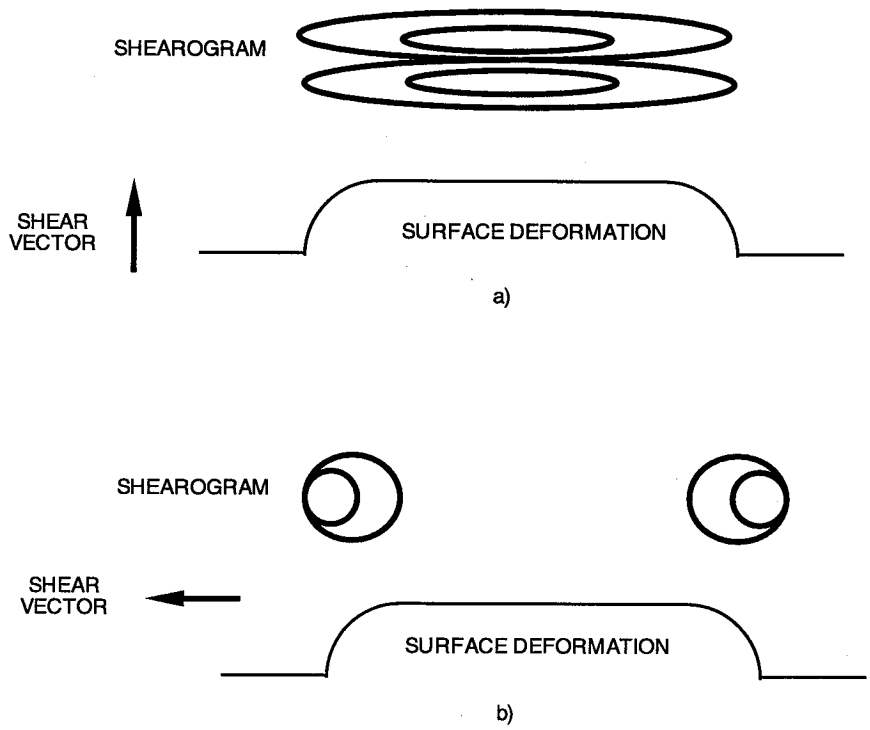

Figure 3-9. Shearograms for a Seam Debond. a) shear vector perpendicular to debond. b) shear vector parallel to debond.

Figures 3-10 and 3-11 show the results of data taken on two seam debonds, 3/4-x-3 inches and 3/4-x-10 inches respectively. The figures show detection values as a function of foam thickness and shear vector orientation. In figure 3-10 it is clearly seen that the detection value is strongly reduced when the shear vector is at 90 degrees, or parallel to the debond for all SOFI thicknesses. However, because this debond is relatively short in length, the shearographic indications remain close enough to provide some visual information that a debond is present. Figure 3-11 shows the results for the 10 inch long seam debond. In this case not only are the detection values greatly reduced when the shear vector is parallel to the debond, but in some cases the debond was not detected at all. This again implies that when doing field inspections on flight hardware where debonds are not likely to always be symmetric, several orientations of shear vector must be used.

It must also be noted that even when the shear vector is rotated to 45 or 135 degrees, the visual indication of a seam debond is not as clear as that when the shear vector is at 0 or 180 degrees. This is not always reflected in the data because even though the visual indication may be reduced, it may not change in detection value based on the grading system established. For example, at a shear vector orientation of 0 degrees, the shearogram of a seam debond may contain a double bullseye with two secondary fringes in each side. This may still be the case when the shear vector is rotated to 45 degrees but the shearographic indication may be compressed or have lower contrast and not be as visually clear as that at 0 degree shear vector.

Figure 3-12 shows the shearograms of the 3/4-x-10-inch debond in 1 inch of SOFI at three shear vector orientations: 0, 45 and 90 degrees. At 0 and 45 degrees the shearographic indications receive the same detection value; however, the shearogram at 0 degree shear vector is visually clearer. At the 90 degree shear vector orientation, the indication all but disappears.

3.4 TESTING WITH VACUUM OFFSET

To simulate shearographic testing of SOFI using a vacuum hood, inspections were made on the test panels using a vacuum offset. An offset simulates the vacuum required to seal the hood against the test object. In these inspections the vacuum level was raised to 5, 10 and 15 inches of water before the reference image was obtained. After the reference image was acquired, the vacuum level was increased to generate a relative surface deformation in the presence of a debond. This procedure neither enhanced nor degraded the detection of the programmed debonds. In fact, the detection values for all the values of vacuum offset were essentially identical to those where no offset was used. Also, the same dependency on detection as a function of pressure differential was observed. There was no increase in debonds detected when the pressure differential between the offset vacuum and the test

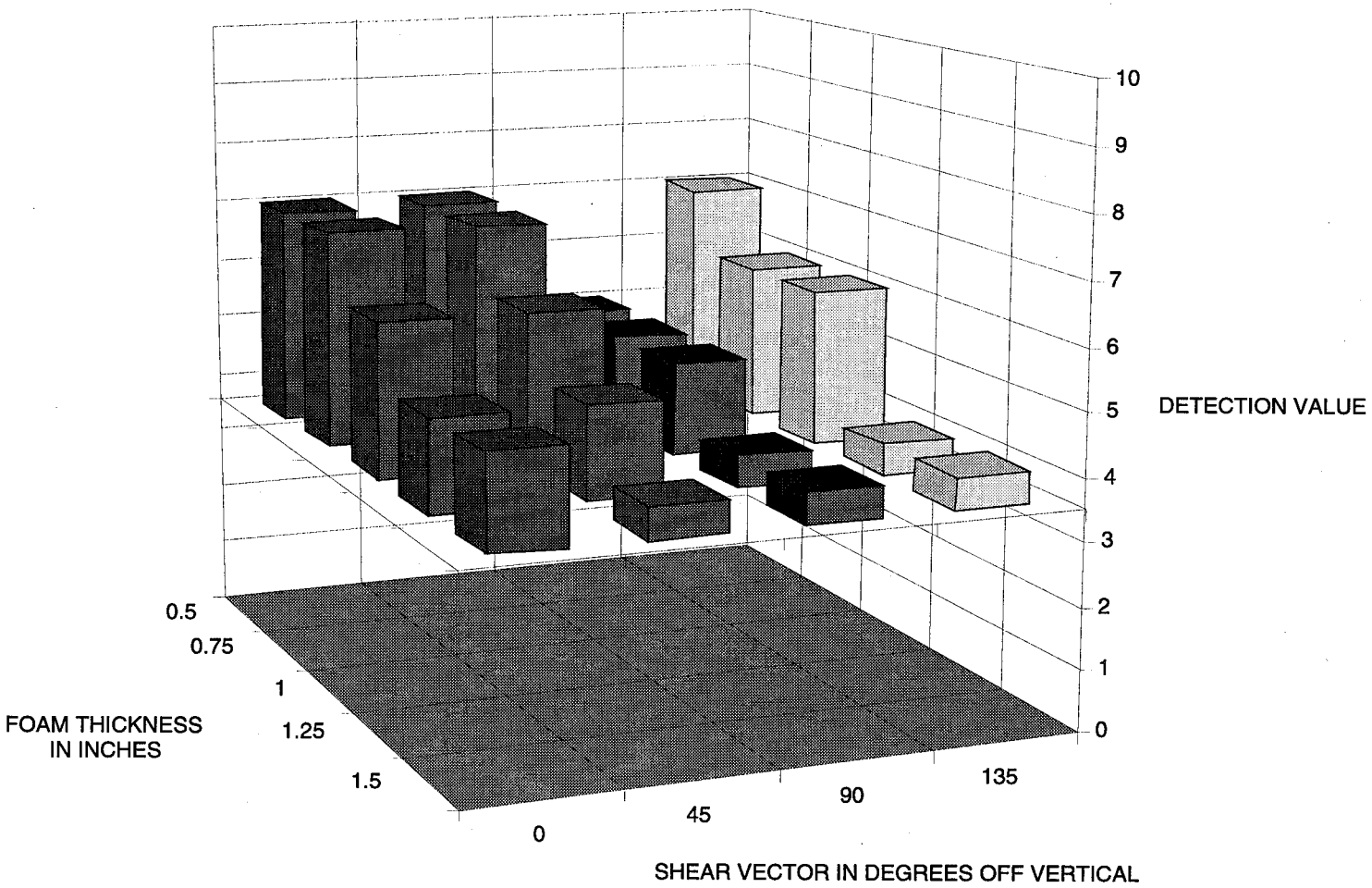

Figure 3-10. Detection Values vs. Shear Vector in all Foam Thicknesses for 0.75-Inch-by-3-Inch Seam Debond

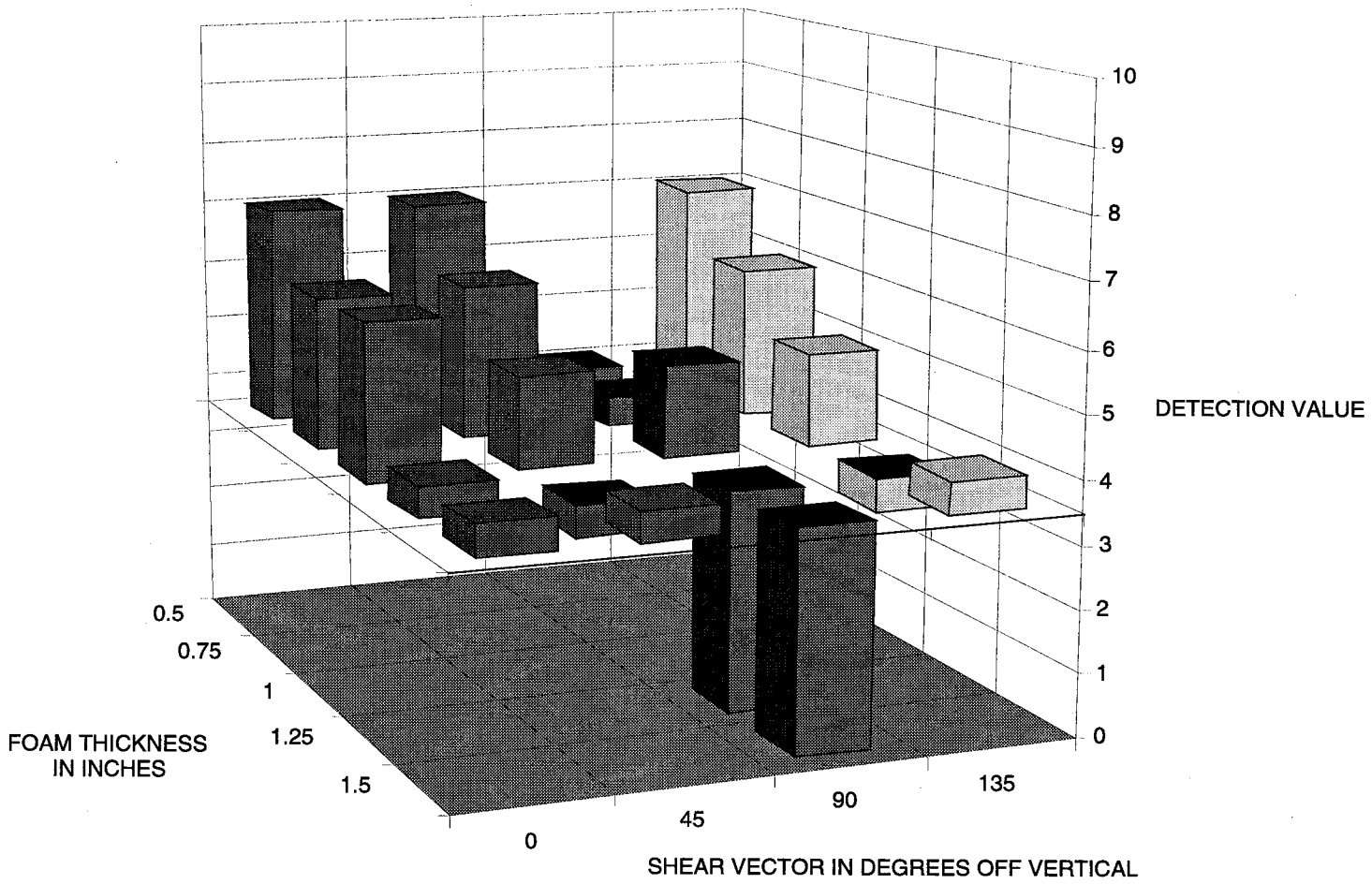

Figure 3-11. Detection Values vs. Shear Vector in all Foam Thicknesses for 0.75-Inch-by-10-Inch Seam Debond

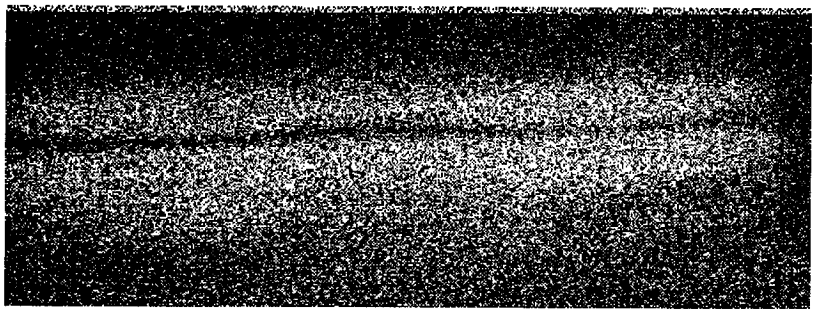

SHEAR VECTOR AT 0 DEGREES (PERPENDICULAR TO SEAM)

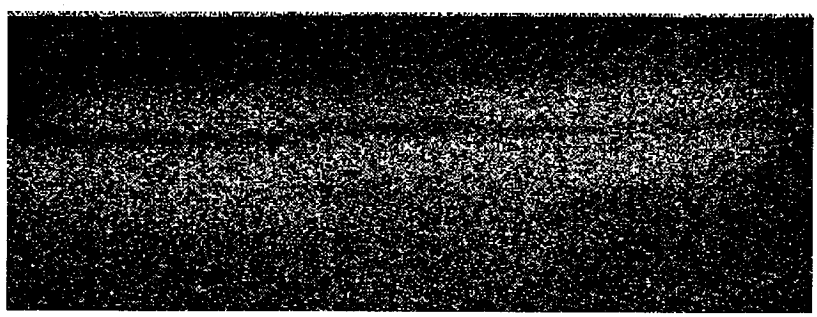

SHEAR VECTOR AT 45 DEGREES

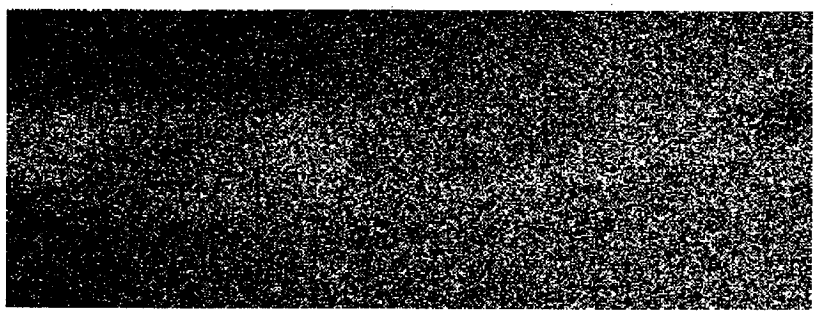

SHEAR VECTOR AT 90 DEGRESS (PARALLEL TO SEAM)

Figure 3-12. Shearograms of a Horizontal Seam Debond With Different Orientations of Shear Vector

vacuum exceeded 1 inch of water, and at a pressure differential of 3 inches of water decorrelation effects begin resulting in image degradation. While this may seem to contradict the discussion on page 3-4 regarding increasing vacuum and detectability, it does not. It is the differential between the pressure at which the reference image is stored (offset vacuum) and the test vacuum that is important. Therefore, if the reference image is obtained at a pressure drop of 10 inches of water, the test vacuum could range from 7 to 13 inches of water before decorrelation set in.

3.5 TESTING WITH 1 DEGREE SHEAR VECTOR CAMERA

By increasing the magnitude of the shear vector, the sensitivity of a shearographic system to out-of-plane surface deformations is increased. In order to determine if a larger magnitude shear vector would increase the detection of debonds in SOFI, a shearographic camera with a 1-degree shear vector was obtained on loan for a short period of time from Laser Technology Inc. Inspections were made on the test panels at the 1-inch nominal SOFI thickness. The increase in shear vector magnitude seamed to increase the fringe visibility in the shearograms. However, the number of fringes present in a shearogram for a specific debond did not increase. The detection values for all defects tested with the 0.5- and 1-degree shear vectors were identical and no defects were detected by the 1-degree camera that were not detected by the 0.5-degree camera. Although the 1-degree camera is more sensitive, it is believed that the detection of defects in SOFI is still limited by the race between the deformation of the surface due to a debond and that of the closed cell structure of SOFI. The increase in sensitivity allows the surface deformation from a debond to be detected earlier in the vacuum pull before the closed cell structure of the SOFI has much chance to react. This results in the increase in fringe visibility (signal-to-noise) in the shearogram. However, by the time the vacuum increases to the point where small debonds may be affected, the SOFI has reacted to a level where decorrelation of the image sets in. The 1-degree shear vector enhanced the visual quality of the shearograms but not the ability of the system to detect debonds in SOFI.

3.6 DATA NOT DISCUSSED

The above discussion is limited to the more common types of debonds likely to be found in the field. As mentioned earlier, the programmed debond set also includes annular debonds, groups of debonds placed in close proximity to determine the ability of the system to spatially discriminate flaws which may be separate but closely spaced, triangles, a long triangular resolution debond, and "L" shaped debonds. Appendix B contains a legend of all the programmed debonds that were created, with their identification number, panel number, geometry and dimensions.

Following the legend is the complete data set containing all the measurements taken on all the programmed debonds, on all the test panels at all SOFI thicknesses. The reader is invited to use the data contained in appendix B to satisfy any curiosity on data not discussed, to add on their own to this report or to verify any of the results presented herein.

SECTION IV

PROBABILITY OF DETECTION ANALYSIS

4.1 PROBABILITY OF DETECTION (POD) ANALYSIS

The probability of detection analysis performed in this report utilized software written by A.P. Berens and P.W. Hovey from the University of Dayton Research Institute under a contract with the U.S. Air Force. The software is called "PODSS" and has the U.S. military identifier UDR-TR-88-12. A brief analytical discussion of the al-gorithms it uses is presented below[6].

4.2 PROBABILITY OF DETECTION FROM SIGNAL RESPONSE DATA

Any measurement instrument generates a response which is somehow dependent on what the device is measuring. Let $\hat{a}$ represent the response of the laser shearograph (the presence, lack of presence or the density of fringes present in the shearographic indication) to a debond of size a. The probability of detection (POD) can be obtained from the relation between $\hat{a}$ and a. Let $g_a(\hat{a})$ represent the probability density of the $\hat{a}$ values for a defect of size a. The POD can then be written as:

$$\mathrm{POD}(a) = \int_{\hat{a}_{\mathrm{dec}}}^{\infty} g_a(\hat{a})\, d\hat{a},$$

where $\hat{a}_{dec}$ is the decision threshold, below which the response of the instrument is not sufficient to identify a defect. The correlating function between $\hat{a}$ and a defines the mean of $g_a(\hat{a})$ and is written as:

$$\hat{a} = \mu(a) + \delta,$$

where $\mu(a)$ is the mean of $g_a(\hat{a})$ and δ is a random error term accounting for the differences between $\hat{a}$ and $\mu(a)$. The distributional properties of determine the probability density $g_a(\hat{a})$ about $\mu(a)$.

Berens and Hovey have had satisfactory results in POD analysis utilizing a linear relation between $\ln(\hat{a})$ and $\ln(a)$ with normally distributed deviations. The model has the form:

$$\ln(\hat{a}) = \beta_0 + \beta_1 \ln(a) + \delta,$$

where δ is normally distributed with zero mean and constant standard deviation, σ_δ.

With the above assumptions, the POD(a) function is calculated as follows:

$$\text{POD}(a) = \text{Probability } [\hat{a} > \hat{a}_{\text{dec}}]$$

$$\text{POD}(a) = \text{Probability } [\ln(\hat{a}) > \ln(\hat{a}_{\text{dec}})]$$

$$\text{POD}(a) = 1 - \Phi\left[\frac{\ln(\hat{a}_{\text{dec}}) - \beta_0 + \beta_1 \ln(a)}{\sigma_\delta}\right] \qquad (1)$$

where Φ is the standard normal distribution function. Using the symmetry properties of the normal distribution function, equation (1) can be reduced to:

$$\text{POD}(a) = \Phi\left\{\frac{\ln(a) - [\ln(\hat{a}_{\text{dec}}) - \beta_0]/\beta_1}{\sigma_\delta/\beta_1}\right\} \qquad (2)$$

Equation (2) is a cumulative log normal distribution function with mean and standard deviation of log defect size given by:

$$\mu = \frac{\ln(\hat{a}_{\text{dec}}) - \beta_0}{\beta_1}$$

$$\sigma = \frac{\sigma_\delta}{\beta_1}$$

The terms β_0, β_1 and σ_δ are estimated by the method of maximum likelihood estimators.

As stated above it is assumed that the $\hat{a}$ values for a defect of size a have a normal distribution with mean and standard deviation given by:

$$\mu_{\ln(\hat{a})} = \beta_0 + \beta_1 \ln(a)$$

$$\sigma_{\ln(\hat{a})} = \sigma_\delta$$

where σ_δ does not depend on the defect size. Berens and Hovey simplify the notation by letting $Y_i = \ln(\hat{a}_i)$ and $X_i = \ln(a_i)$. The random variable:

$$Z = \frac{Y - (\beta_0 + \beta_1 X)}{\sigma_\delta}$$

has a standard normal distribution. Let $\phi(z)$ represent the density function of the standard normal distribution:

$$\phi(z) = \frac{1}{\sqrt{2\pi}} \exp[-(z_2^2)]$$

and $\Phi(z)$ represent the cumulative normal distribution:

$$\Phi(z) = \int_{-\infty}^{z} \phi(\xi) d\xi \ .$$

The likelihood function is then partitioned into three regions:

Region R: the region in which $\hat{a}$ values were recorded. (i.e., above the decision threshold and below the saturation limit of the instrument)

Region T: $\hat{a}$ values are below the decision threshold

Region S: $\hat{a}$ values are the saturation limit of the instrument and cannot be recorded

The likelihood function for the entire sample is the product of the likelihood functions for the three regions and can be written as:

$$L(\beta_0, \beta_1, \sigma_\delta) = \prod_R L_R \prod_T L_T \prod_S L_S \ .$$

Where

$$L_R = \prod_{i=1}^{r} \frac{1}{\sigma} \phi(Z_i)$$

$$L_T = \prod_{i=1}^{t} \Phi_i(a_{th})$$

$$L_S = \prod_{i=1}^{s} [1 - \Phi_i(a_{sat})]$$

because $1/\sigma\ \phi(Z_i)dz$ is the probability of observing $\hat{a}_i$ for the ith defect in R, $\Phi_i(a_{th})$ is the probability of obtaining an $\hat{a}_i$ value below the recording threshold for the ith

defect is S, and $1-\Phi_i(a_{sat})$ is the probability of obtaining an $\hat{a}$ value above the saturation limit for the ith defect in T. The log of the likelihood function is:

$$\ln[L(\beta_0,\beta_1,\sigma_\delta)] = -r\ln(\sigma) - \frac{1}{2\sigma^2}\sum_R [Y_i - (\beta_0+\beta_1 X_i)]^2 + \sum_T \ln\Phi_i(a_{th}) + \sum_S \ln[1-\Phi_i(a_{sat})]$$

where r is the number of defects in R, or the number of defects that are above the decision threshold and below the instrument saturation.

The maximum likelihood estimators are given by maximizing the likelihood function with respect to each term β_0, β_1 and σ_δ. Therefore, the maximum likelihood estimators are the solutions to:

$$0 = \frac{\partial \ln(L)}{\partial \beta_0} = \frac{1}{\sigma}\left[\sum_R Z_i + \sum_S V(Z_i) - \sum_T W(Z_i)\right]$$

$$0 = \frac{\partial \ln(L)}{\partial \beta_1} = \frac{1}{\sigma}\left[\sum_R Z_i X_i + \sum_S X_i V(Z_i) - \sum_T X_i W(Z_i)\right]$$

$$0 = \frac{\partial \ln(L)}{\partial \sigma} = \frac{1}{\sigma}\left[-r + \sum_R Z_i^2 + \sum_S Z_i V(Z_i) - \sum_T Z_i W(Z_i)\right]$$

where :

$$V(Z_i) = \frac{\phi(Z_i)}{1-\Phi(Z_i)}$$

$$W(Z_i) = \frac{\phi(Z_i)}{\Phi(Z_i)}$$

These equations are solved iteratively by standard numerical methods. Excellent choices for the initial estimates of the iterative process are the intercept, slope and standard deviation of residuals obtained from a standard linear regression analysis on the linear relation between $\hat{a}$ and a on the values of $\hat{a}$ for which a valid response was obtained.

SECTION V

POD CURVES BASED ON TEST RESULTS

5.1 DISCUSSION OF POD

The POD curves are shown in figures 5-1 through 5-23. These curves are consistent with the data presented in section III of this report. As would be expected, at the thinner SOFI thicknesses the POD curves begin to rise at very small defect sizes and the curves transition to high POD's very quickly. This is due to the very high detection rate of all defects in the thinner SOFI thicknesses. As the SOFI thickness increases, however, the curves shift to the right and the transition to high POD's occurs more strongly detected.

5.2 PODS FOR CIRCULAR DEBONDS

Figures 5-1 through 5-5 show the PODs plotted as a function of circular defect size in all SOFI thicknesses when viewing the entire panel. As expected, the thinner the SOFI the higher the POD. It is clear from these figures that in the full panel views, the small debonds do not show up well even when the SOFI is thin. This phenomenon was discussed earlier; however, it is clearly illustrated in this set of figures. For example, if one looks at the POD of a debond that is the same diameter as the SOFI thickness, in general, the larger debonds are more easily detected independent of SOFI thickness. Figure 5-1 gives a POD of approximately 0.75 for a 0.5-inch diameter debond in 0.5 inch of SOFI, while figure 5-2 gives a 0.87 for a 0.75-inch debond in 0.75 SOFI. Figure 5-3 gives a 0.99 for a 1-inch debond in 1 inch of SOFI; figure 5-4 gives a 0.98 for a 1.25-inch debond in 1.25 inch of SOFI; figure 5-4 gives a 0.98 for a 1.25-inch debond in 1.25 inch of SOFI; and figure 5-5 gives a 0.98 for a 1.5-inch of SOFI.

Figures 5-6 through 5-10 show the results from the circular debonds when inspected in the subarea views. As stated earlier, the effective resolution of the shearograph is increased as the surface to be inspected is zoomed in on, and in general, the detectability of a debond was enhanced when a smaller area is viewed. Again, using the criteria of debond diameter equal to the thickness of the SOFI, figure 5-6 shows that the POD of a 0.5-inch debond is essentially 1. The 0.75-inch foam/defect comparison is 0.95 and subsequent figures show the POD to be 0.98 or greater. The importance of this observation is that small debond detection is enhanced when the field of view is smaller. Therefore, the trade-off in speed of large area inspections with detection size criteria needs to be addressed.

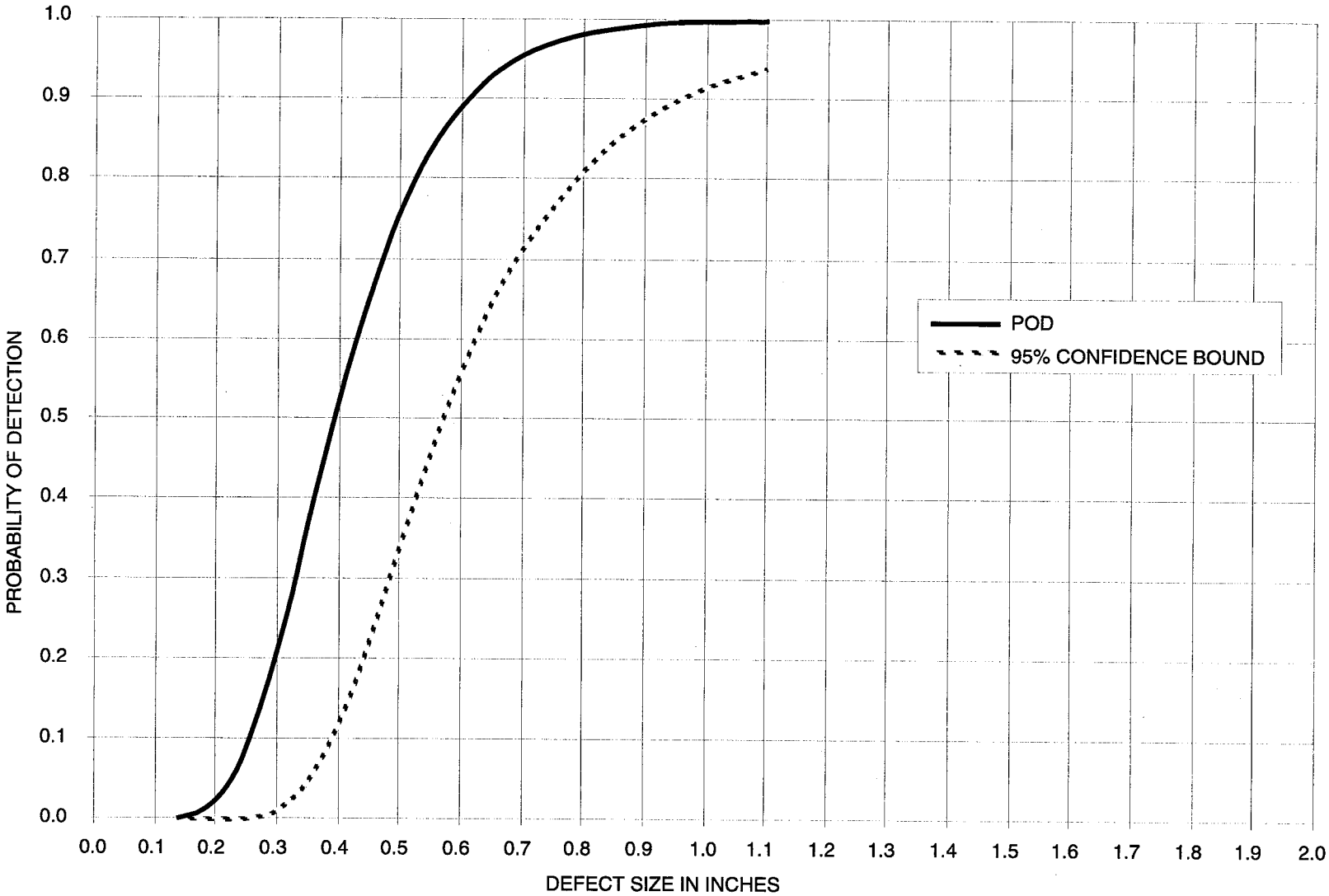

Figure 5-1. Probability of Detection of Circular Debonds on 0.5-Inch-Thick SOFI (Full Panel View)

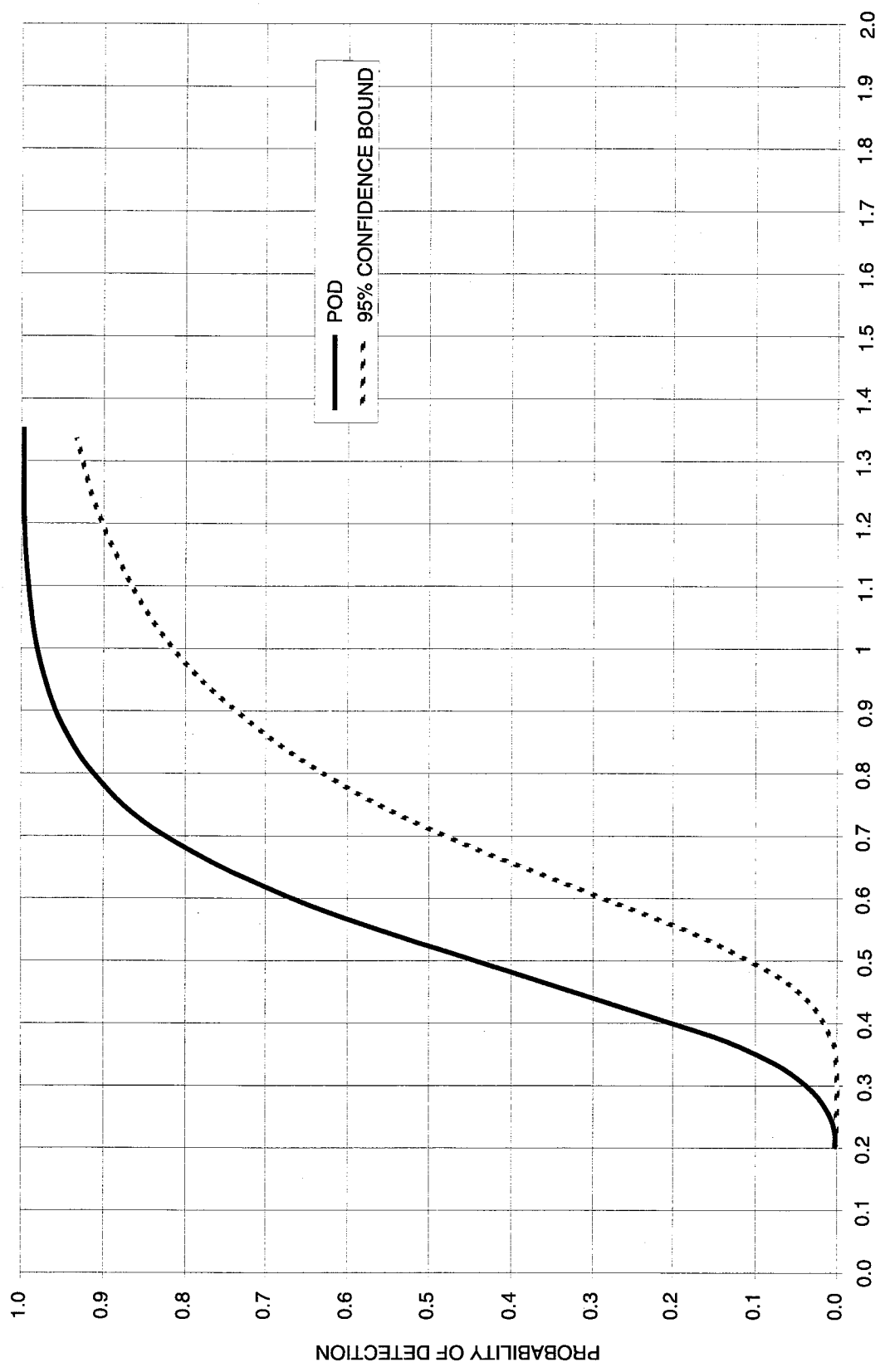

Figure 5-2. Probability of Detection of Circular Debonds on 0.75-Inch-Thick SOFI (Full Panel View)

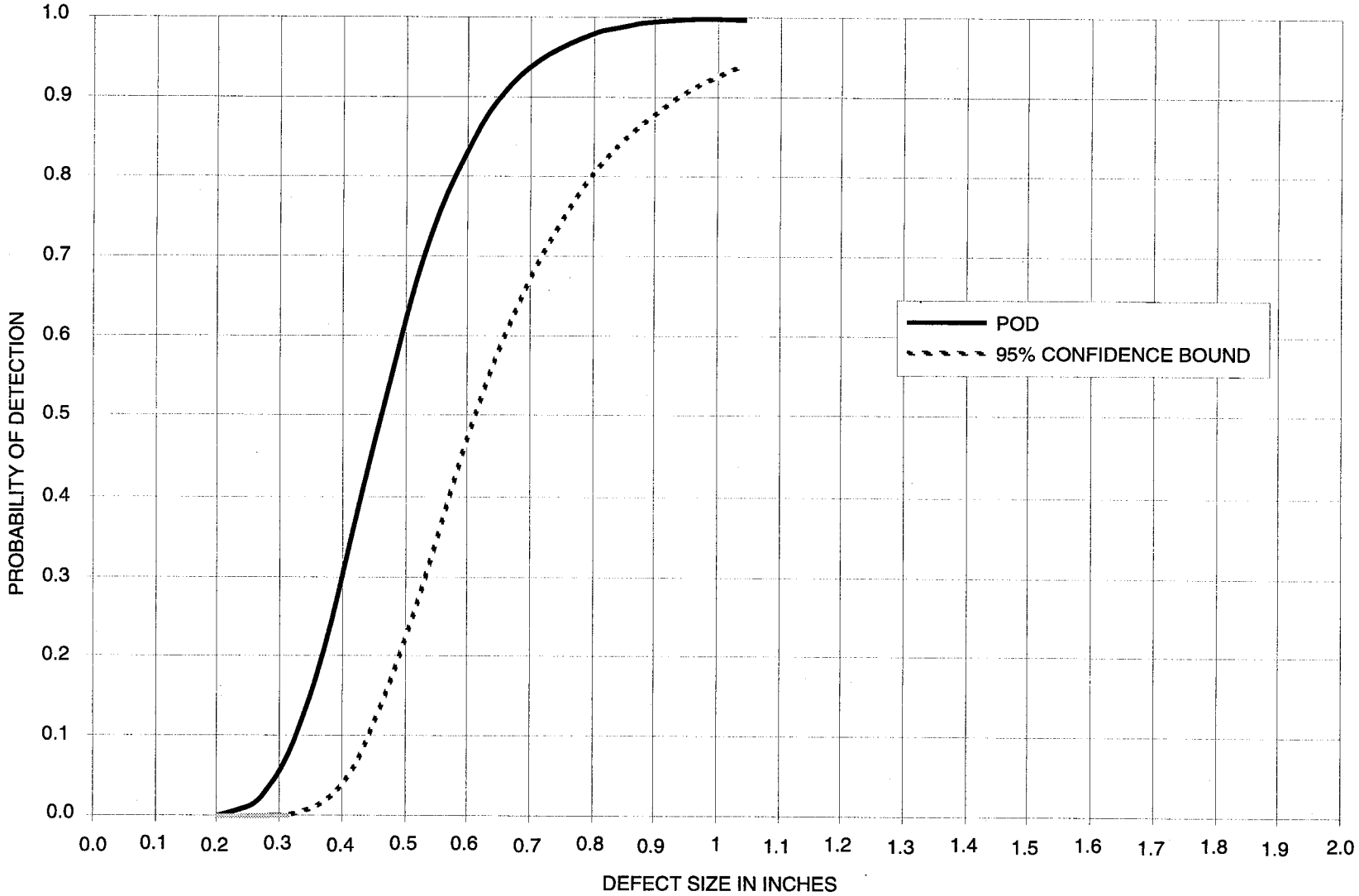

Figure 5-3. Probability of Detection of Circular Debonds in 1.0-Inch-Thick SOFI (Full Panel View)

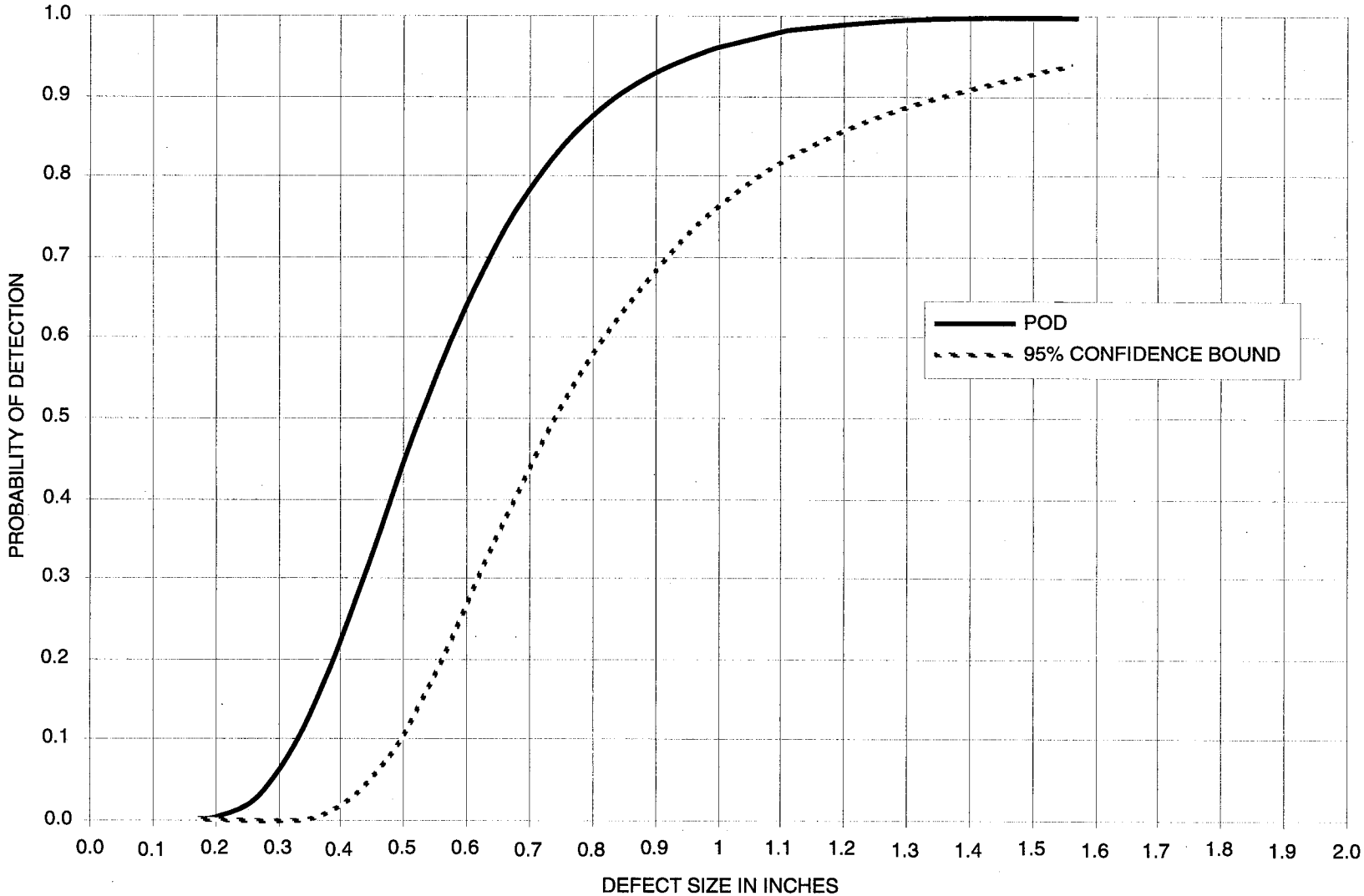

Figure 5-4. Probability of Detection of Circular Debonds in 1.25-Inch-Thick SOFI (Full Panel View)

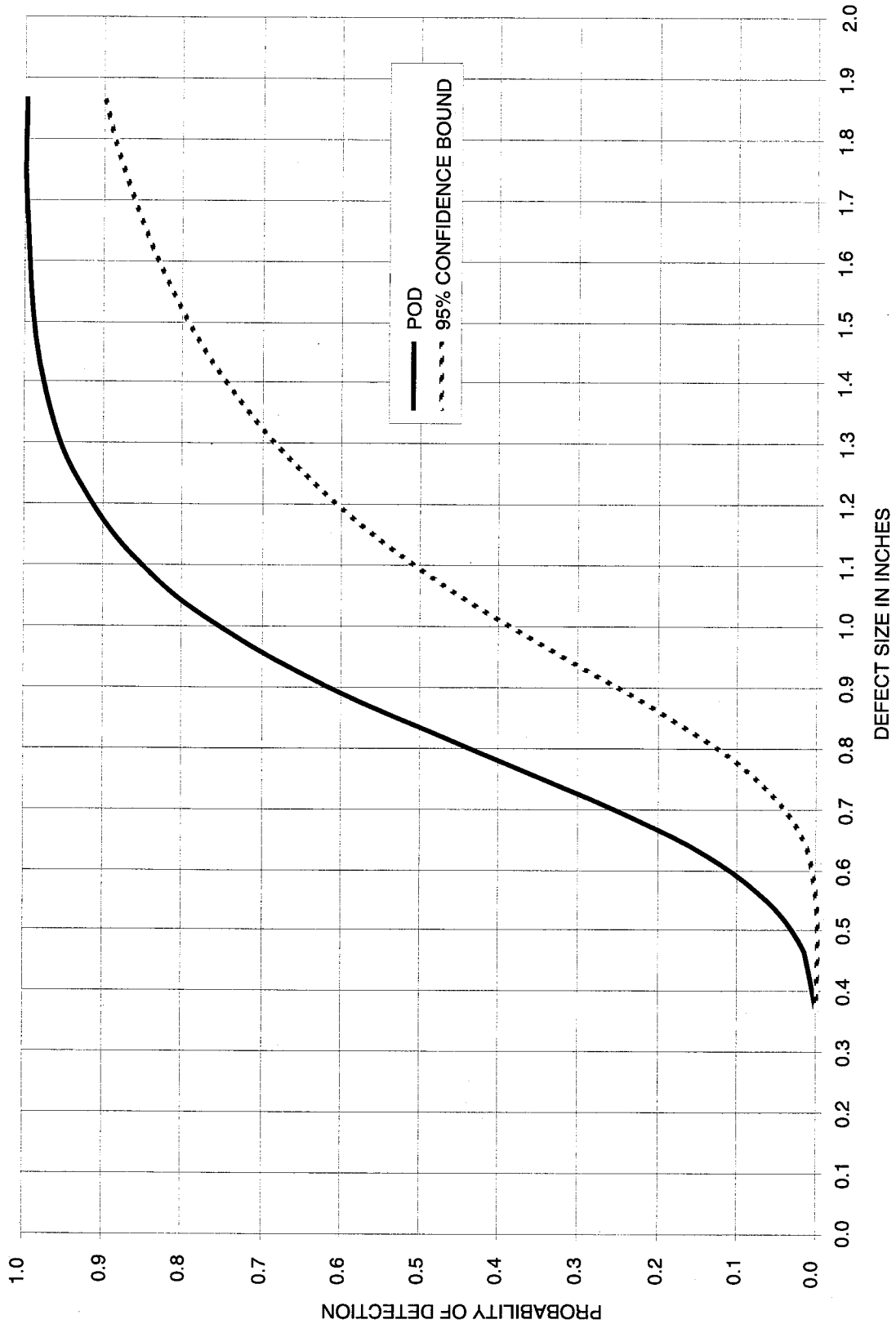

Figure 5-5. Probability of Detection of Circular Debonds on 1.5-Inch-Thick SOFI (Full Panel View)

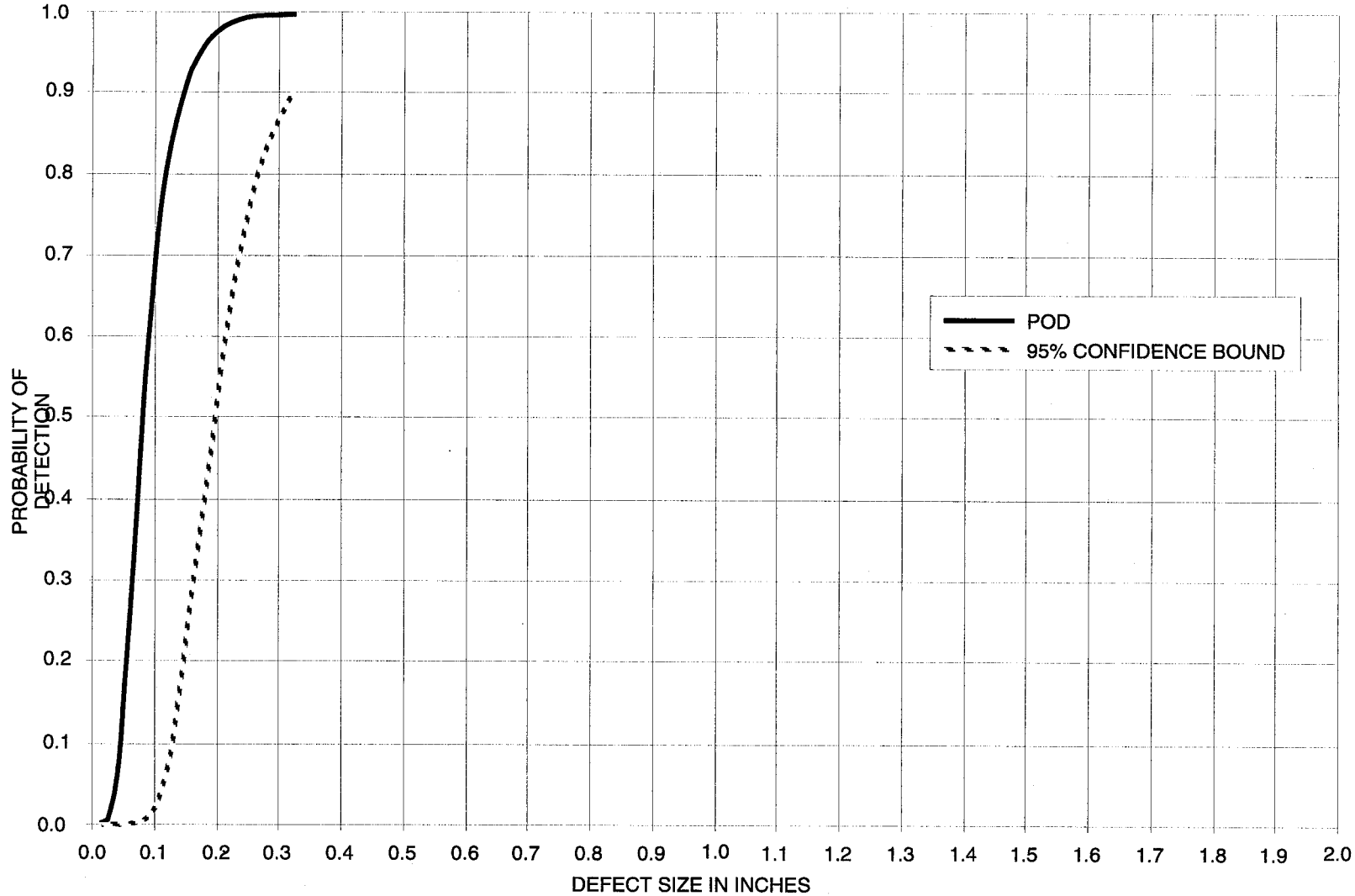

Figure 5-6. Probability of Detection of Circular Debonds in 0.5-Inch-Thick SOFI (Subarea)

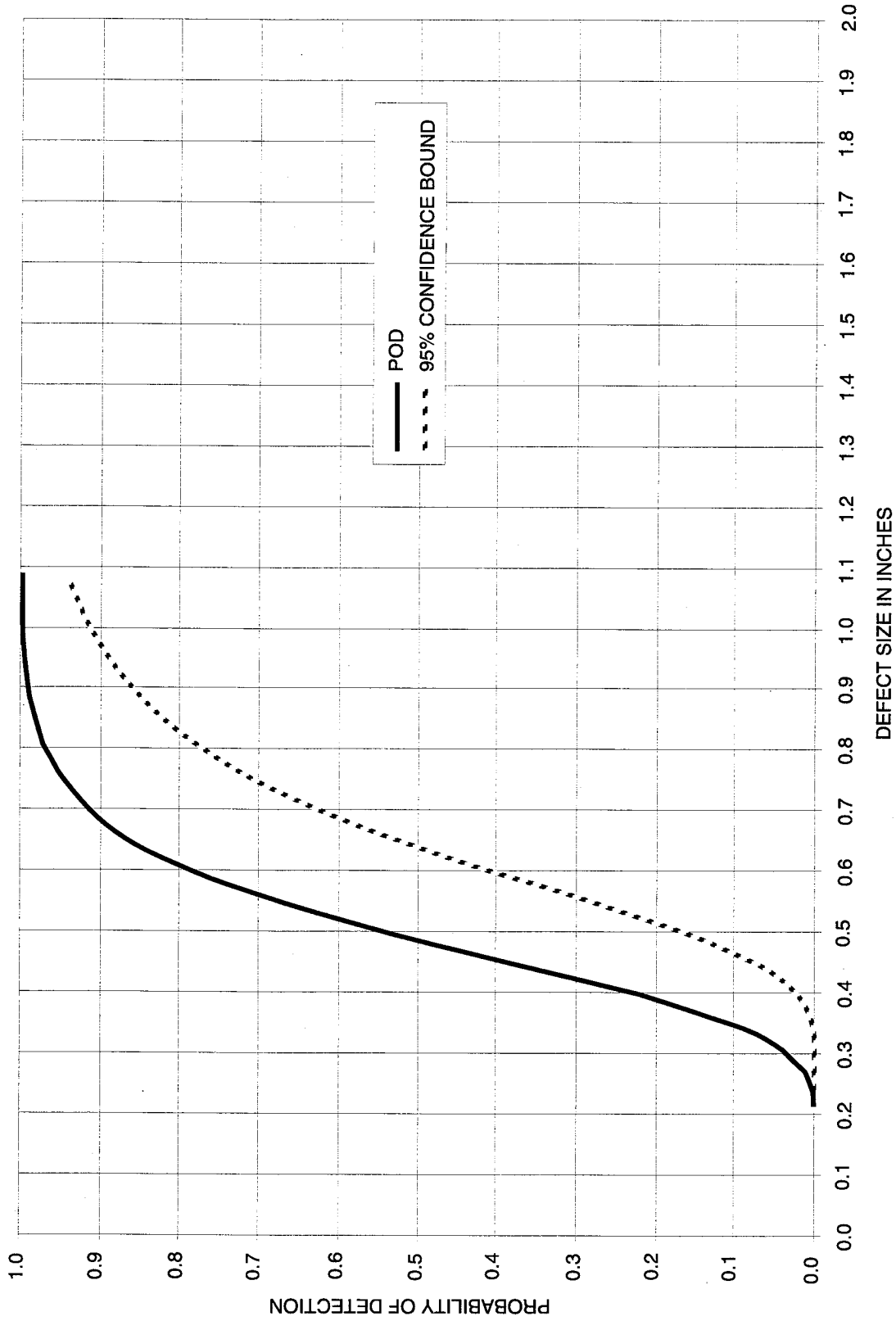

Figure 5-7. Probability of Detection of Circular Debonds in 0.75-Inch-Thick SOFI (Subarea)

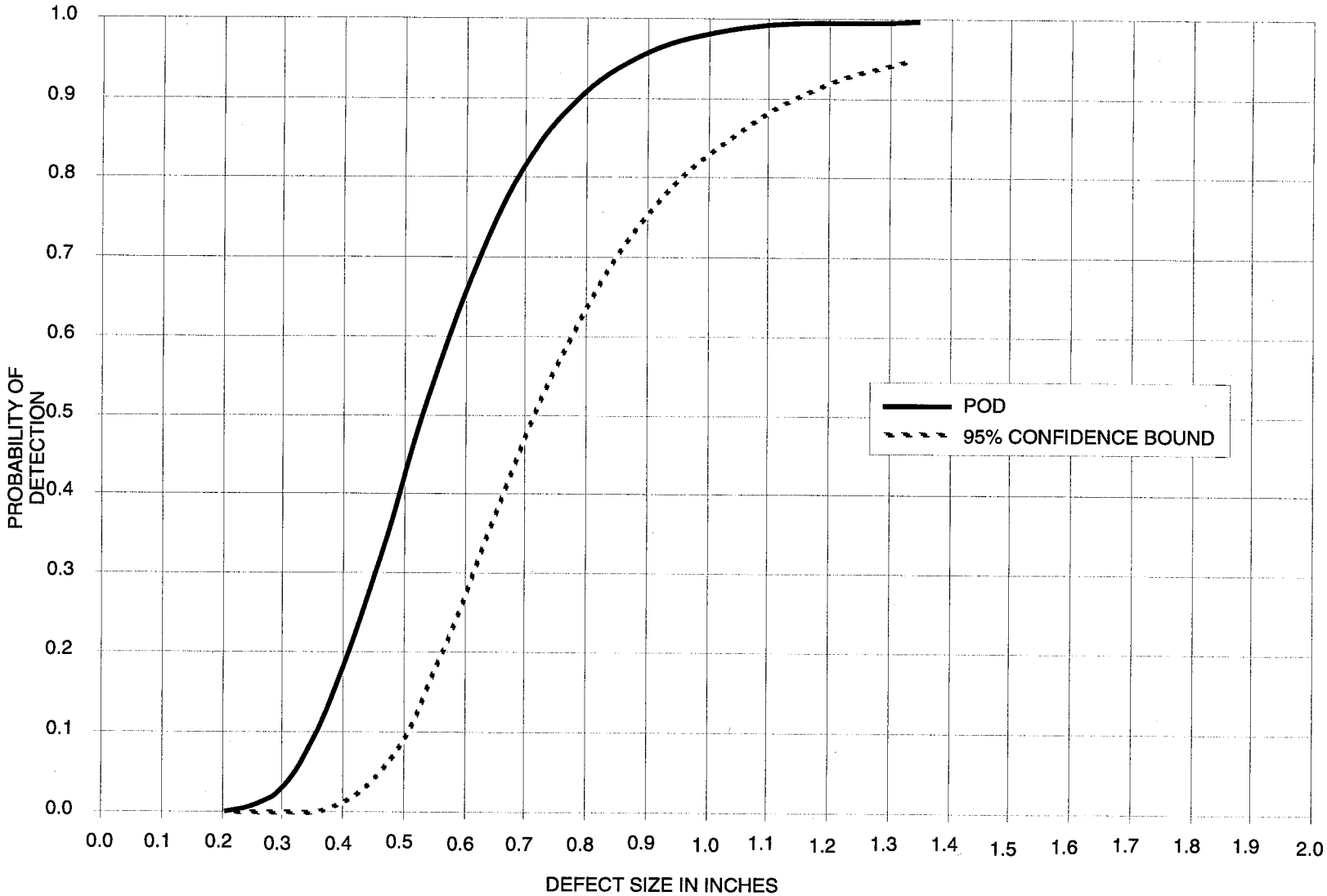

Figure 5-8. Probability of Detection of Circular Debonds in 1.0-Inch-Thick SOFI (Subarea)

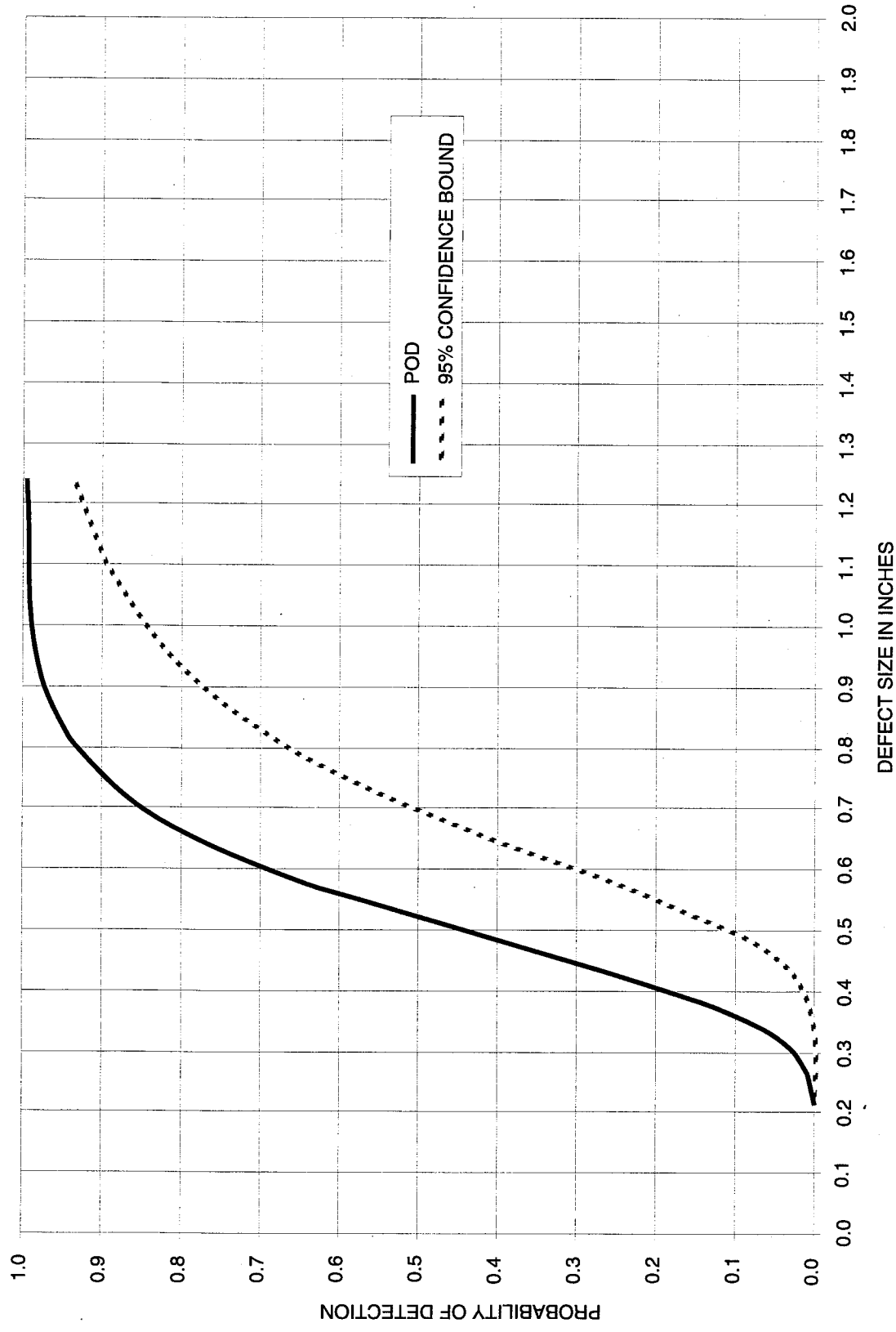

Figure 5-9. Probability of Detection of Circular Debonds in 1.25-Inch-Thick SOFI (Subarea)

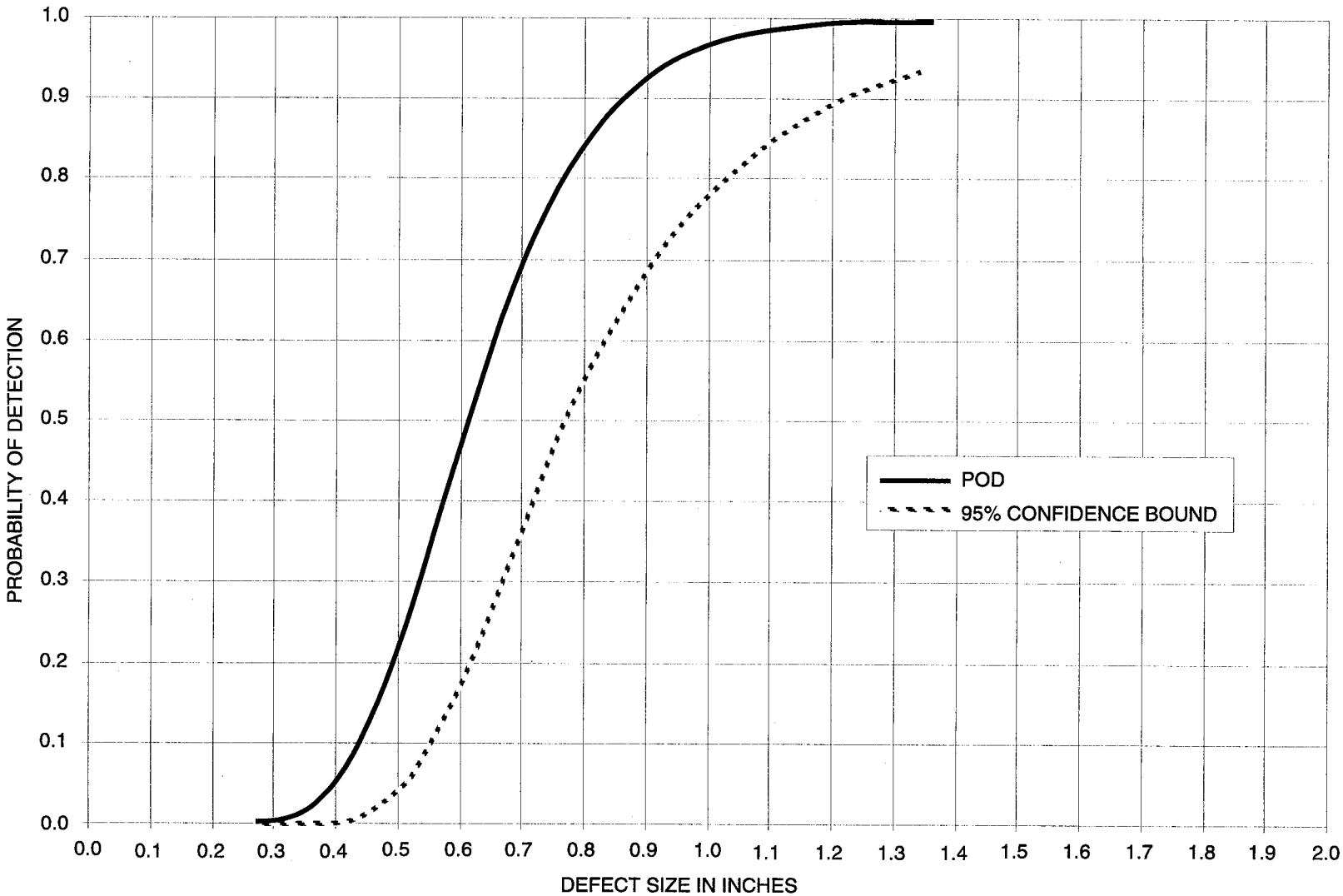

Figure 5-10. Probability of Detection of Circular Debonds in 1.5-Inch-Thick SOFI (Subarea)

5.3 PODS FOR SQUARE DEBONDS

Figures 5-11 through 5-15 show full panel views of the square debonds: as stated earlier the square debonds were more easily detected. In comparison with the circular debonds at the full panel views, square debonds with the same size as the SOFI thickness all showed PODs of 0.95 or greater.

Figures 5-16 through 5-20 show the PODs of the square debonds when the field of view was reduced for subarea inspections. The detectability of the debonds again improves with the smaller field of view because of the higher effective resolution.

5.4 PODS FOR SEAM DEBONDS

A POD analysis was conducted on the data from the two seam debonds presented in section III. The results are shown in figures 5-21 through 5-24. As was expected, the POD of these asymmetric debonds exhibit a strong dependency on the shear vector orientation. This is an important point because it is suspected that this type debond constitutes a large percentage of debonds that may be present in SOFI on the Orbiter external tank. Figures 5-21 and 5-22 show the 10-inch-by-75-inch seam and the dependence of the POD on shear vector. Figures 5-23 and 5-24 show the 3-inch-by-0.75 inch seam. As can be seen from these figures, the length of the seam debond also plays a large role in its ability to be detected. The POD for the shorter debond is higher than that of the longer debond in both the full panel and subarea views. When the shear vector is parallel to the seam debond, the shearographic indications at the ends of the debond are more easily visually correlated for shorter seam debonds. In fact, for longer debonds with parallel shear vectors, the shearographic indication may be interpreted as two separate debonds. Applying a similar width/SOFI criteria to the seam debonds, it is seen when the SOFI is 0.75 inch thick and the shearing angle is perpendicular to the long axis of the seam all PODs were essentially 1.

5.5 PROBABILITY OF FALSE DETECTION

The probability of false detection is equally important as the probability of true detection. Scraping, reinspecting or reconfiguring a piece of flight hardware due to a false detection of a nonexistent flaw can be extremely time consuming and expensive. If a particular NDT tool produces a significant amount of false detections, it may be considered noneffective and useless.

No defects were detected in any of the three test panels, at any of the thicknesses, that were not programmed debonds. However, the shearographic indications of

some of the smaller debonds in the thicker SOFI thicknesses were vague and difficult to interpret (detection values of 1 and 2).

If the detection grading criteria established in this report is adhered to, considering defects with a detection value of 4 or greater as a true detection, should result in a extremely low false detection rate. (**Note:** This statement is made, for the time being, with no quantifiable evidence. It is based solely on experience and hundreds of hours of shearographic testing on SOFI.) Detection value 4 is the point where a debond produces a shearographic indication consisting of a uniformly bright doublet with no secondary fringes.

Considering, as an example, page B-34, it is seen that defect 16, a 1-inch circular debond receives a detection value of 5 in the full panel view for all shear vectors and vacuum drops at a SOFI thickness of 1 inch. NASA Operations is primarily concerned about detecting debonds of 2 inches in diameter or greater in the 1-inch nominal thickness of SOFI. Therefore, using a detection value of 4 or greater as the detection threshold to reduce the probability of false detects does not reduce the usefulness of laser shearography for locating debonds in SOFI.

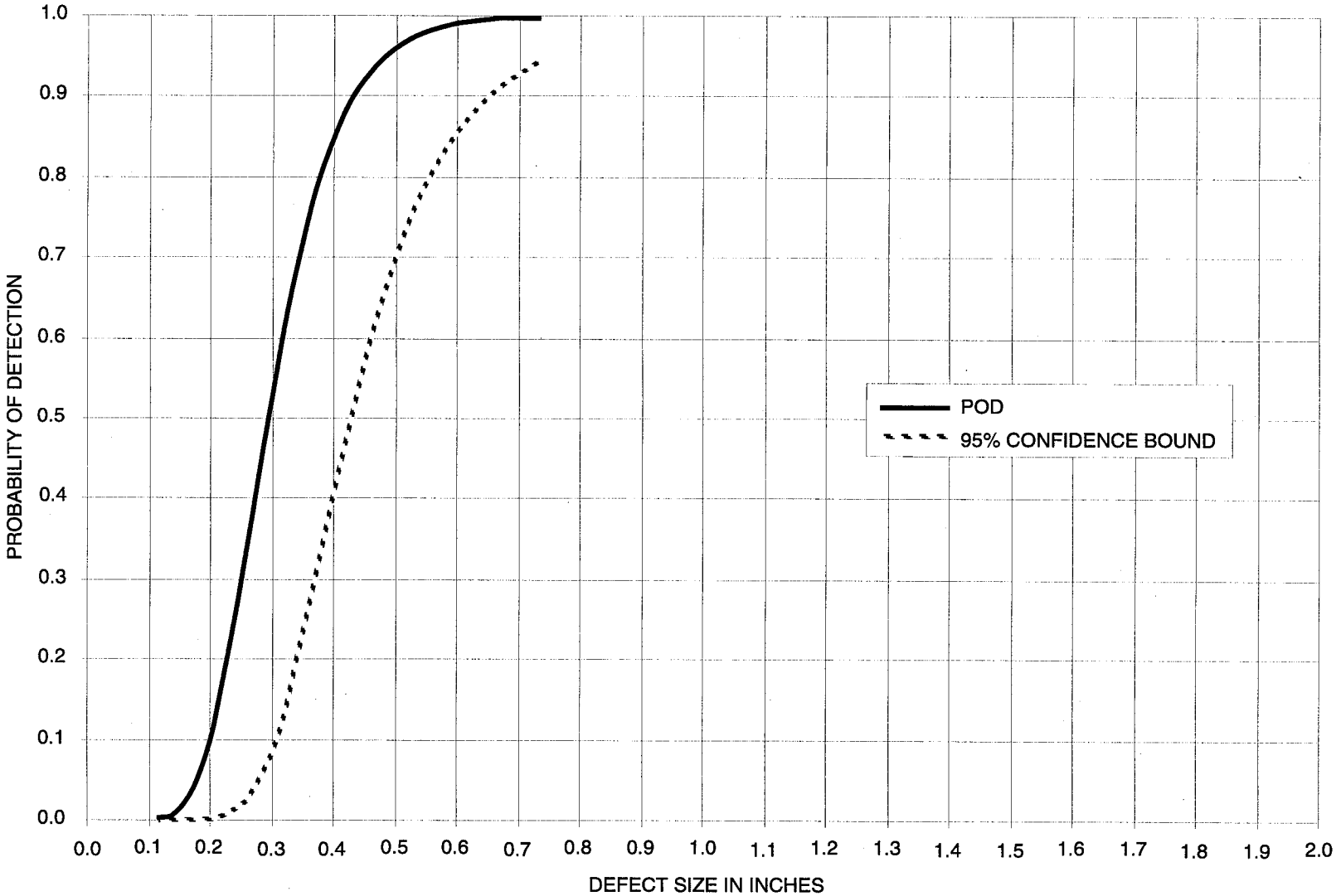

Figure 5-11. Probability of Detection of Square Debonds in 0.5-Inch-Thick SOFI (Full Panel View)

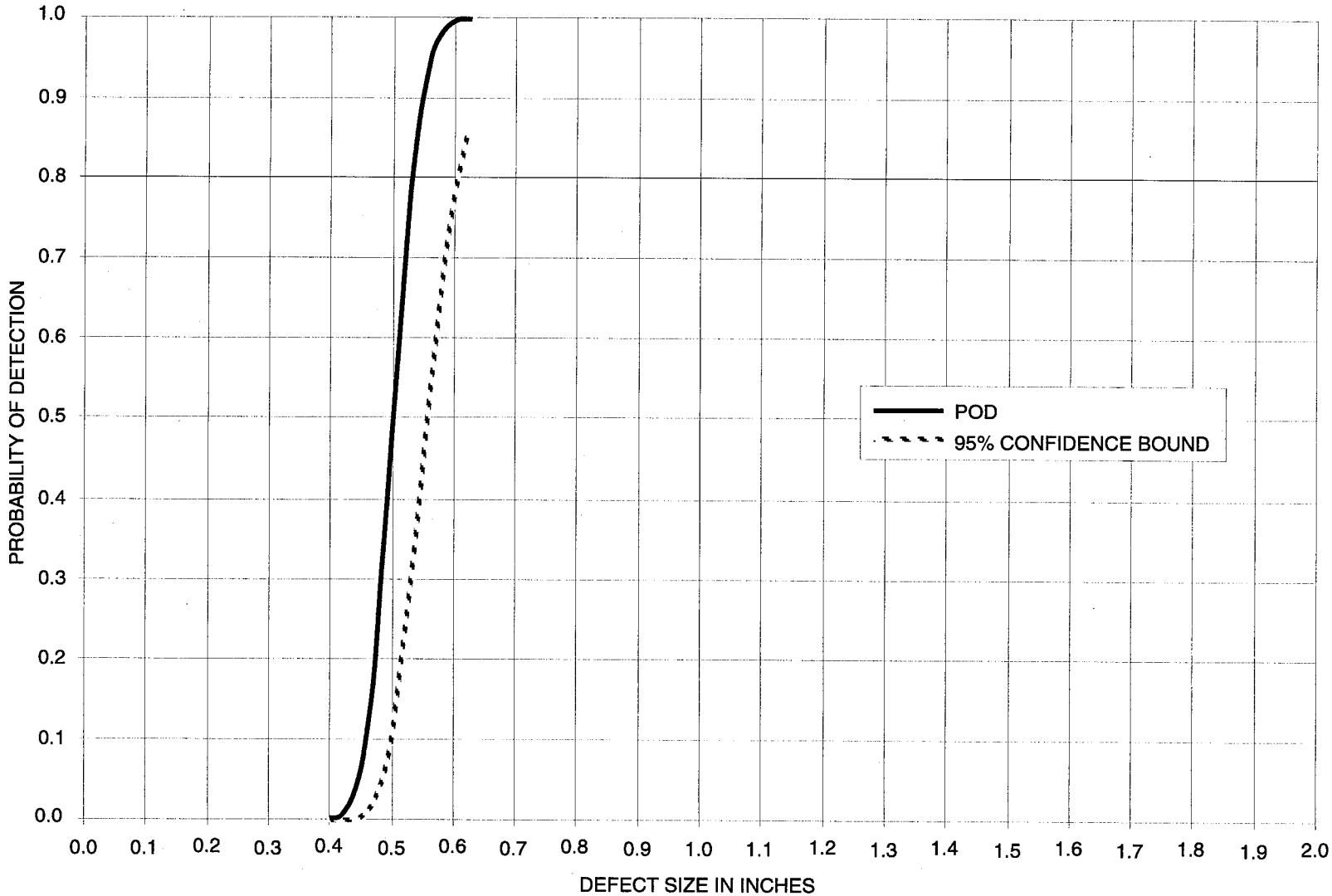

Figure 5-12. Probability of Detection of Square Debonds in 0.75-Inch-Thick SOFI (Full Panel View)

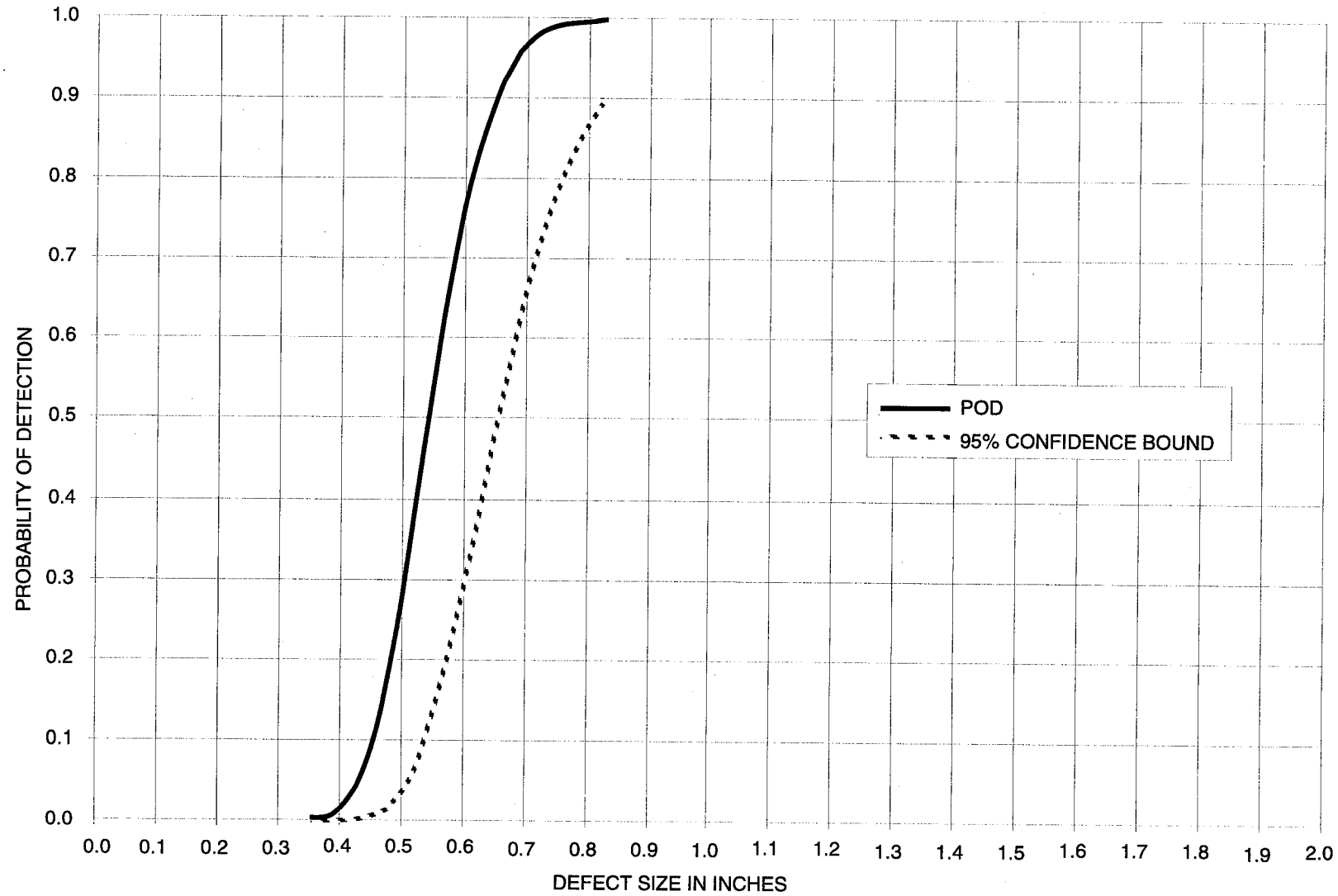

Figure 5-13. Probability of Detection of Square Debonds in 1.0-Inch-Thick SOFI (Full Panel View)

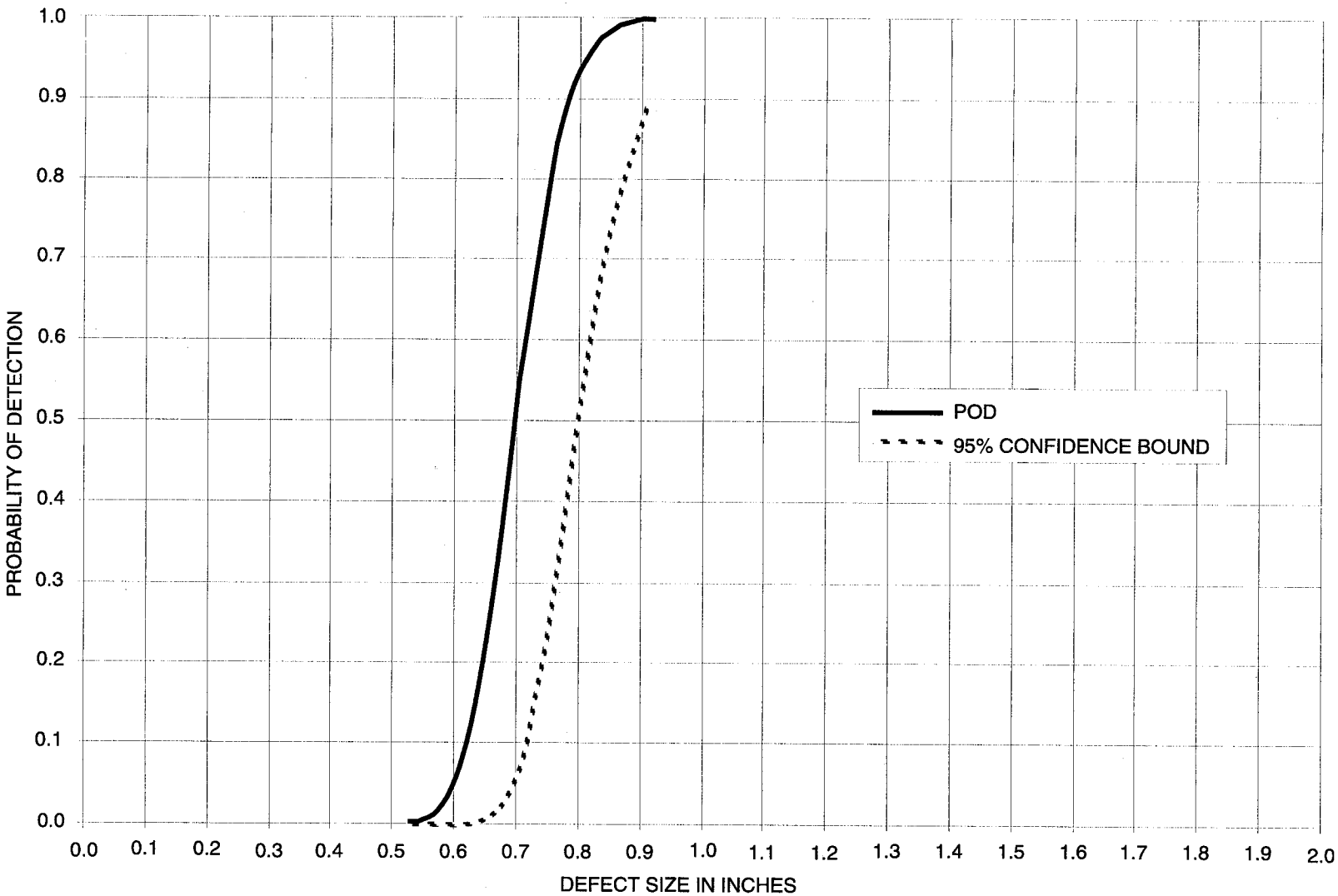

Figure 5-14. Probability of Detection of Square Debonds in 1.25-Inch-Thick SOFI (Full Panel View)

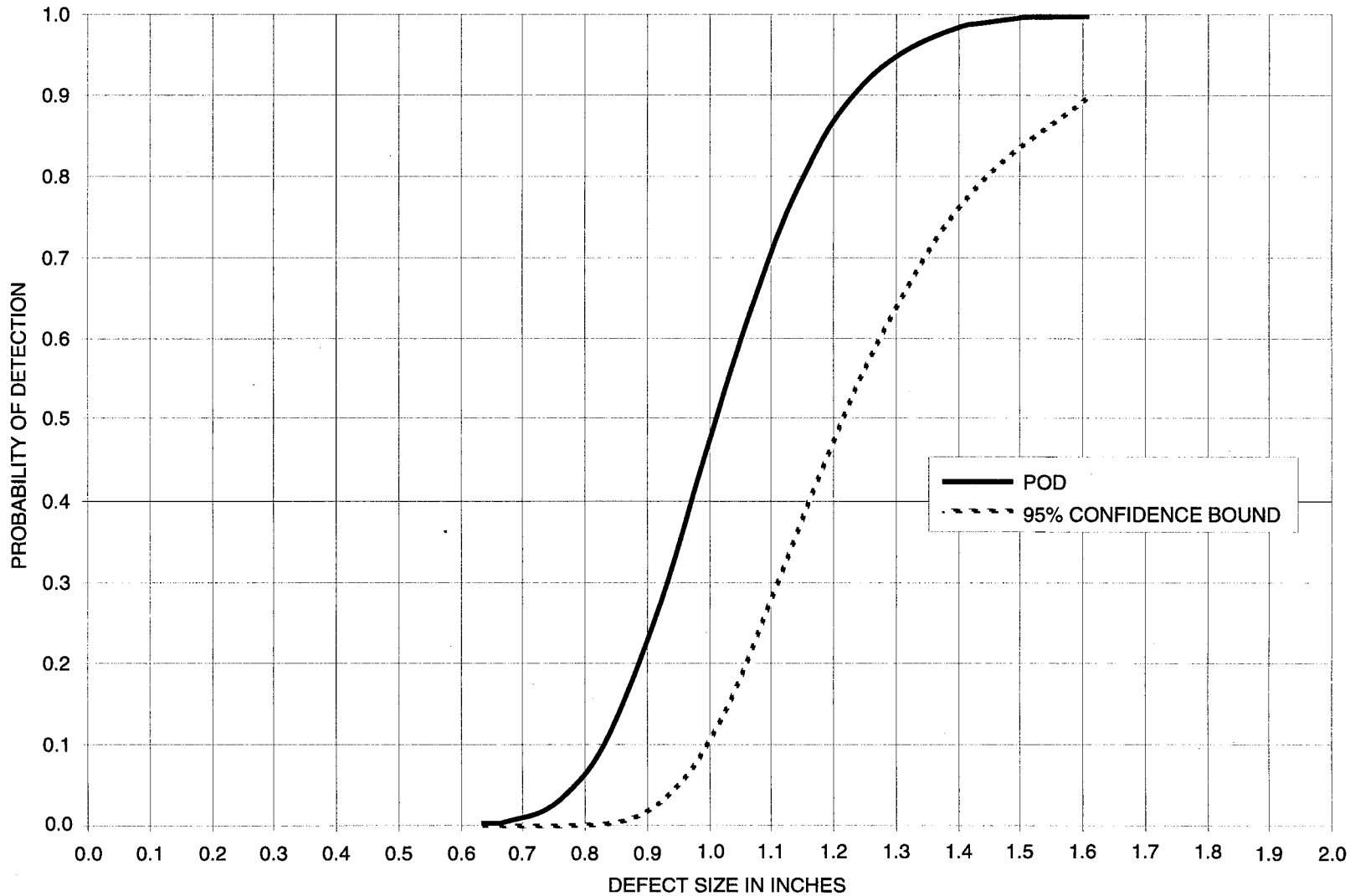

Figure 5-15. Probability of Detection of Square Debonds in 1.5-Inch-Thick SOFI (Full Panel View)

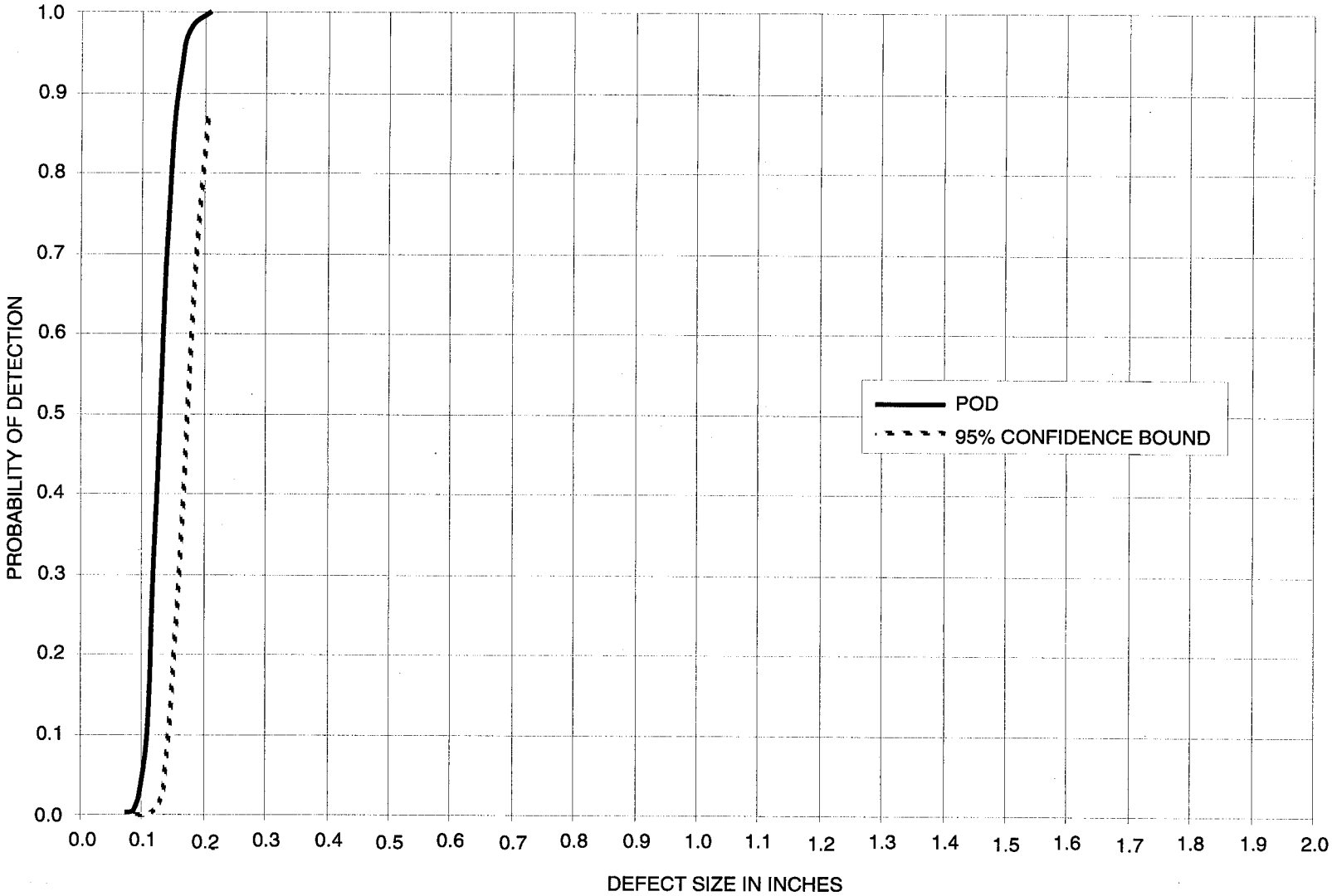

Figure 5-16. Probability of Detection of Square Debonds in 0.5-Inch-Thick SOFI (Subarea)

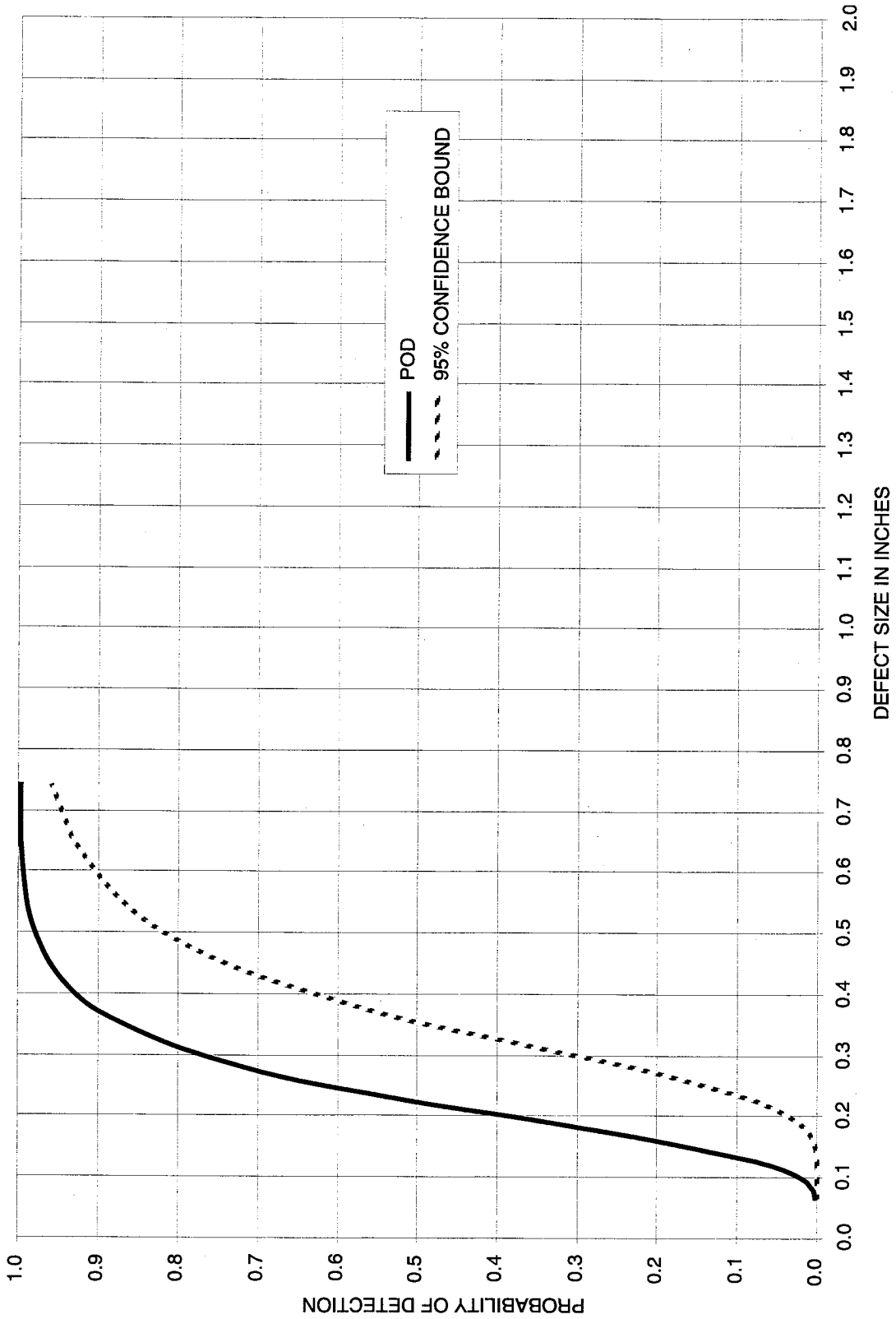

Figure 5-17. Probability of Detection of Square Debonds in 0.75-Inch-Thick SOFI (Subareas)

Figure 5-18. Probability of Detection of Square Debonds in 1.0-Inch-Thick SOFI (Subareas)

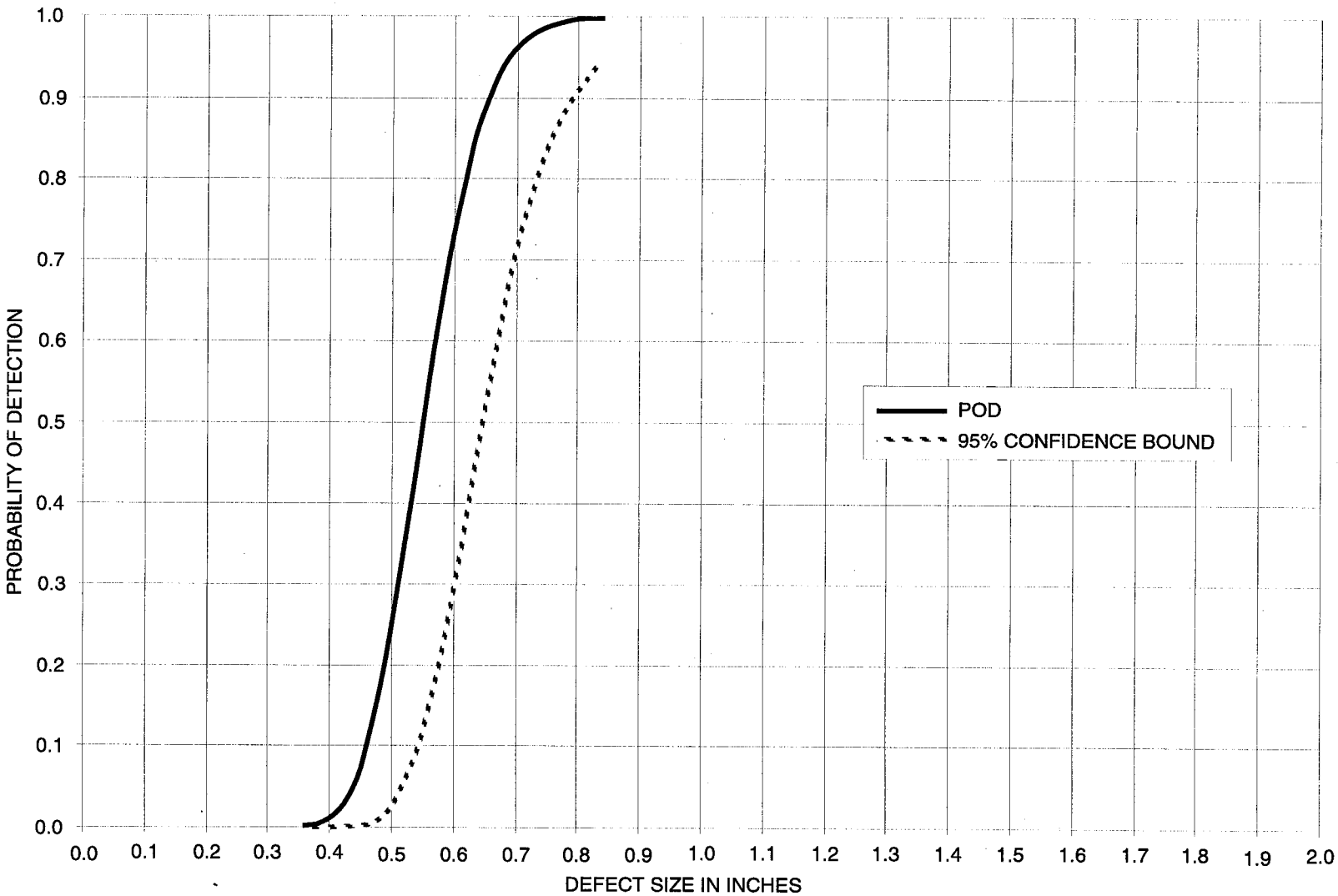

Figure 5-19. Probability of Detection of Square Debonds in 1.25-Inch-Thick SOFI (Subareas)

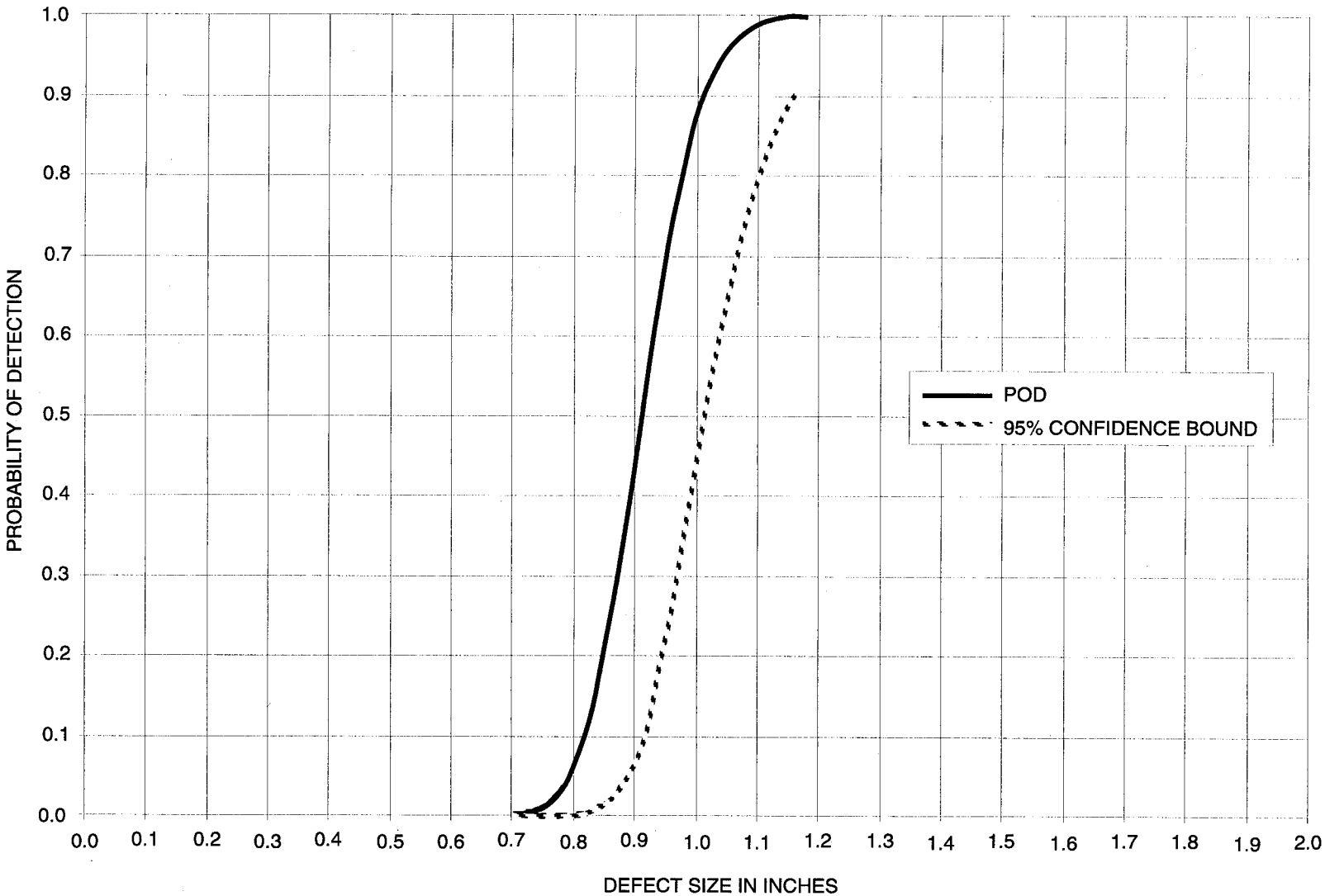

Figure 5-20. Probability of Detection of Square Debonds in 1.5-Inch-Thick SOFI (Subareas)

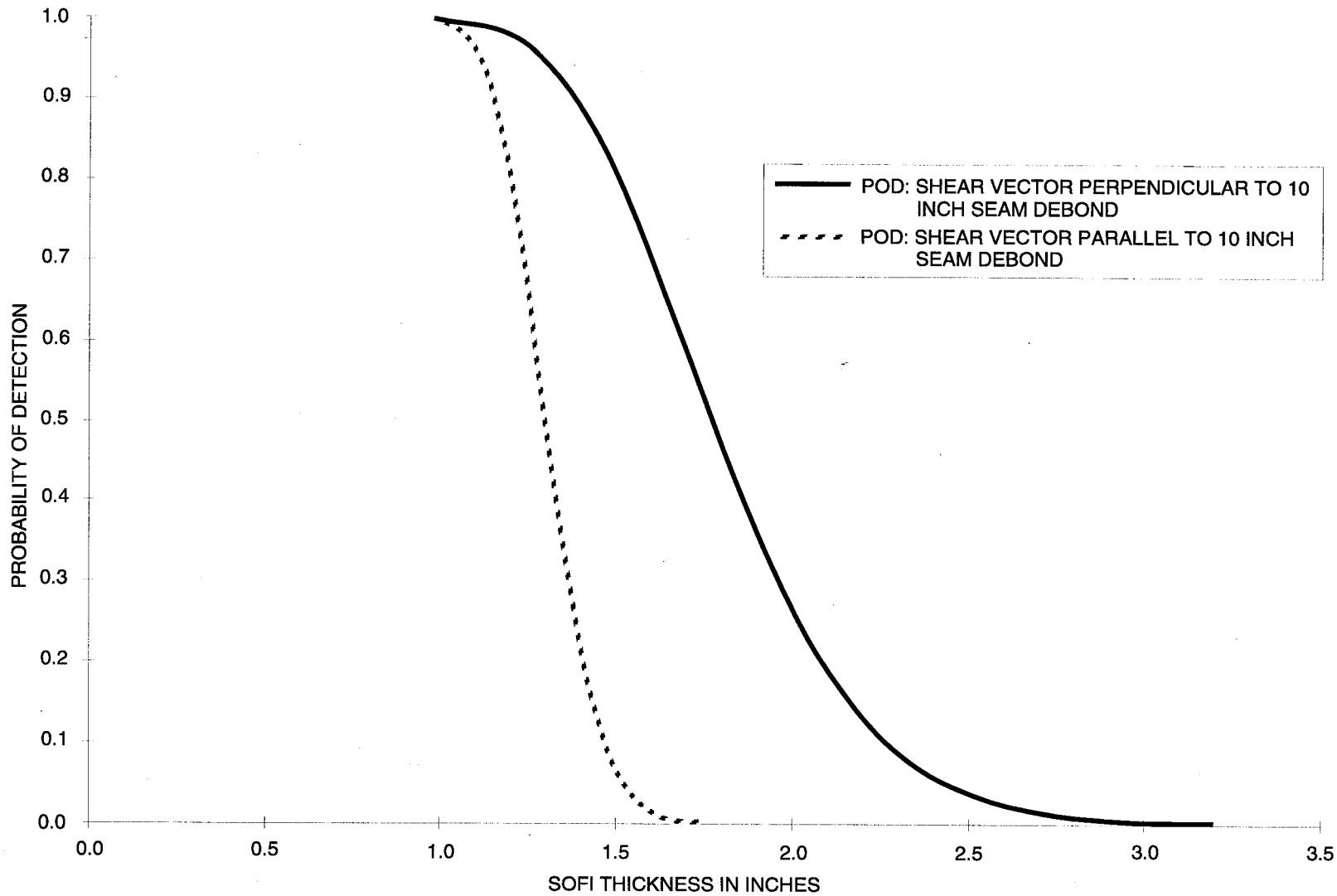

Figure 5-21. Probability of Detection of 10-Inch Seam Debond as Function of Shear Vector and SOFI Thickness (Full Panel View)

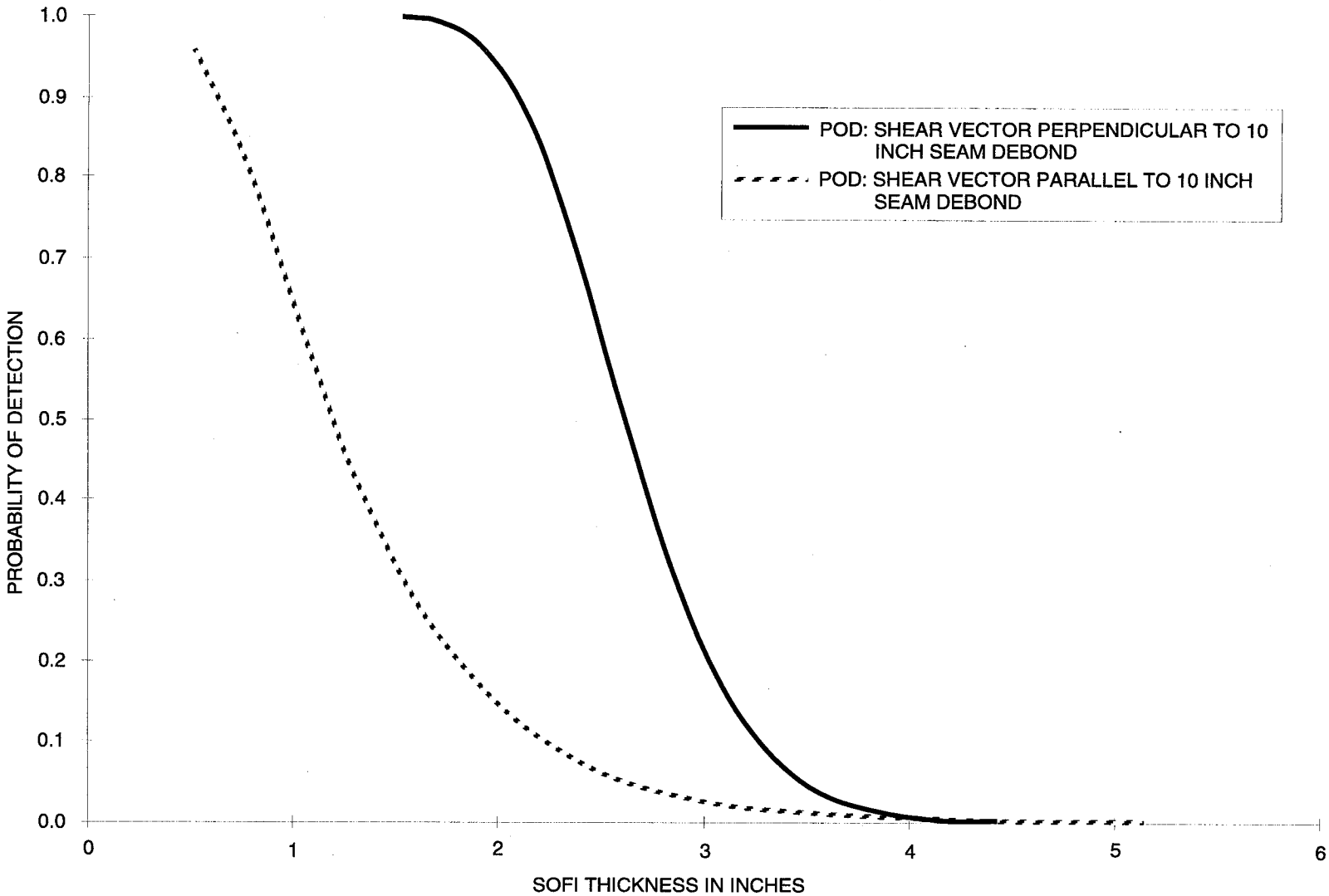

Figure 5-22. Probability of Detection of 10-Inch Seam Debond as Function of Shear Vector and SOFI Thickness (Subarea)

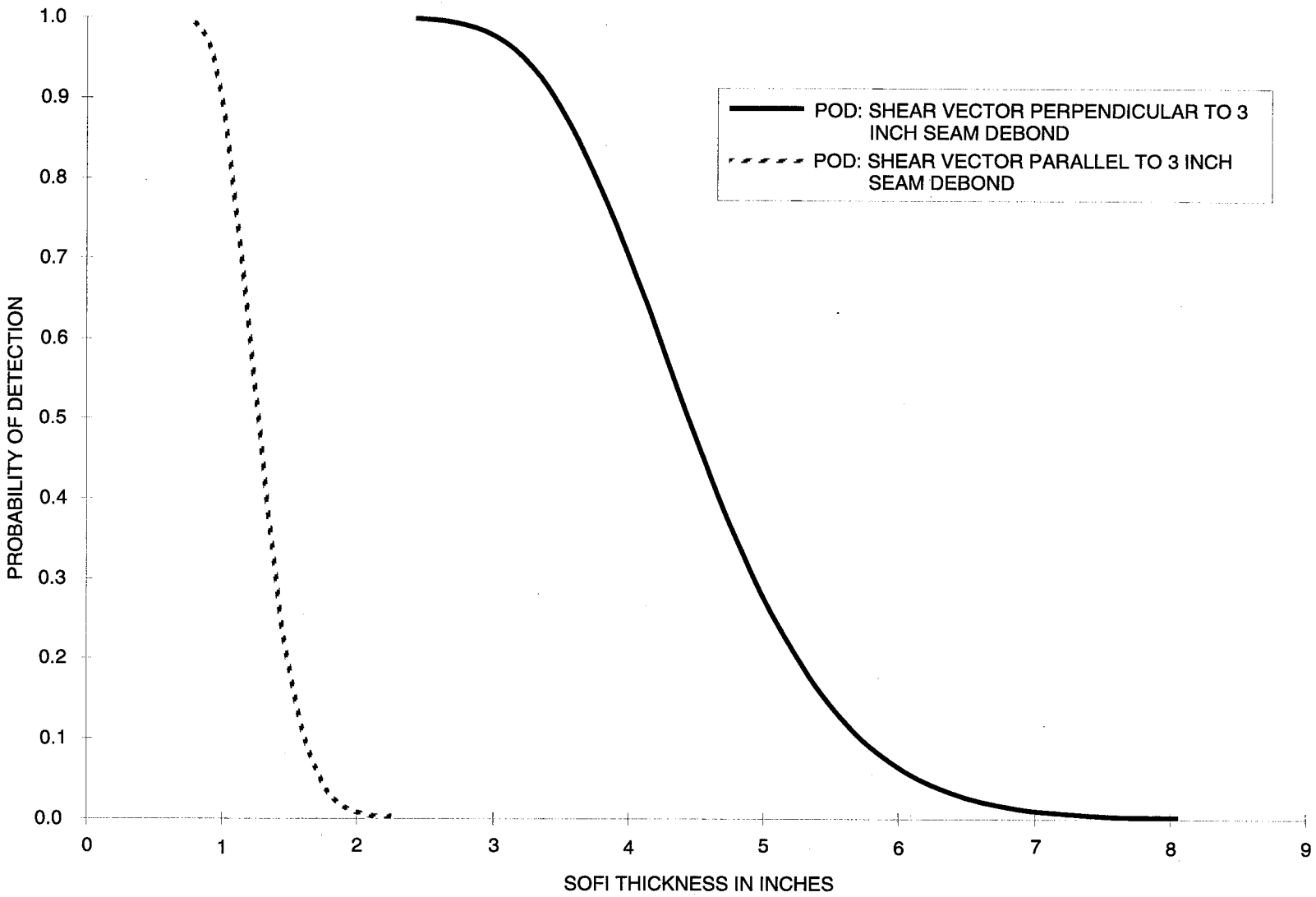

Figure 5-23. Probability of Detection of 3-Inch Seam Debond as Function of Shear Vector and SOFI Thickness (Full Panel View)

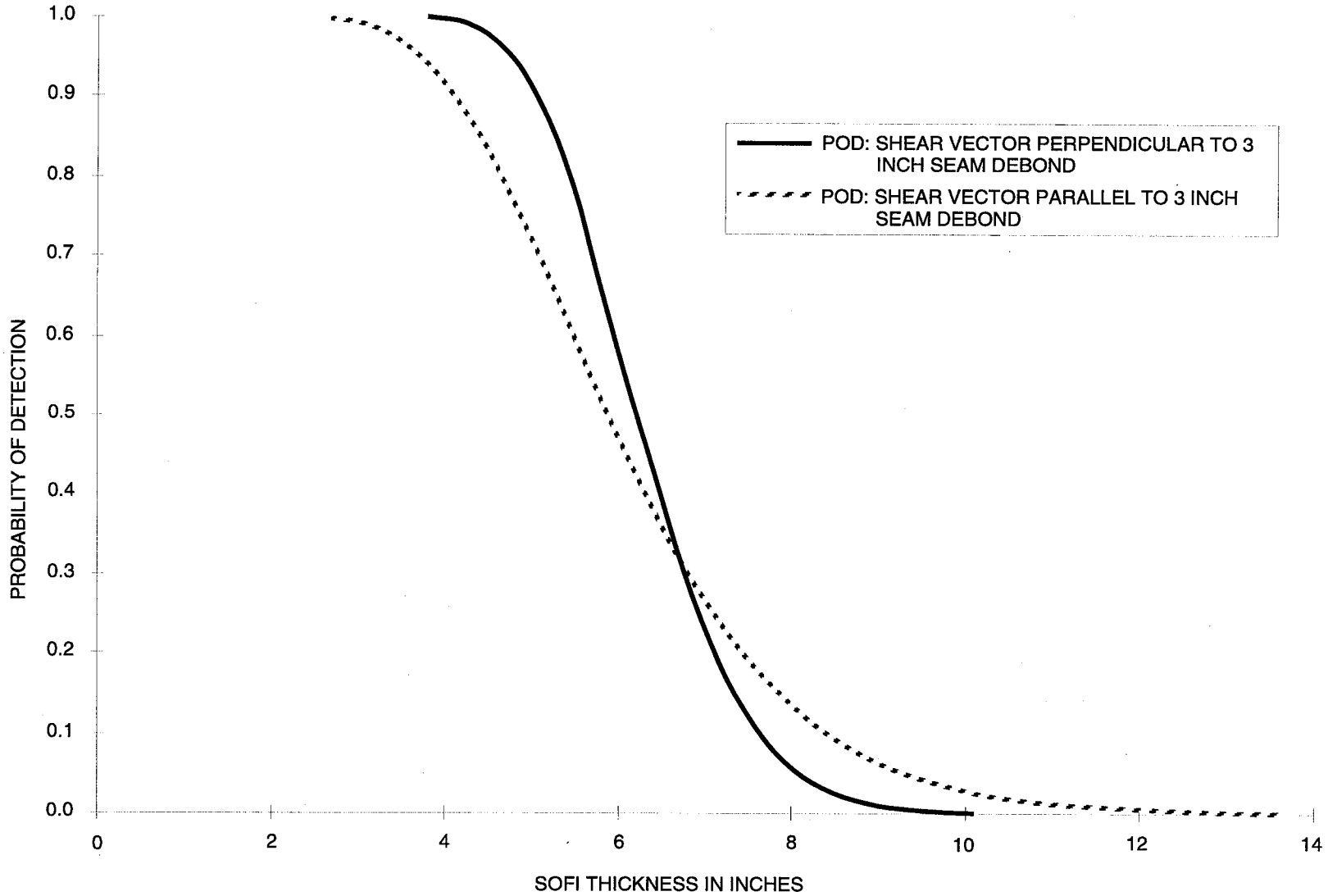

Figure 5-24. Probability of Detection of 3-Inch Seam Debond as Function of Shear Vector and SOFI Thickness (Subarea)

SECTION VI

CONCLUSIONS

From the data presented in this report, laser shearography is shown to be a very powerful tool for the detection of debonds in SOFI foam. The vacuum levels needed for surface excitement are very low and cause no damage to the surface of the SOFI or apply any significant level of force to the bond between the SOFI and the substrate.

Because SOFI is a relatively soft, closed cell material when a vacuum is applied to it, the entire surface under inspection deforms. Therefore, there is a race between the deformation of the surface due to a debond and that due to the individual expansions of the cells. At low pressure drops, the surface deflection caused by the expansion of the larger volume of air present at a debond wins out. However, as the vacuum increases, the deformations caused by the closed cells grow to a point where the image decorrelates and the defect can no longer be distinuguished. Because of this phenomenon, large pressure drops are not efficacious and need not be used.

A small integrated vacuum hood, containing a shearographic camera and laser source, can be manufactured to facilitate shearographic inspection in tight and difficult to reach areas.

Because of the insensitivity to ambient vibration, this technique can be used in the field. While testing in the VAB, vibrations in the floor could be felt. This occurred during movement of the large doors and the crawler-transporter. This may have introduced some variability in the data, but it did not prevent the use of the instrument.

The sensitivity of laser shearography to debonds in SOFI has been shown to be more than adequate. NASA Operations is primarily concerned about detecting debonds of 2 inches in diameter or greater in the 1-inch nominal thickness of SOFI. In the test performed for this report, a defect of 1.5 inches in diameter/side was always detected even in 1.5 inches of SOFI with a 2-foot square field of view. Therefore, large defect inspections using large fields of view may be conducted. If smaller defects become a concern, the field of view may be decreased.

It must be emphasized, however, that all inspections should be conducted with multiple shear vector orientations for results that can be considered reliable. Shear vectors of 0, 45, and 90 degrees from a vertical orientation seem sufficient to detect most asymmetric debonds. A shearographic system with a remotely controlled

shear vector orientation should be considered to facilitate field inspections with multiple shear vector orientations.

Inspection of the programmed test panels with vacuum offset to simulate the use of an integrated vaccum hood (i.e., a hood with camera and laser source incorporated into the hood) produced results virtually identical to those obtained with no vacuum offset. This implies that results of actual field inspections of the ET SOFI utilizing an integrated vacuum hood should be similar to the results presented in this report. Therefore, this data should represent a reasonable baseline for field inspections of ET SOFI using shearography with vacuum stressing.

APPENDIX A

UNAVERAGED DATA TAKEN DURING SHEAROGRAPHY TESTS

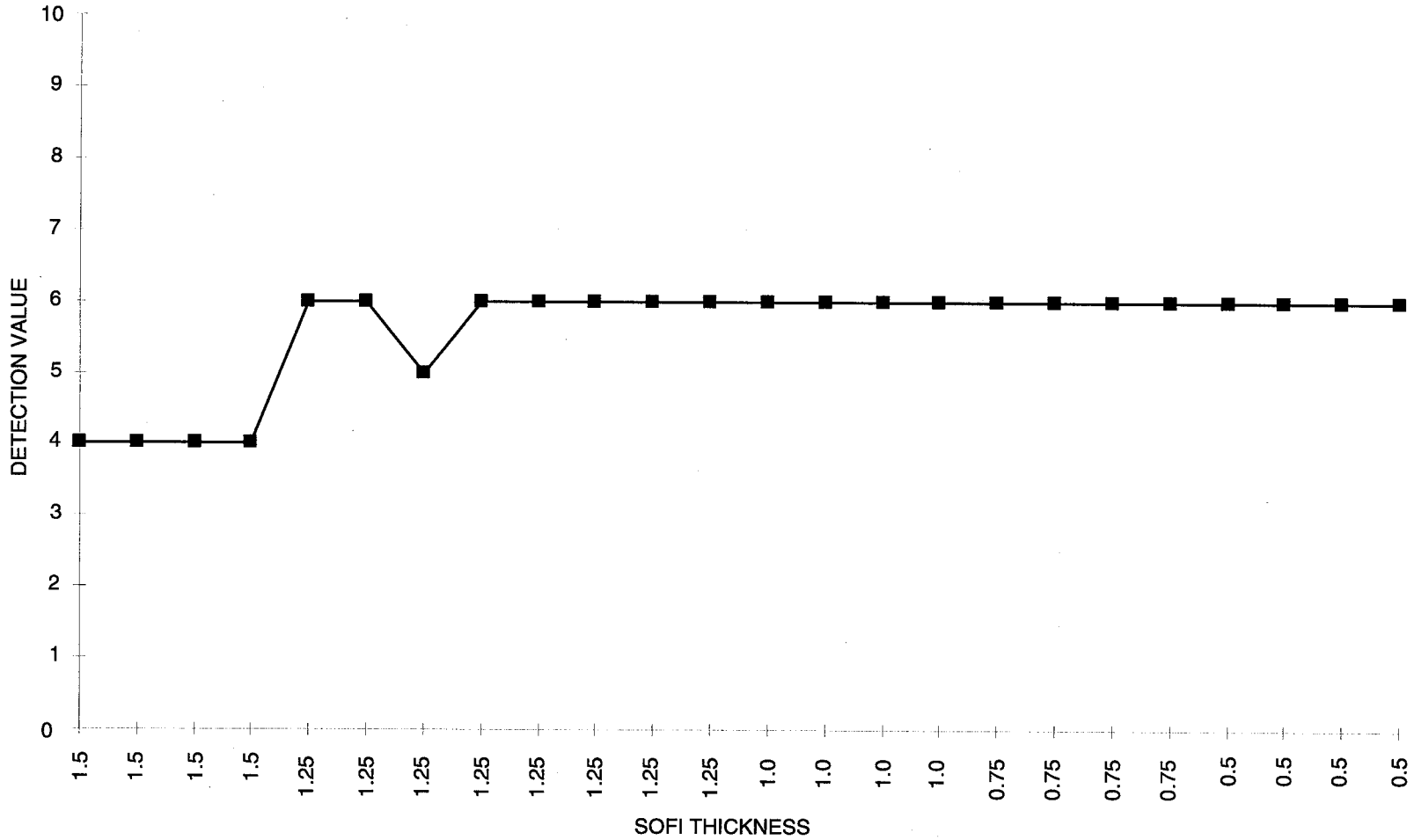

Detection Values of 1-Inch Circular Debond vs. SOFI Thickness

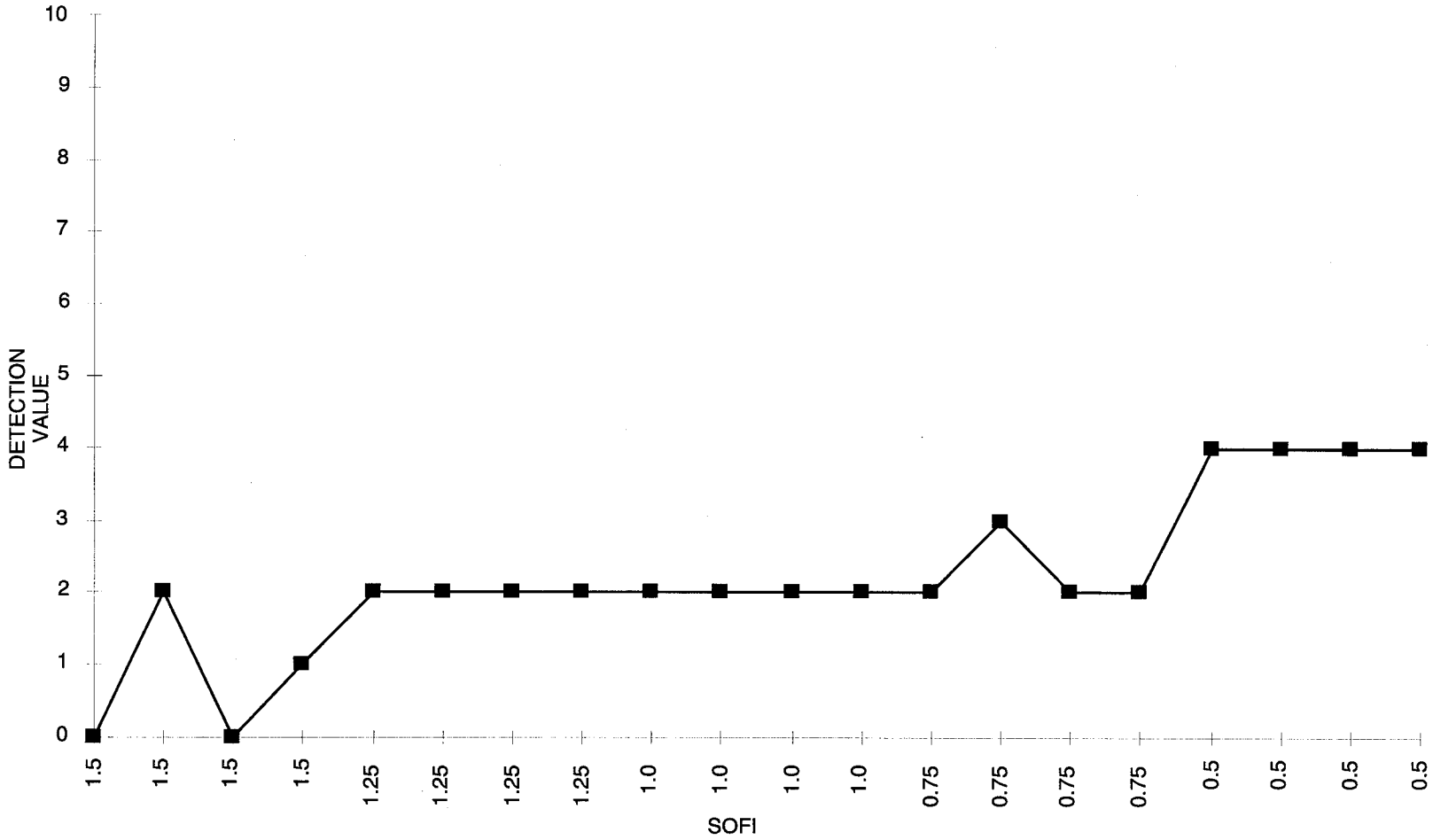

Detection Values of 0.5-Inch Circular Debond vs. SOFI Thickness

Detection Values of 0.75-Inch Circular Debond vs. SOFI Thickness

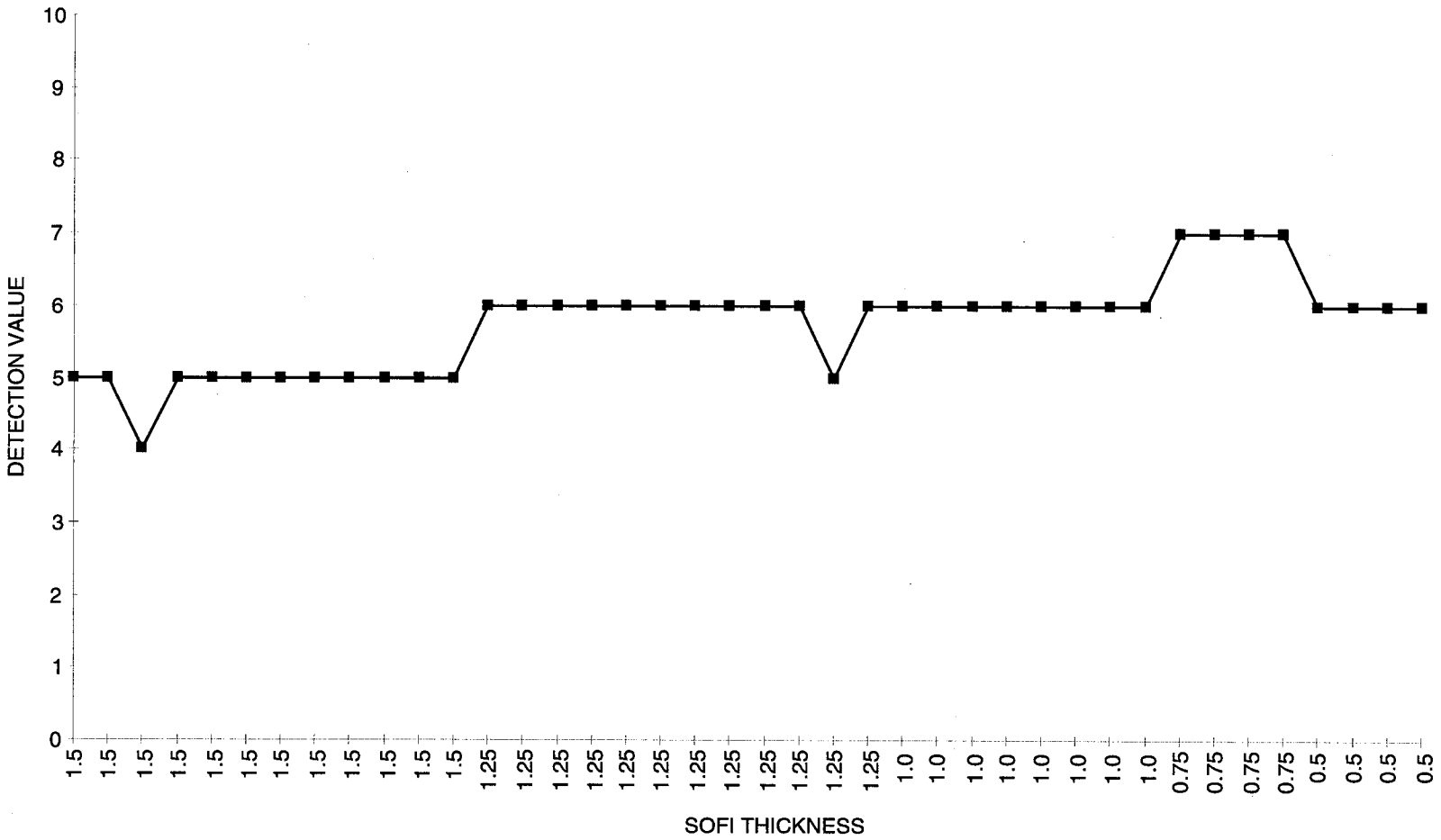

Detection Values of 1.5-Inch Circular Debond vs. SOFI Thickness

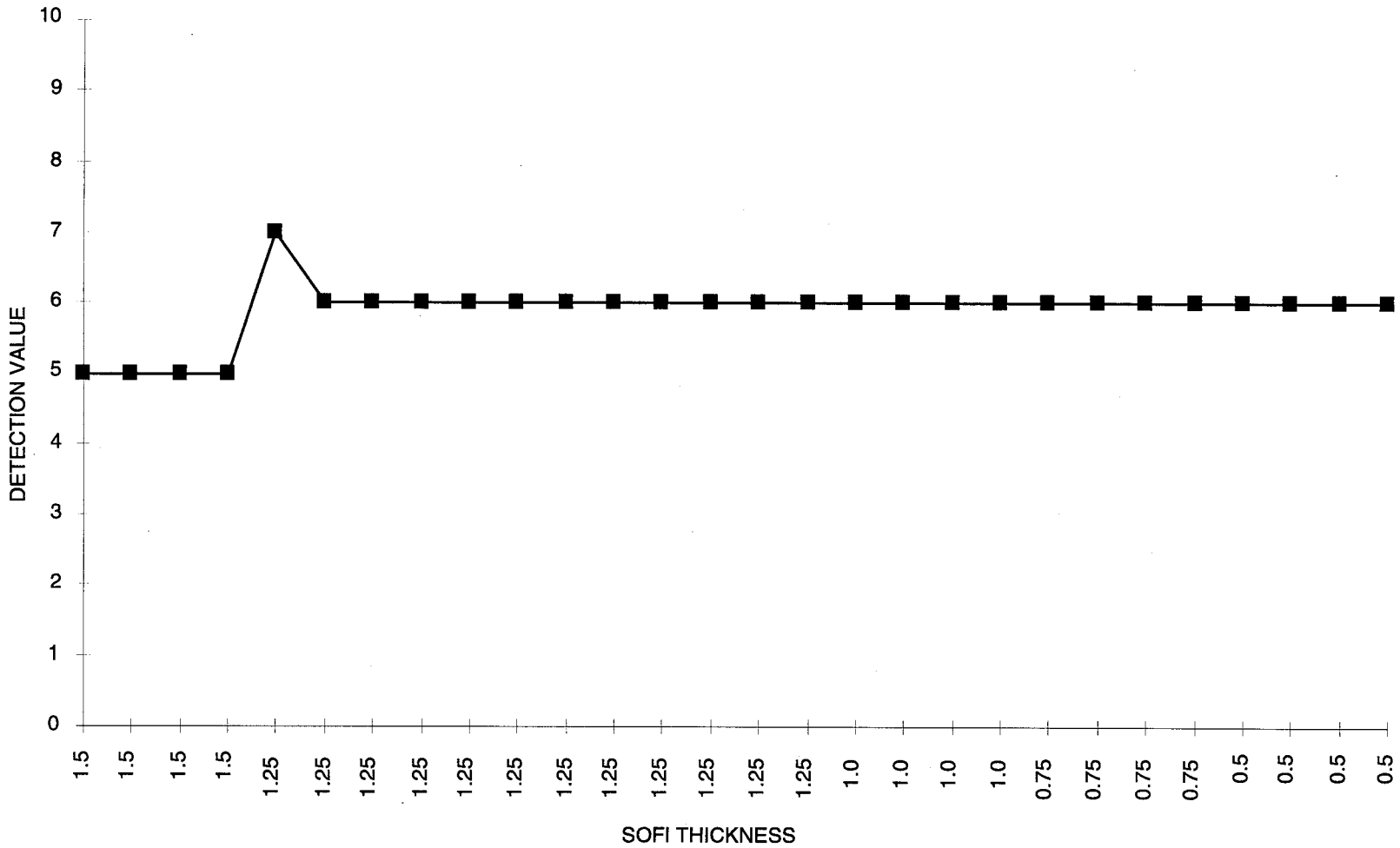

Detection Values of 2-Inch Circular Debond vs. SOFI Thickness

Detection Values of 0.5-Inch Square Debond vs. SOFI Thickness

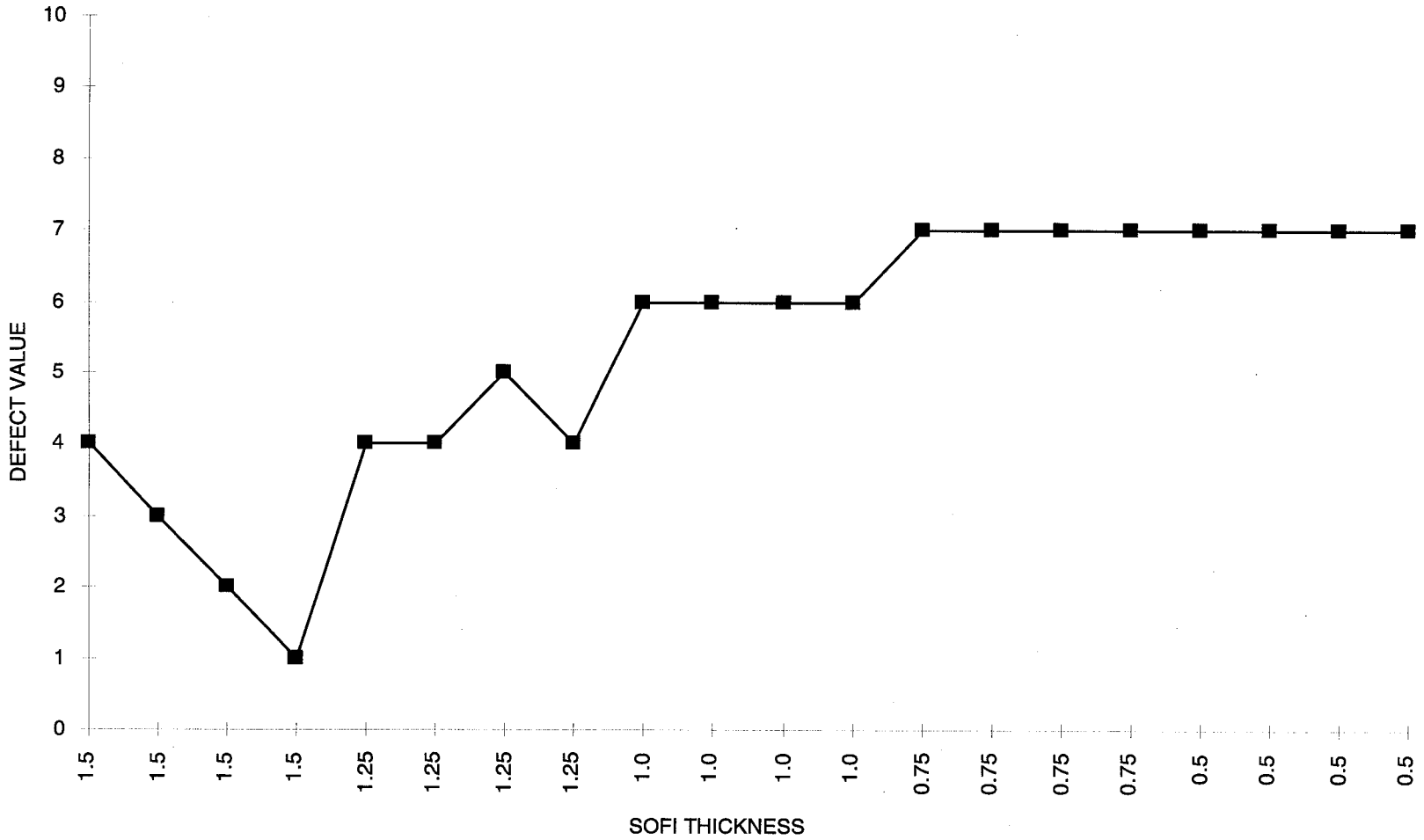

Detection Values of 1-Inch Square Debond vs. SOFI Thickness

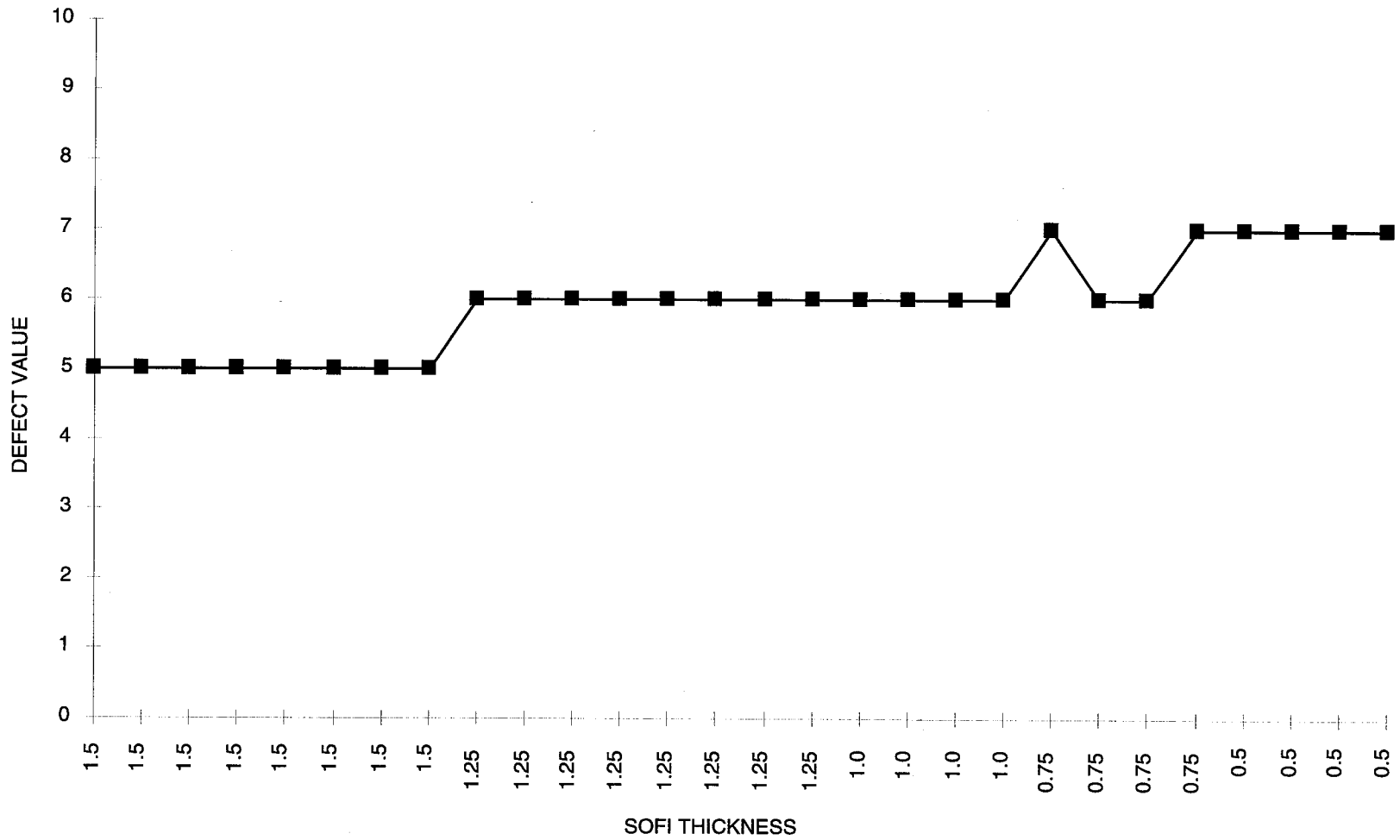

Detection Values of 1.5-Inch Square Debond vs. SOFI Thickness

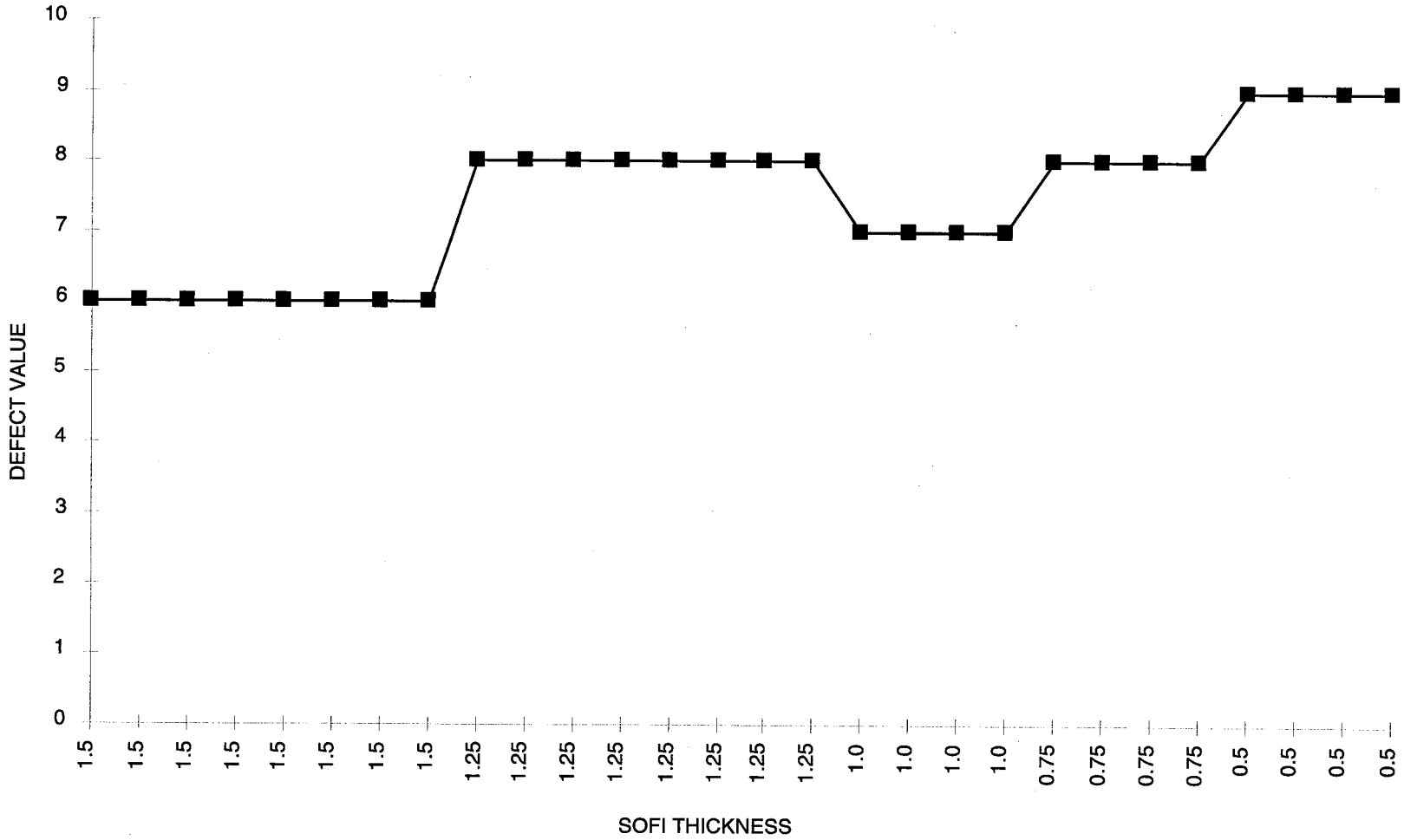

Detection Values of 2-Inch Square Debond vs. SOFI Thickness

APPENDIX B

DEFECT LEGEND AND RAW DATA

DEBOND LEGEND

NOTE: SEE B-3 FOR PHOTOS OF TEST PANEL PRIOR TO SOFI APPLICATION

DEFECT	PANEL	DESCRIPTION
1	5	Triangular Debond - 1" base by 0.75" height
2	5	Anular Debond - 2.5" diameter with 0.5" hole
3	5	L Debond - 0.75" by 2.5"
4	5	Rectangular Debond - 4" by 5 "
5	5	L Debond - 1" by 3"
6	5	Triangular Debond - 2" base by 1.25" height
7	5	Rectangular Debond - 1" by 2"
8	5	Rectangular Debond - 3" by 0.75" (*Seam*)
9	5	Anular Debond - 1.25" diameter with 0.5" hole
10	5	Cross Debond - 3" by 1"
11	3	Square Debond - 1"
12	3	Circular Debond - 1.5"
13	3	Square Debond - 1.5"
14	3	Circular Debond - 0.5"
15	3	Circular Debond - 2"
16	3	Circular Debond - 1"
17	3	Square Debond - 0.5"
18	3	Circular Debond - 0.75"
19	3	Square Debond - 2"
20	4	Square Section of Bubble Wrap - 2"
21	4	Rectangular Debond - 10" by 0.75" (*Seam*)
22	4	Rectangular Debond - 10" by 0.75" (*Seam not used*)
23	4	Square Debond Pair - 0.5" with 1" Separation
24	4	Circular Debond Triple - 0.75" with 0.75" Separation
NASA	4	NASA Debond - See Figure 1-5
Wedge	4	Wedge (Resolution Target)

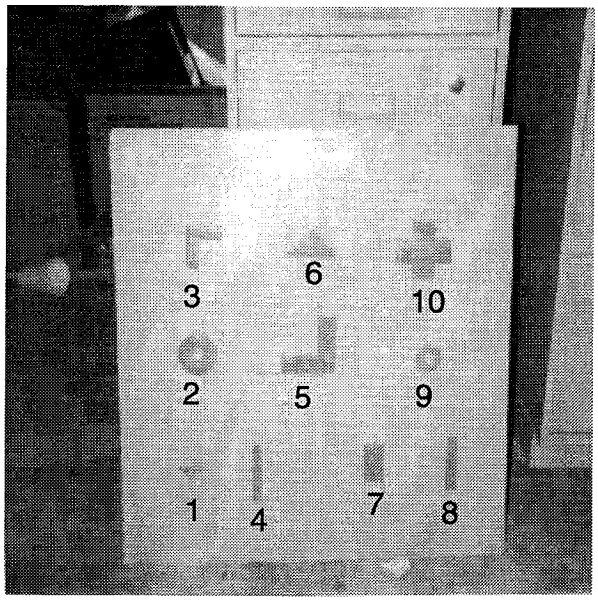

PANEL 5

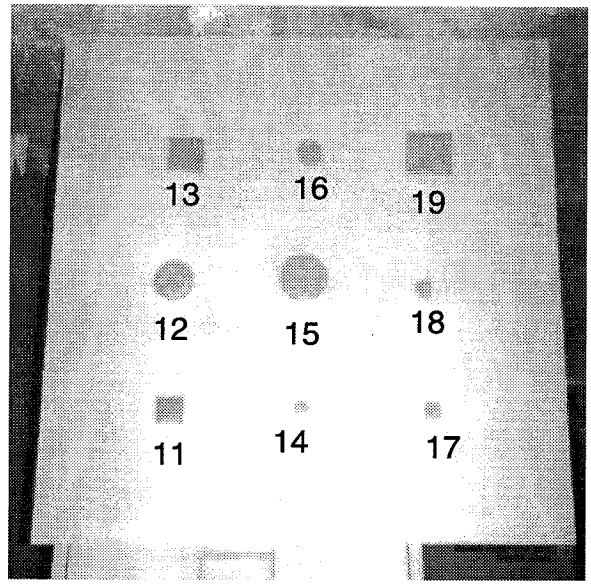

PANEL 3

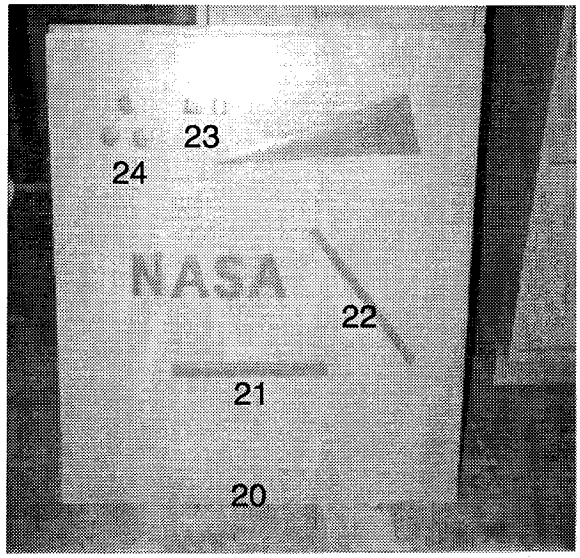

PANEL 4

Test Panels with Programmed Debonds Before SOFI Application

Defect	Thickness	Panel	Laser Power	Orientation	Vacuum	Value
1	1.5	5	500	0	1	1
1	1.5	5	500	45	1	0
1	1.5	5	500	90	1	2
1	1.5	5	500	135	1	2
1	1.25	5	500	0	1	0
1	1.25	5	500	45	1	2
1	1.25	5	500	135	1	0
1	1	5	500	0	1	0
1	1	5	500	0	5	0
1	1	5	500	0	10	0
1	1	5	500	0	15	0
1	1	5	500	45	1	0
1	1	5	500	45	5	0
1	1	5	500	45	10	0
1	1	5	500	45	15	0
1	1	5	500	90	1	0
1	1	5	500	90	5	0
1	1	5	500	90	10	0
1	1	5	500	90	15	0
1	1	5	500	135	1	0
1	1	5	500	135	5	0
1	1	5	500	135	10	0
1	1	5	500	135	15	0
1	0.75	5	500	0	1	4
1	0.75	5	500	45	1	4
1	0.75	5	500	90	1	5
1	0.75	5	500	135	1	4
1	0.5	5	500	0	1	5
1	0.5	5	500	45	1	5
1	0.5	5	500	90	1	5
1	0.5	5	500	135	1	5

Defect	Thickness	Panel	Laser Power	Orientation	Vacuum	Value
1	1.5	5	100	0	1	4
1	1.5	5	100	45	1	2
1	1.5	5	100	90	1	4
1	1.5	5	100	135	1	4
1	1.25	5	100	0	1	4
1	1.25	5	100	45	1	4
1	1.25	5	100	90	1	4
1	1.25	5	100	135	1	3
1	1	5	100	0	1	3
1	1	5	100	0	10	3
1	1	5	100	45	1	3
1	1	5	100	45	10	3
1	1	5	100	90	1	3
1	1	5	100	90	10	2
1	1	5	100	135	1	3
1	1	5	100	135	10	3
1	0.75	5	100	0	1	5
1	0.75	5	100	45	1	5
1	0.75	5	100	90	1	5
1	0.75	5	100	135	1	5
1	0.5	5	100	0	1	6
1	0.5	5	100	45	1	6
1	0.5	5	100	90	1	6
1	0.5	5	100	135	1	6

Defect	Thickness	Panel	Laser Power	Orientation	Vacuum	Value
2	1.5	5	500	0	1	3
2	1.5	5	500	45	1	3
2	1.5	5	500	90	1	4
2	1.5	5	500	135	1	4
2	1.25	5	500	0	1	4
2	1.25	5	500	45	1	4
2	1.25	5	500	90	1	5
2	1.25	5	500	135	1	4
2	1	5	500	0	1	4
2	1	5	500	0	5	4
2	1	5	500	0	10	4
2	1	5	500	0	15	4
2	1	5	500	45	1	4
2	1	5	500	45	5	4
2	1	5	500	45	10	4
2	1	5	500	45	15	4
2	1	5	500	90	1	5
2	1	5	500	90	5	5
2	1	5	500	90	10	5
2	1	5	500	90	15	5
2	1	5	500	135	1	3
2	1	5	500	135	5	3
2	1	5	500	135	10	3
2	1	5	500	135	15	3
2	0.75	5	500	0	1	5
2	0.75	5	500	45	1	5
2	0.75	5	500	90	1	4
2	0.75	5	500	135	1	4
2	0.5	5	500	0	1	6
2	0.5	5	500	45	1	6
2	0.5	5	500	90	1	5
2	0.5	5	500	135	1	5

Defect	Thickness	Panel	Laser Power	Orientation	Vacuum	Value
2	1.5	5	100	0	1	5
2	1.5	5	100	45	1	5
2	1.5	5	100	90	1	5
2	1.5	5	100	135	1	5
2	1.25	5	100	0	1	5
2	1.25	5	100	45	1	4
2	1.25	5	100	90	1	5
2	1.25	5	100	135	1	5
2	1.25	5	100	0	1	4
2	1.25	5	100	45	1	4
2	1.25	5	100	90	1	5
2	1.25	5	100	135	1	5
2	1	5	100	0	1	5
2	1	5	100	0	10	4
2	1	5	100	45	1	4
2	1	5	100	45	10	4
2	1	5	100	90	1	5
2	1	5	100	90	10	4
2	1	5	100	135	1	4
2	1	5	100	135	10	4
2	0.75	5	100	0	1	6
2	0.75	5	100	45	1	5
2	0.75	5	100	90	1	5
2	0.75	5	100	135	1	5
2	0.5	5	100	0	1	7
2	0.5	5	100	45	1	6
2	0.5	5	100	90	1	6
2	0.5	5	100	135	1	7

Defect	Thickness	Panel	Laser Power	Orientation	Vacuum	Value
3	1.5	5	500	0	1	1
3	1.5	5	500	45	1	3
3	1.5	5	500	90	1	2
3	1.5	5	500	135	1	3
3	1.25	5	500	0	1	4
3	1.25	5	500	45	1	3
3	1.25	5	500	90	1	4
3	1.25	5	500	135	1	0
3	1	5	500	0	1	3
3	1	5	500	0	5	3
3	1	5	500	0	10	3
3	1	5	500	0	15	3
3	1	5	500	45	1	4
3	1	5	500	45	5	4
3	1	5	500	45	10	4
3	1	5	500	45	15	4
3	1	5	500	90	1	5
3	1	5	500	90	5	5
3	1	5	500	90	10	5
3	1	5	500	90	15	5
3	1	5	500	135	1	2
3	1	5	500	135	5	2
3	1	5	500	135	10	2
3	1	5	500	135	15	2
3	0.75	5	500	0	1	5
3	0.75	5	500	45	1	4
3	0.75	5	500	90	1	4
3	0.75	5	500	135	1	4
3	0.5	5	500	0	1	6
3	0.5	5	500	45	1	5
3	0.5	5	500	90	1	5
3	0.5	5	500	135	1	5

Defect	Thickness	Panel	Laser Power	Orientation	Vacuum	Value
3	1.5	5	100	0	1	3
3	1.5	5	100	45	1	1
3	1.5	5	100	90	1	5
3	1.5	5	100	135	1	4
3	1.25	5	100	0	1	4
3	1.25	5	100	45	1	0
3	1.25	5	100	90	1	3
3	1.25	5	100	135	1	0
3	1.25	5	100	0	1	4
3	1.25	5	100	45	1	3
3	1.25	5	100	90	1	4
3	1.25	5	100	135	1	4
3	0.75	5	100	0	1	5
3	0.75	5	100	45	1	5
3	0.75	5	100	90	1	6
3	0.75	5	100	135	1	5
3	0.5	5	100	0	1	6
3	0.5	5	100	45	1	6
3	0.5	5	100	90	1	6
3	0.5	5	100	135	1	6

Defect	Thickness	Panel	Laser Power	Orientation	Vacuum	Value
4	1.5	5	500	0	1	0
4	1.5	5	500	45	1	0
4	1.5	5	500	90	1	0
4	1.5	5	500	135	1	0
4	1.25	5	500	0	1	0
4	1.25	5	500	45	1	0
4	1.25	5	500	90	1	0
4	1.25	5	500	135	1	0
4	1	5	500	0	1	0
4	1	5	500	0	5	0
4	1	5	500	0	10	0
4	1	5	500	0	15	0
4	1	5	500	45	1	0
4	1	5	500	45	5	0
4	1	5	500	45	10	0
4	1	5	500	45	15	0
4	1	5	500	90	1	0
4	1	5	500	90	5	0
4	1	5	500	90	10	0
4	1	5	500	90	15	0
4	1	5	500	135	1	3
4	1	5	500	135	5	3
4	1	5	500	135	10	4
4	1	5	500	135	15	4
4	0.75	5	500	0	1	6
4	0.75	5	500	45	1	5
4	0.75	5	500	90	1	2
4	0.75	5	500	135	1	4
4	0.5	5	500	0	1	6
4	0.5	5	500	45	1	6
4	0.5	5	500	90	1	4
4	0.5	5	500	135	1	5

Defect	Thickness	Panel	Laser Power	Orientation	Vacuum	Value
4	1.5	5	100	0	1	4
4	1.5	5	100	45	1	0
4	1.5	5	100	90	1	0
4	1.5	5	100	135	1	0
4	1.25	5	100	0	1	3
4	1.25	5	100	45	1	0
4	1.25	5	100	90	1	0
4	1.25	5	100	135	1	2
4	1	5	100	0	1	4
4	1	5	100	0	10	4
4	1	5	100	45	1	3
4	1	5	100	45	10	3
4	1	5	100	90	1	2
4	1	5	100	90	10	2
4	1	5	100	135	1	4
4	1	5	100	135	10	3
4	0.75	5	100	0	1	5
4	0.75	5	100	45	1	5
4	0.75	5	100	90	1	3
4	0.75	5	100	135	1	5
4	0.5	5	100	0	1	6
4	0.5	5	100	45	1	6
4	0.5	5	100	90	1	4
4	0.5	5	100	135	1	6

Defect	Thickness	Panel	Laser Power	Orientation	Vacuum	Value
5	1.5	5	500	0	1	4
5	1.5	5	500	45	1	4
5	1.5	5	500	90	1	4
5	1.5	5	500	135	1	3
5	1.25	5	500	0	1	5
5	1.25	5	500	45	1	5
5	1.25	5	500	90	1	4
5	1.25	5	500	135	1	4
5	1	5	500	0	1	5
5	1	5	500	0	5	5
5	1	5	500	0	10	5
5	1	5	500	0	15	5
5	1	5	500	45	1	5
5	1	5	500	45	5	5
5	1	5	500	45	10	5
5	1	5	500	45	15	5
5	1	5	500	90	1	5
5	1	5	500	90	5	5
5	1	5	500	90	10	5
5	1	5	500	90	15	5
5	1	5	500	135	1	5
5	1	5	500	135	5	5
5	1	5	500	135	10	5
5	1	5	500	135	15	5
5	0.75	5	500	0	1	6
5	0.75	5	500	45	1	6
5	0.75	5	500	90	1	5
5	0.75	5	500	135	1	5
5	0.5	5	500	0	1	6
5	0.5	5	500	45	1	7
5	0.5	5	500	90	1	5
5	0.5	5	500	135	1	5

Defect	Thickness	Panel	Laser Power	Orientation	Vacuum	Value
5	1.5	5	100	0	1	5
5	1.5	5	100	45	1	5
5	1.5	5	100	90	1	5
5	1.5	5	100	135	1	5
5	1.5	5	100	0	1	5
5	1.5	5	100	45	1	4
5	1.5	5	100	90	1	5
5	1.5	5	100	135	1	4
5	1.25	5	100	0	1	4
5	1.25	5	100	45	1	5
5	1.25	5	100	90	1	5
5	1.25	5	100	135	1	5
5	1.25	5	100	0	1	5
5	1.25	5	100	45	1	5
5	1.25	5	100	90	1	5
5	1.25	5	100	135	1	5
5	1	5	100	0	1	6
5	1	5	100	0	10	6
5	1	5	100	45	1	6
5	1	5	100	45	10	6
5	1	5	100	90	1	6
5	1	5	100	90	10	6
5	1	5	100	135	1	6
5	1	5	100	135	10	6
5	0.75	5	100	0	1	6
5	0.75	5	100	45	1	6
5	0.75	5	100	90	1	5
5	0.75	5	100	135	1	5
5	0.5	5	100	0	1	7
5	0.5	5	100	45	1	7
5	0.5	5	100	90	1	6
5	0.5	5	100	135	1	7

Defect	Thickness	Panel	Laser Power	Orientation	Vacuum	Value
6	1.5	5	500	0	1	3
6	1.5	5	500	45	1	4
6	1.5	5	500	90	1	5
6	1.5	5	500	135	1	3
6	1.25	5	500	0	1	5
6	1.25	5	500	45	1	5
6	1.25	5	500	90	1	5
6	1.25	5	500	135	1	5
6	1	5	500	0	1	5
6	1	5	500	0	5	5
6	1	5	500	0	10	5
6	1	5	500	0	15	5
6	1	5	500	45	1	5
6	1	5	500	45	5	5
6	1	5	500	45	10	5
6	1	5	500	45	15	5
6	1	5	500	90	1	5
6	1	5	500	90	5	5
6	1	5	500	90	10	5
6	1	5	500	90	15	5
6	1	5	500	135	1	5
6	1	5	500	135	5	5
6	1	5	500	135	10	5
6	1	5	500	135	15	5
6	0.75	5	500	0	1	6
6	0.75	5	500	45	1	5
6	0.75	5	500	90	1	5
6	0.75	5	500	135	1	6
6	0.5	5	500	0	1	6
6	0.5	5	500	45	1	6
6	0.5	5	500	90	1	5
6	0.5	5	500	135	1	5

Defect	Thickness	Panel	Laser Power	Orientation	Vacuum	Value
6	1.5	5	100	0	1	5
6	1.5	5	100	45	1	4
6	1.5	5	100	90	1	5
6	1.5	5	100	135	1	5
6	1.25	5	100	0	1	5
6	1.25	5	100	45	1	5
6	1.25	5	100	90	1	5
6	1.25	5	100	135	1	5
6	1	5	100	0	1	6
6	1	5	100	0	10	6
6	1	5	100	45	1	6
6	1	5	100	45	10	6
6	1	5	100	90	1	6
6	1	5	100	90	10	6
6	1	5	100	135	1	6
6	1	5	100	135	10	6
6	0.75	5	100	0	1	6
6	0.75	5	100	45	1	6
6	0.75	5	100	90	1	7
6	0.75	5	100	135	1	7
6	0.5	5	100	0	1	6
6	0.5	5	100	45	1	5
6	0.5	5	100	90	1	6
6	0.5	5	100	135	1	6

Defect	Thickness	Panel	Laser Power	Orientation	Vacuum	Value
7	1.5	5	500	0	1	4
7	1.5	5	500	45	1	2
7	1.5	5	500	90	1	3
7	1.5	5	500	135	1	5
7	1.25	5	500	0	1	5
7	1.25	5	500	45	1	4
7	1.25	5	500	90	1	4
7	1.25	5	500	135	1	5
7	1	5	500	0	1	5
7	1	5	500	0	5	5
7	1	5	500	0	10	5
7	1	5	500	0	15	5
7	1	5	500	45	1	5
7	1	5	500	45	5	5
7	1	5	500	45	10	5
7	1	5	500	45	15	5
7	1	5	500	90	1	4
7	1	5	500	90	5	4
7	1	5	500	90	10	4
7	1	5	500	90	15	4
7	1	5	500	135	1	5
7	1	5	500	135	5	5
7	1	5	500	135	10	5
7	1	5	500	135	15	5
7	0.75	5	500	0	1	6
7	0.75	5	500	45	1	5
7	0.75	5	500	90	1	5
7	0.75	5	500	135	1	5
7	0.5	5	500	0	1	6
7	0.5	5	500	45	1	6
7	0.5	5	500	90	1	5
7	0.5	5	500	135	1	6

Defect	Thickness	Panel	Laser Power	Orientation	Vacuum	Value
7	1.5	5	100	0	1	4
7	1.5	5	100	45	1	4
7	1.5	5	100	90	1	4
7	1.5	5	100	135	1	5
7	1.5	5	100	0	1	6
7	1.5	5	100	45	1	5
7	1.5	5	100	90	1	5
7	1.5	5	100	135	1	5
7	1.25	5	100	0	1	5
7	1.25	5	100	45	1	5
7	1.25	5	100	90	1	5
7	1.25	5	100	135	1	5
7	1.25	5	100	0	1	6
7	1.25	5	100	45	1	5
7	1.25	5	100	90	1	5
7	1.25	5	100	135	1	5
7	1	5	100	0	1	6
7	1	5	100	0	10	6
7	1	5	100	45	1	6
7	1	5	100	45	10	5
7	1	5	100	90	1	5
7	1	5	100	90	10	5
7	1	5	100	135	1	6
7	1	5	100	135	10	5
7	0.75	5	100	0	1	7
7	0.75	5	100	45	1	7
7	0.75	5	100	90	1	5
7	0.75	5	100	135	1	6
7	0.5	5	100	0	1	7
7	0.5	5	100	45	1	7
7	0.5	5	100	90	1	6
7	0.5	5	100	135	1	7

Defect	Thickness	Panel	Laser Power	Orientation	Vacuum	Value
8	1.5	5	500	0	1	4
8	1.5	5	500	45	1	0
8	1.5	5	500	90	1	0
8	1.5	5	500	135	1	3
8	1.25	5	500	0	1	5
8	1.25	5	500	45	1	2
8	1.25	5	500	90	1	2
8	1.25	5	500	135	1	3
8	1	5	500	0	1	5
8	1	5	500	0	5	5
8	1	5	500	0	10	5
8	1	5	500	0	15	5
8	1	5	500	45	1	4
8	1	5	500	45	5	4
8	1	5	500	45	10	4
8	1	5	500	45	15	4
8	1	5	500	90	1	4
8	1	5	500	90	5	4
8	1	5	500	90	10	4
8	1	5	500	90	15	4
8	1	5	500	135	1	4
8	1	5	500	135	5	4
8	1	5	500	135	10	4
8	1	5	500	135	15	4
8	0.75	5	500	0	1	6
8	0.75	5	500	45	1	5
8	0.75	5	500	90	1	5
8	0.75	5	500	135	1	6
8	0.5	5	500	0	1	6
8	0.5	5	500	45	1	6
8	0.5	5	500	90	1	5
8	0.5	5	500	135	1	6

Defect	Thickness	Panel	Laser Power	Orientation	Vacuum	Value
8	1.5	5	100	0	1	5
8	1.5	5	100	45	1	4
8	1.5	5	100	90	1	4
8	1.5	5	100	135	1	4
8	1.25	5	100	0	1	5
8	1.25	5	100	45	1	5
8	1.25	5	100	90	1	4
8	1.25	5	100	135	1	4
8	1	5	100	0	1	6
8	1	5	100	0	10	6
8	1	5	100	45	1	6
8	1	5	100	45	10	5
8	1	5	100	90	1	5
8	1	5	100	90	10	5
8	1	5	100	135	1	6
8	1	5	100	135	10	5
8	0.75	5	100	0	1	7
8	0.75	5	100	45	1	7
8	0.75	5	100	90	1	5
8	0.75	5	100	135	1	6
8	0.5	5	100	0	1	7
8	0.5	5	100	45	1	7
8	0.5	5	100	90	1	5
8	0.5	5	100	135	1	7

Defect	Thickness	Panel	Laser Power	Orientation	Vacuum	Value
9	1.5	5	500	0	1	4
9	1.5	5	500	45	1	4
9	1.5	5	500	90	1	4
9	1.5	5	500	135	1	4
9	1.25	5	500	0	1	5
9	1.25	5	500	45	1	4
9	1.25	5	500	90	1	5
9	1.25	5	500	135	1	5
9	1	5	500	0	1	5
9	1	5	500	0	5	5
9	1	5	500	0	10	5
9	1	5	500	0	15	5
9	1	5	500	45	1	5
9	1	5	500	45	5	5
9	1	5	500	45	10	5
9	1	5	500	45	15	5
9	1	5	500	90	1	5
9	1	5	500	90	5	5
9	1	5	500	90	10	5
9	1	5	500	90	15	5
9	1	5	500	135	1	5
9	1	5	500	135	5	5
9	1	5	500	135	10	5
9	1	5	500	135	15	5
9	0.75	5	500	0	1	6
9	0.75	5	500	45	1	5
9	0.75	5	500	90	1	5
9	0.75	5	500	135	1	6
9	0.5	5	500	0	1	6
9	0.5	5	500	45	1	6
9	0.5	5	500	90	1	6
9	0.5	5	500	135	1	6

Defect	Thickness	Panel	Laser Power	Orientation	Vacuum	Value
9	1.5	5	100	0	1	5
9	1.5	5	100	45	1	5
9	1.5	5	100	90	1	5
9	1.5	5	100	135	1	5
9	1.25	5	100	0	1	5
9	1.25	5	100	45	1	5
9	1.25	5	100	90	1	5
9	1.25	5	100	135	1	5
9	1	5	100	0	1	6
9	1	5	100	0	10	6
9	1	5	100	45	1	6
9	1	5	100	45	10	6
9	1	5	100	90	1	5
9	1	5	100	90	10	5
9	1	5	100	135	1	6
9	1	5	100	135	10	6
9	0.75	5	100	0	1	6
9	0.75	5	100	45	1	6
9	0.75	5	100	90	1	6
9	0.75	5	100	135	1	6
9	0.5	5	100	0	1	6
9	0.5	5	100	45	1	6
9	0.5	5	100	90	1	6
9	0.5	5	100	135	1	6

Defect	Thickness	Panel	Laser Power	Orientation	Vacuum	Value
10	1.5	5	500	0	1	6
10	1.5	5	500	45	1	6
10	1.5	5	500	90	1	7
10	1.5	5	500	135	1	7
10	1.25	5	500	0	1	6
10	1.25	5	500	45	1	6
10	1.25	5	500	90	1	6
10	1.25	5	500	135	1	6
10	1	5	500	0	1	6
10	1	5	500	0	5	6
10	1	5	500	0	10	6
10	1	5	500	0	15	6
10	1	5	500	45	1	6
10	1	5	500	45	5	6
10	1	5	500	45	10	6
10	1	5	500	45	15	6
10	1	5	500	90	1	7
10	1	5	500	90	5	7
10	1	5	500	90	10	7
10	1	5	500	90	15	7
10	1	5	500	135	1	7
10	1	5	500	135	5	7
10	1	5	500	135	10	7
10	1	5	500	135	15	7
10	0.75	5	500	0	1	7
10	0.75	5	500	45	1	7
10	0.75	5	500	90	1	7
10	0.75	5	500	135	1	7
10	0.5	5	500	0	1	7
10	0.5	5	500	45	1	7
10	0.5	5	500	90	1	7
10	0.5	5	500	135	1	7

Defect	Thickness	Panel	Laser Power	Orientation	Vacuum	Value
10	1.5	5	100	0	1	7
10	1.5	5	100	45	1	7
10	1.5	5	100	90	1	7
10	1.5	5	100	135	1	7
10	1.25	5	100	0	1	6
10	1.25	5	100	45	1	6
10	1.25	5	100	90	1	6
10	1.25	5	100	135	1	6
10	1	5	100	0	1	6
10	1	5	100	0	10	6
10	1	5	100	45	1	6
10	1	5	100	45	10	6
10	1	5	100	90	1	6
10	1	5	100	90	10	6
10	1	5	100	135	1	6
10	1	5	100	135	10	6
10	0.75	5	100	0	1	8
10	0.75	5	100	45	1	7
10	0.75	5	100	90	1	8
10	0.75	5	100	135	1	8
10	0.5	5	100	0	1	8
10	0.5	5	100	45	1	8
10	0.5	5	100	90	1	8
10	0.5	5	100	135	1	8

Defect	Thickness	Panel	Laser Power	Orientation	Vacuum	Value
11	1.5	3	500	0	1	4
11	1.5	3	500	45	1	3
11	1.5	3	500	90	1	0
11	1.5	3	500	135	1	3
11	1.25	3	500	0	1	4
11	1.25	3	500	45	1	4
11	1.25	3	500	90	1	4
11	1.25	3	500	135	1	4
11	1	3	500	0	1	6
11	1	3	500	0	5	6
11	1	3	500	0	10	6
11	1	3	500	0	15	6
11	1	3	500	45	1	5
11	1	3	500	45	5	5
11	1	3	500	45	10	5
11	1	3	500	45	15	5
11	1	3	500	90	1	5
11	1	3	500	90	5	5
11	1	3	500	90	10	5
11	1	3	500	90	15	5
11	1	3	500	135	1	5
11	1	3	500	135	5	5
11	1	3	500	135	10	5
11	1	3	500	135	15	5
11	0.75	3	500	0	1	5
11	0.75	3	500	45	1	5
11	0.75	3	500	90	1	5
11	0.75	3	500	135	1	5
11	0.5	3	500	0	1	6
11	0.5	3	500	45	1	6
11	0.5	3	500	90	1	6
11	0.5	3	500	135	1	6

Defect	Thickness	Panel	Laser Power	Orientation	Vacuum	Value
11	1.5	3	100	0	1	4
11	1.5	3	100	45	1	3
11	1.5	3	100	90	1	2
11	1.5	3	100	135	1	1
11	1.25	3	100	0	1	4
11	1.25	3	100	45	1	4
11	1.25	3	100	90	1	5
11	1.25	3	100	135	1	4
11	1	3	100	0	1	6
11	1	3	100	0	10	6
11	1	3	100	45	1	6
11	1	3	100	45	10	5
11	1	3	100	90	1	6
11	1	3	100	90	10	6
11	1	3	100	135	1	6
11	1	3	100	135	10	6
11	0.75	3	100	0	1	7
11	0.75	3	100	45	1	7
11	0.75	3	100	90	1	7
11	0.75	3	100	135	1	7
11	0.5	3	100	0	1	7
11	0.5	3	100	45	1	7
11	0.5	3	100	90	1	7
11	0.5	3	100	135	1	7

Defect	Thickness	Panel	Laser Power	Orientation	Vacuum	Value
12	1.5	3	500	0	1	5
12	1.5	3	500	45	1	4
12	1.5	3	500	90	1	3
12	1.5	3	500	135	1	4
12	1.25	3	500	0	1	4
12	1.25	3	500	45	1	5
12	1.25	3	500	90	1	5
12	1.25	3	500	135	1	5
12	1	3	500	0	1	6
12	1	3	500	0	5	6
12	1	3	500	0	10	6
12	1	3	500	0	15	6
12	1	3	500	45	1	6
12	1	3	500	45	5	5
12	1	3	500	45	10	5
12	1	3	500	45	15	5
12	1	3	500	90	1	5
12	1	3	500	90	5	5
12	1	3	500	90	10	5
12	1	3	500	90	15	5
12	1	3	500	135	1	5
12	1	3	500	135	5	5
12	1	3	500	135	10	5
12	1	3	500	135	15	5
12	0.75	3	500	0	1	6
12	0.75	3	500	45	1	6
12	0.75	3	500	90	1	6
12	0.75	3	500	135	1	6
12	0.5	3	500	0	1	6
12	0.5	3	500	45	1	6
12	0.5	3	500	90	1	6
12	0.5	3	500	135	1	6

Defect	Thickness	Panel	Laser Power	Orientation	Vacuum	Value
12	1.5	3	100	0	1	5
12	1.5	3	100	45	1	5
12	1.5	3	100	90	1	4
12	1.5	3	100	135	1	5
12	1.5	3	100	0	1	5
12	1.5	3	100	45	1	5
12	1.5	3	100	90	1	5
12	1.5	3	100	135	1	5
12	1.5	3	100	0	1	5
12	1.5	3	100	45	1	5
12	1.5	3	100	90	1	5
12	1.5	3	100	135	1	5
12	1.25	3	100	0	1	6
12	1.25	3	100	45	1	6
12	1.25	3	100	90	1	6
12	1.25	3	100	135	1	6
12	1.25	3	100	0	1	6
12	1.25	3	100	45	1	6
12	1.25	3	100	90	1	6
12	1.25	3	100	135	1	6
12	1.25	3	100	0	1	6
12	1.25	3	100	45	1	6
12	1.25	3	100	90	1	5
12	1.25	3	100	135	1	6
12	1	3	100	0	1	6
12	1	3	100	0	10	6
12	1	3	100	45	1	6
12	1	3	100	45	10	6
12	1	3	100	90	1	6
12	1	3	100	90	10	6
12	1	3	100	135	1	6
12	1	3	100	135	10	6
12	1	3	100	0	1	6
12	1	3	100	0	10	6
12	1	3	100	45	1	6
12	1	3	100	45	10	6
12	1	3	100	90	1	6
12	1	3	100	90	10	6
12	1	3	100	135	1	6
12	1	3	100	135	10	6
12	0.75	3	100	0	1	7
12	0.75	3	100	45	1	7
12	0.75	3	100	90	1	7
12	0.75	3	100	135	1	7
12	0.5	3	100	0	1	6
12	0.5	3	100	45	1	6
12	0.5	3	100	90	1	6
12	0.5	3	100	135	1	6

Defect	Thickness	Panel	Laser Power	Orientation	Vacuum	Value
13	1.5	3	500	0	1	5
13	1.5	3	500	45	1	4
13	1.5	3	500	90	1	5
13	1.5	3	500	135	1	4
13	1.25	3	500	0	1	5
13	1.25	3	500	45	1	6
13	1.25	3	500	90	1	6
13	1.25	3	500	135	1	6
13	1	3	500	0	1	6
13	1	3	500	0	5	6
13	1	3	500	0	10	6
13	1	3	500	0	15	6
13	1	3	500	45	1	6
13	1	3	500	45	5	5
13	1	3	500	45	10	5
13	1	3	500	45	15	5
13	1	3	500	90	1	5
13	1	3	500	90	5	5
13	1	3	500	90	10	5
13	1	3	500	90	15	5
13	1	3	500	135	1	5
13	1	3	500	135	5	5
13	1	3	500	135	10	5
13	1	3	500	135	15	5
13	0.75	3	500	0	1	6
13	0.75	3	500	45	1	6
13	0.75	3	500	90	1	6
13	0.75	3	500	135	1	6
13	0.5	3	500	0	1	6
13	0.5	3	500	45	1	6
13	0.5	3	500	90	1	6
13	0.5	3	500	135	1	6

Defect	Thickness	Panel	Laser Power	Orientation	Vacuum	Value
13	1.5	3	100	0	1	5
13	1.5	3	100	45	1	5
13	1.5	3	100	90	1	5
13	1.5	3	100	135	1	5
13	1.5	3	100	0	1	5
13	1.5	3	100	45	1	5
13	1.5	3	100	90	1	5
13	1.5	3	100	135	1	5
13	1.25	3	100	0	1	6
13	1.25	3	100	45	1	6
13	1.25	3	100	90	1	6
13	1.25	3	100	135	1	6
13	1.25	3	100	0	1	6
13	1.25	3	100	45	1	6
13	1.25	3	100	90	1	6
13	1.25	3	100	135	1	6
13	1	3	100	0	1	6
13	1	3	100	0	10	6
13	1	3	100	45	1	6
13	1	3	100	45	10	4
13	1	3	100	90	1	6
13	1	3	100	90	10	6
13	1	3	100	135	1	6
13	1	3	100	135	10	6
13	0.75	3	100	0	1	7
13	0.75	3	100	45	1	6
13	0.75	3	100	90	1	6
13	0.75	3	100	135	1	7
13	0.5	3	100	0	1	7
13	0.5	3	100	45	1	7
13	0.5	3	100	90	1	7
13	0.5	3	100	135	1	7

Defect	Thickness	Panel	Laser Power	Orientation	Vacuum	Value
14	1.5	3	500	0	1	0
14	1.5	3	500	45	1	0
14	1.5	3	500	90	1	0
14	1.5	3	500	135	1	0
14	1.25	3	500	0	1	0
14	1.25	3	500	45	1	0
14	1.25	3	500	90	1	2
14	1.25	3	500	135	1	1
14	1	3	500	0	1	0
14	1	3	500	0	5	0
14	1	3	500	0	10	0
14	1	3	500	0	15	0
14	1	3	500	45	1	0
14	1	3	500	45	5	0
14	1	3	500	45	10	0
14	1	3	500	45	15	0
14	1	3	500	90	1	0
14	1	3	500	90	5	0
14	1	3	500	90	10	0
14	1	3	500	90	15	0
14	1	3	500	135	1	0
14	1	3	500	135	5	0
14	1	3	500	135	10	0
14	1	3	500	135	15	0
14	0.75	3	500	0	1	2
14	0.75	3	500	45	1	0
14	0.75	3	500	90	1	0
14	0.75	3	500	135	1	0
14	0.5	3	500	0	1	0
14	0.5	3	500	45	1	0
14	0.5	3	500	90	1	0
14	0.5	3	500	135	1	0

Defect	Thickness	Panel	Laser Power	Orientation	Vacuum	Value
14	1.5	3	100	0	1	0
14	1.5	3	100	45	1	2
14	1.5	3	100	90	1	0
14	1.5	3	100	135	1	1
14	1.25	3	100	0	1	2
14	1.25	3	100	45	1	2
14	1.25	3	100	90	1	2
14	1.25	3	100	135	1	2
14	0.75	3	100	0	1	2
14	0.75	3	100	45	1	3
14	0.75	3	100	90	1	2
14	0.75	3	100	135	1	2
14	0.5	3	100	0	1	4
14	0.5	3	100	45	1	4
14	0.5	3	100	90	1	4
14	0.5	3	100	135	1	4

Defect	Thickness	Panel	Laser Power	Orientation	Vacuum	Value
15	1.5	3	500	0	1	5
15	1.5	3	500	45	1	5
15	1.5	3	500	90	1	5
15	1.5	3	500	135	1	5
15	1.25	3	500	0	1	6
15	1.25	3	500	45	1	5
15	1.25	3	500	90	1	6
15	1.25	3	500	135	1	5
15	1	3	500	0	1	6
15	1	3	500	0	5	6
15	1	3	500	0	10	6
15	1	3	500	0	15	6
15	1	3	500	45	1	5
15	1	3	500	45	5	5
15	1	3	500	45	10	5
15	1	3	500	45	15	5
15	1	3	500	90	1	5
15	1	3	500	90	5	5
15	1	3	500	90	10	5
15	1	3	500	90	15	5
15	1	3	500	135	1	5
15	1	3	500	135	5	5
15	1	3	500	135	10	5
15	1	3	500	135	15	5
15	0.75	3	500	0	1	5
15	0.75	3	500	45	1	5
15	0.75	3	500	90	1	5
15	0.75	3	500	135	1	5
15	0.5	3	500	0	1	6
15	0.5	3	500	45	1	6
15	0.5	3	500	90	1	6
15	0.5	3	500	135	1	6

Defect	Thickness	Panel	Laser Power	Orientation	Vacuum	Value
15	1.5	3	100	0	1	5
15	1.5	3	100	45	1	5
15	1.5	3	100	90	1	5
15	1.5	3	100	135	1	5
15	1.25	3	100	0	1	7
15	1.25	3	100	45	1	6
15	1.25	3	100	90	1	6
15	1.25	3	100	135	1	6
15	1.25	3	100	0	1	6
15	1.25	3	100	45	1	6
15	1.25	3	100	90	1	6
15	1.25	3	100	135	1	6
15	1.25	3	100	0	1	6
15	1.25	3	100	45	1	6
15	1.25	3	100	90	1	6
15	1.25	3	100	135	1	6
15	1	3	100	0	1	6
15	1	3	100	0	10	6
15	1	3	100	45	1	6
15	1	3	100	45	10	6
15	1	3	100	90	1	6
15	1	3	100	90	10	6
15	1	3	100	135	1	6
15	1	3	100	135	10	6
15	0.75	3	100	0	1	6
15	0.75	3	100	45	1	6
15	0.75	3	100	90	1	6
15	0.75	3	100	135	1	6
15	0.5	3	100	0	1	6
15	0.5	3	100	45	1	6
15	0.5	3	100	90	1	6
15	0.5	3	100	135	1	6

Defect	Thickness	Panel	Laser Power	Orientation	Vacuum	Value
16	1.5	3	500	0	1	4
16	1.5	3	500	45	1	4
16	1.5	3	500	90	1	4
16	1.5	3	500	135	1	4
16	1.25	3	500	0	1	5
16	1.25	3	500	45	1	6
16	1.25	3	500	90	1	4
16	1.25	3	500	135	1	5
16	1	3	500	0	1	5
16	1	3	500	0	5	5
16	1	3	500	0	10	5
16	1	3	500	0	15	5
16	1	3	500	45	1	5
16	1	3	500	45	5	5
16	1	3	500	45	10	5
16	1	3	500	45	15	5
16	1	3	500	90	1	5
16	1	3	500	90	5	5
16	1	3	500	90	10	5
16	1	3	500	90	15	5
16	1	3	500	135	1	5
16	1	3	500	135	5	5
16	1	3	500	135	10	5
16	1	3	500	135	15	5
16	0.75	3	500	0	1	5
16	0.75	3	500	45	1	5
16	0.75	3	500	90	1	5
16	0.75	3	500	135	1	5
16	0.5	3	500	0	1	6
16	0.5	3	500	45	1	6
16	0.5	3	500	90	1	6
16	0.5	3	500	135	1	6

Defect	Thickness	Panel	Laser Power	Orientation	Vacuum	Value
16	1.5	3	100	0	1	4
16	1.5	3	100	45	1	4
16	1.5	3	100	90	1	4
16	1.5	3	100	135	1	4
16	1.25	3	100	0	1	6
16	1.25	3	100	45	1	6
16	1.25	3	100	90	1	5
16	1.25	3	100	135	1	6
16	1.25	3	100	0	1	6
16	1.25	3	100	45	1	6
16	1.25	3	100	90	1	6
16	1.25	3	100	135	1	6
16	1	3	100	0	1	6
16	1	3	100	0	10	6
16	1	3	100	45	1	6
16	1	3	100	45	10	6
16	1	3	100	90	1	6
16	1	3	100	90	10	6
16	1	3	100	135	1	6
16	1	3	100	135	10	6
16	0.75	3	100	0	1	6
16	0.75	3	100	45	1	6
16	0.75	3	100	90	1	6
16	0.75	3	100	135	1	6
16	0.5	3	100	0	1	6
16	0.5	3	100	45	1	6
16	0.5	3	100	90	1	6
16	0.5	3	100	135	1	6

Defect	Thickness	Panel	Laser Power	Orientation	Vacuum	Value
17	1.5	3	500	0	1	0
17	1.5	3	500	45	1	0
17	1.5	3	500	90	1	0
17	1.5	3	500	135	1	0
17	1.25	3	500	0	1	0
17	1.25	3	500	45	1	0
17	1.25	3	500	90	1	0
17	1.25	3	500	135	1	0
17	1	3	500	0	1	4
17	1	3	500	0	5	4
17	1	3	500	0	10	4
17	1	3	500	0	15	4
17	1	3	500	45	1	4
17	1	3	500	45	5	4
17	1	3	500	45	10	4
17	1	3	500	45	15	4
17	1	3	500	90	1	4
17	1	3	500	90	5	4
17	1	3	500	90	10	4
17	1	3	500	90	15	4
17	1	3	500	135	1	4
17	1	3	500	135	5	4
17	1	3	500	135	10	4
17	1	3	500	135	15	4
17	0.75	3	500	0	1	4
17	0.75	3	500	45	1	3
17	0.75	3	500	90	1	3
17	0.75	3	500	135	1	3
17	0.5	3	500	0	1	3
17	0.5	3	500	45	1	4
17	0.5	3	500	90	1	5
17	0.5	3	500	135	1	5

Defect	Thickness	Panel	Laser Power	Orientation	Vacuum	Value
17	1.5	3	100	0	1	3
17	1.5	3	100	45	1	0
17	1.5	3	100	90	1	0
17	1.5	3	100	135	1	0
17	1.25	3	100	0	1	4
17	1.25	3	100	45	1	3
17	1.25	3	100	90	1	3
17	1.25	3	100	135	1	3
17	1	3	100	0	1	5
17	1	3	100	0	10	5
17	1	3	100	45	1	4
17	1	3	100	45	10	4
17	1	3	100	90	1	4
17	1	3	100	90	10	4
17	1	3	100	135	1	3
17	1	3	100	135	10	3
17	0.75	3	100	0	1	4
17	0.75	3	100	45	1	4
17	0.75	3	100	90	1	4
17	0.75	3	100	135	1	4
17	0.5	3	100	0	1	5
17	0.5	3	100	45	1	5
17	0.5	3	100	90	1	5
17	0.5	3	100	135	1	5

Defect	Thickness	Panel	Laser Power	Orientation	Vacuum	Value
18	1.5	3	500	0	1	1
18	1.5	3	500	45	1	0
18	1.5	3	500	90	1	0
18	1.5	3	500	135	1	0
18	1.25	3	500	0	1	5
18	1.25	3	500	45	1	4
18	1.25	3	500	90	1	3
18	1.25	3	500	135	1	4
18	1	3	500	0	1	4
18	1	3	500	0	5	4
18	1	3	500	0	10	4
18	1	3	500	0	15	4
18	1	3	500	45	1	4
18	1	3	500	45	5	4
18	1	3	500	45	10	4
18	1	3	500	45	15	4
18	1	3	500	90	1	4
18	1	3	500	90	5	4
18	1	3	500	90	10	4
18	1	3	500	90	15	4
18	1	3	500	135	1	4
18	1	3	500	135	5	4
18	1	3	500	135	10	4
18	1	3	500	135	15	4
18	0.75	3	500	0	1	4
18	0.75	3	500	45	1	2
18	0.75	3	500	90	1	4
18	0.75	3	500	135	1	4
18	0.5	3	500	0	1	5
18	0.5	3	500	45	1	5
18	0.5	3	500	90	1	5
18	0.5	3	500	135	1	5

Defect	Thickness	Panel	Laser Power	Orientation	Vacuum	Value
18	1.5	3	100	0	1	4
18	1.5	3	100	45	1	3
18	1.5	3	100	90	1	3
18	1.5	3	100	135	1	4
18	1.5	3	100	0	1	4
18	1.5	3	100	45	1	4
18	1.5	3	100	90	1	2
18	1.5	3	100	135	1	3
18	1.25	3	100	0	1	5
18	1.25	3	100	45	1	5
18	1.25	3	100	90	1	4
18	1.25	3	100	135	1	4
18	1.25	3	100	0	1	4
18	1.25	3	100	45	1	3
18	1.25	3	100	90	1	3
18	1.25	3	100	135	1	4
18	1	3	100	0	1	5
18	1	3	100	0	10	4
18	1	3	100	45	1	3
18	1	3	100	45	10	4
18	1	3	100	90	1	3
18	1	3	100	90	10	4
18	1	3	100	135	1	5
18	1	3	100	135	10	4
18	0.75	3	100	0	1	4
18	0.75	3	100	45	1	4
18	0.75	3	100	90	1	4
18	0.75	3	100	135	1	4
18	0.5	3	100	0	1	6
18	0.5	3	100	45	1	6
18	0.5	3	100	90	1	6
18	0.5	3	100	135	1	6

Defect	Thickness	Panel	Laser Power	Orientation	Vacuum	Value
19	1.5	3	500	0	1	6
19	1.5	3	500	45	1	5
19	1.5	3	500	90	1	5
19	1.5	3	500	135	1	5
19	1.25	3	500	0	1	7
19	1.25	3	500	45	1	7
19	1.25	3	500	90	1	6
19	1.25	3	500	135	1	8
19	1	3	500	0	1	7
19	1	3	500	0	5	7
19	1	3	500	0	10	7
19	1	3	500	0	15	7
19	1	3	500	45	1	7
19	1	3	500	45	5	7
19	1	3	500	45	10	7
19	1	3	500	45	15	7
19	1	3	500	90	1	7
19	1	3	500	90	5	7
19	1	3	500	90	10	7
19	1	3	500	90	15	7
19	1	3	500	135	1	7
19	1	3	500	135	5	7
19	1	3	500	135	10	7
19	1	3	500	135	15	7
19	0.75	3	500	0	1	7
19	0.75	3	500	45	1	7
19	0.75	3	500	90	1	7
19	0.75	3	500	135	1	7
19	0.5	3	500	0	1	8
19	0.5	3	500	45	1	8
19	0.5	3	500	90	1	8
19	0.5	3	500	135	1	8

Defect	Thickness	Panel	Laser Power	Orientation	Vacuum	Value
19	1.5	3	100	0	1	6
19	1.5	3	100	45	1	6
19	1.5	3	100	90	1	6
19	1.5	3	100	135	1	6
19	1.5	3	100	0	1	6
19	1.5	3	100	45	1	6
19	1.5	3	100	90	1	6
19	1.5	3	100	135	1	6
19	1.25	3	100	0	1	8
19	1.25	3	100	45	1	8
19	1.25	3	100	90	1	8
19	1.25	3	100	135	1	8
19	1.25	3	100	0	1	8
19	1.25	3	100	45	1	8
19	1.25	3	100	90	1	8
19	1.25	3	100	135	1	8
19	1	3	100	0	1	7
19	1	3	100	0	10	7
19	1	3	100	45	1	7
19	1	3	100	45	10	7
19	1	3	100	90	1	7
19	1	3	100	90	10	7
19	1	3	100	135	1	7
19	1	3	100	135	10	7
19	0.75	3	100	0	1	8
19	0.75	3	100	45	1	8
19	0.75	3	100	90	1	8
19	0.75	3	100	135	1	8
19	0.5	3	100	0	1	9
19	0.5	3	100	45	1	9
19	0.5	3	100	90	1	9
19	0.5	3	100	135	1	9

Defect	Thickness	Panel	Laser Power	Orientation	Vacuum	Value
20	1.5	4	500	0	1	5
20	1.5	4	500	45	1	5
20	1.5	4	500	90	1	5
20	1.5	4	500	135	1	5
20	1.25	4	500	0	1	6
20	1.25	4	500	45	1	6
20	1.25	4	500	90	1	5
20	1.25	4	500	135	1	5
20	1	4	500	0	1	6
20	1	4	500	0	5	6
20	1	4	500	0	10	6
20	1	4	500	0	15	6
20	1	4	500	45	1	5
20	1	4	500	45	5	5
20	1	4	500	45	10	5
20	1	4	500	45	15	5
20	1	4	500	90	1	6
20	1	4	500	90	5	6
20	1	4	500	90	10	6
20	1	4	500	90	15	6
20	1	4	500	135	1	5
20	1	4	500	135	5	5
20	1	4	500	135	10	5
20	1	4	500	135	15	5
20	0.75	4	500	0	1	5
20	0.75	4	500	45	1	5
20	0.75	4	500	90	1	5
20	0.75	4	500	135	1	5
20	0.5	4	500	0	1	6
20	0.5	4	500	45	1	6
20	0.5	4	500	90	1	6
20	0.5	4	500	135	1	6

Defect	Thickness	Panel	Laser Power	Orientation	Vacuum	Value
20	1.5	4	100	0	1	6
20	1.5	4	100	45	1	5
20	1.5	4	100	90	1	6
20	1.5	4	100	135	1	6
20	1.25	4	100	0	1	6
20	1.25	4	100	45	1	6
20	1.25	4	100	90	1	5
20	1.25	4	100	135	1	5
20	1	4	100	0	1	6
20	1	4	100	0	10	6
20	1	4	100	45	1	6
20	1	4	100	45	10	6
20	1	4	100	90	1	6
20	1	4	100	90	10	6
20	1	4	100	135	1	6
20	1	4	100	135	10	6
20	0.75	4	100	0	1	6
20	0.75	4	100	45	1	6
20	0.75	4	100	90	1	6
20	0.75	4	100	135	1	6
20	0.5	4	100	0	1	7
20	0.5	4	100	45	1	7
20	0.5	4	100	90	1	7
20	0.5	4	100	135	1	7

Defect	Thickness	Panel	Laser Power	Orientation	Vacuum	Value
21	1.5	4	500	0	1	0
21	1.5	4	500	45	1	0
21	1.5	4	500	90	1	0
21	1.5	4	500	135	1	0
21	1.25	4	500	0	1	4
21	1.25	4	500	45	1	2
21	1.25	4	500	90	1	0
21	1.25	4	500	135	1	3
21	1	4	500	0	1	5
21	1	4	500	0	5	5
21	1	4	500	0	10	5
21	1	4	500	0	15	5
21	1	4	500	45	1	5
21	1	4	500	45	5	5
21	1	4	500	45	10	5
21	1	4	500	45	15	5
21	1	4	500	90	1	4
21	1	4	500	90	5	4
21	1	4	500	90	10	4
21	1	4	500	90	15	4
21	1	4	500	135	1	5
21	1	4	500	135	5	5
21	1	4	500	135	10	5
21	1	4	500	135	15	5
21	0.75	4	500	0	1	5
21	0.75	4	500	45	1	5
21	0.75	4	500	90	1	5
21	0.75	4	500	135	1	5
21	0.5	4	500	0	1	6
21	0.5	4	500	45	1	6
21	0.5	4	500	90	1	6
21	0.5	4	500	135	1	6

Defect	Thickness	Panel	Laser Power	Orientation	Vacuum	Value
21	1.5	4	100	0	1	4
21	1.5	4	100	45	1	4
21	1.5	4	100	90	1	0
21	1.5	4	100	135	1	4
21	1.25	4	100	0	1	4
21	1.25	4	100	45	1	3
21	1.25	4	100	90	1	0
21	1.25	4	100	135	1	3
21	1	4	100	0	1	6
21	1	4	100	0	10	6
21	1	4	100	45	1	5
21	1	4	100	45	10	5
21	1	4	100	90	1	5
21	1	4	100	90	10	5
21	1	4	100	135	1	5
21	1	4	100	135	10	5
21	0.75	4	100	0	1	6
21	0.75	4	100	45	1	6
21	0.75	4	100	90	1	4
21	0.75	4	100	135	1	6
21	0.5	4	100	0	1	7
21	0.5	4	100	45	1	7
21	0.5	4	100	90	1	4
21	0.5	4	100	135	1	7

Defect	Thickness	Panel	Laser Power	Orientation	Vacuum	Value
22	1.5	4	500	0	1	3
22	1.5	4	500	45	1	2
22	1.5	4	500	90	1	3
22	1.5	4	500	135	1	0
22	1.25	4	500	0	1	3
22	1.25	4	500	45	1	3
22	1.25	4	500	90	1	2
22	1.25	4	500	135	1	0
22	1	4	500	0	1	4
22	1	4	500	0	5	4
22	1	4	500	0	10	4
22	1	4	500	0	15	4
22	1	4	500	45	1	4
22	1	4	500	45	5	4
22	1	4	500	45	10	4
22	1	4	500	45	15	4
22	1	4	500	90	1	4
22	1	4	500	90	5	4
22	1	4	500	90	10	4
22	1	4	500	90	15	4
22	1	4	500	135	1	0
22	1	4	500	135	5	0
22	1	4	500	135	10	0
22	1	4	500	135	15	0
22	0.75	4	500	0	1	5
22	0.75	4	500	45	1	5
22	0.75	4	500	90	1	5
22	0.75	4	500	135	1	5
22	0.5	4	500	0	1	6
22	0.5	4	500	45	1	6
22	0.5	4	500	90	1	6
22	0.5	4	500	135	1	6

Defect	Thickness	Panel	Laser Power	Orientation	Vacuum	Value
221.5	4	100	0	1	4	
221.5	4	100	45	1	4	
221.5	4	100	90	1	2	
221.5	4	100	135	1	0	
221	4	100	0	1	4	
221	4	100	0	10	4	
221	4	100	45	1	3	
221	4	100	45	10	4	
221	4	100	90	1	4	
221	4	100	90	10	4	
221	4	100	135	1	0	
221	4	100	135	10	0	

Defect	Thickness	Panel	Laser Power	Orientation	Vacuum	Value
23	1.5	4	500	0	1	0
23	1.5	4	500	45	1	0
23	1.5	4	500	90	1	0
23	1.5	4	500	135	1	0
23	1.25	4	500	0	1	0
23	1.25	4	500	45	1	0
23	1.25	4	500	90	1	0
23	1.25	4	500	135	1	0
23	1	4	500	0	1	3
23	1	4	500	0	5	3
23	1	4	500	0	10	3
23	1	4	500	0	15	3
23	1	4	500	45	1	2
23	1	4	500	45	5	2
23	1	4	500	45	10	2
23	1	4	500	45	15	2
23	1	4	500	90	1	0
23	1	4	500	90	5	3
23	1	4	500	90	10	4
23	1	4	500	90	15	4
23	1	4	500	135	1	3
23	1	4	500	135	5	3
23	1	4	500	135	10	3
23	1	4	500	135	15	3
23	0.75	4	500	0	1	5
23	0.75	4	500	45	1	5
23	0.75	4	500	90	1	5
23	0.75	4	500	135	1	5
23	0.5	4	500	0	1	6
23	0.5	4	500	45	1	6
23	0.5	4	500	90	1	6
23	0.5	4	500	135	1	6

Defect	Thickness	Panel	Laser Power	Orientation	Vacuum	Value
23	1.5	4	100	0	1	0
23	1.5	4	100	45	1	0
23	1.5	4	100	90	1	0
23	1.5	4	100	135	1	0
23	1.25	4	100	0	1	4
23	1.25	4	100	45	1	0
23	1.25	4	100	90	1	0
23	1.25	4	100	135	1	0
23	1	4	100	0	1	4
23	1	4	100	0	10	5
23	1	4	100	45	1	4
23	1	4	100	45	10	5
23	1	4	100	90	1	3
23	1	4	100	90	10	3
23	1	4	100	135	1	3
23	1	4	100	135	10	4
23	0.75	4	100	0	1	5
23	0.75	4	100	45	1	4
23	0.75	4	100	90	1	4
23	0.75	4	100	135	1	5
23	0.5	4	100	0	1	6
23	0.5	4	100	45	1	6
23	0.5	4	100	90	1	6
23	0.5	4	100	135	1	6

Defect	Thickness	Panel	Laser Power	Orientation	Vacuum	Value
24	1.5	4	500	0	1	0
24	1.5	4	500	45	1	0
24	1.5	4	500	90	1	0
24	1.5	4	500	135	1	0
24	1.25	4	500	0	1	0
24	1.25	4	500	45	1	0
24	1.25	4	500	90	1	0
24	1.25	4	500	135	1	0
24	1	4	500	0	1	4
24	1	4	500	0	5	4
24	1	4	500	0	10	4
24	1	4	500	0	15	4
24	1	4	500	45	1	0
24	1	4	500	45	5	0
24	1	4	500	45	10	0
24	1	4	500	45	15	0
24	1	4	500	90	1	0
24	1	4	500	90	5	0
24	1	4	500	90	10	4
24	1	4	500	90	15	4
24	1	4	500	135	1	0
24	1	4	500	135	5	3
24	1	4	500	135	10	3
24	1	4	500	135	15	3
24	0.75	4	500	0	1	5
24	0.75	4	500	45	1	5
24	0.75	4	500	90	1	5
24	0.75	4	500	135	1	5
24	0.5	4	500	0	1	6
24	0.5	4	500	45	1	6
24	0.5	4	500	90	1	6
24	0.5	4	500	135	1	6

Defect	Thickness	Panel	Laser Power	Orientation	Vacuum	Value
24	1.5	4	100	0	1	3
24	1.5	4	100	45	1	1
24	1.5	4	100	90	1	0
24	1.5	4	100	135	1	0
24	1.25	4	100	0	1	4
24	1.25	4	100	45	1	3
24	1.25	4	100	90	1	3
24	1.25	4	100	135	1	3
24	1	4	100	0	1	4
24	1	4	100	0	10	4
24	1	4	100	45	1	3
24	1	4	100	45	10	4
24	1	4	100	90	1	3
24	1	4	100	90	10	3
24	1	4	100	135	1	4
24	1	4	100	135	10	4
24	0.75	4	100	0	1	5
24	0.75	4	100	45	1	4
24	0.75	4	100	90	1	4
24	0.75	4	100	135	1	5
24	0.5	4	100	0	1	6
24	0.5	4	100	45	1	6
24	0.5	4	100	90	1	6
24	0.5	4	100	135	1	6

APPENDIX C

LIST OF REFERENCES

1. Owner-Peterson, M., "Digital Speckle Pattern Shearing Interferometry: Limitations and Prospects," Appl. Opt. 30, 2730-2738 (1991)

2. Hung, Y. Y., "Shearography: A New Optical Method for Strain Measurement and Nondestructive Testing," Opt. Eng., 391-395 (May/June, 1982)

3. LTI Report Advanced Shearography NDT demonstration, MFSC, 28 January to February 2,1991

4. LTI Report Shearography Inspection of Spaced Shuttle ET Jack Pad SOFI Close-out," KSC. 20 June 1994

5. Martin Marietta Report, "Shearographic NDE for External Tank TPS," T.D. 3.6.2.1-651-R14

6. A.P. Berens, "NDE Reliability Data Analysis," Metals Handbook, Volume 17, 9th Ed.: Nondestructive Evaluation and Quality Control

REPORT DOCUMENTATION PAGE

Form Approved
OMB No. 0704-0188

1. AGENCY USE ONLY (Leave blank)	2. REPORT DATE	3. REPORT TYPE AND DATES COVERED
	March 1997	Technical Memorandum - 1997

4. TITLE AND SUBTITLE

Laser Shearographic Inspection for Debonds in Sprayed On Foam Insulation (SOFI)

5. FUNDING NUMBERS

6. AUTHOR(S)

F. W. Adams, J. Hooker, and S. Simmons

7. PERFORMING ORGANIZATION NAME(S) AND ADDRESS(ES)

NASA John F. Kennedy Space Center
Kennedy Space Center, Florida 32899

8. PERFORMING ORGANIZATION REPORT NUMBER

9. SPONSORING / MONITORING AGENCY NAME(S) AND ADDRESS(ES)

National Aeronautics and Space Administration
Washington, D.C. 20546

10. SPONSORING / MONITORING AGENCY REPORT NUMBER

NASA TM- 112648

11. SUPPLEMENTARY NOTES

F. W. Adams, NASA, Kennedy Space Center
J. Hooker and S. Simmons, I-NET, Inc. (work funded by NASA Contract NAS 10-11943)
Responsible individual: F. W. Adams, DL-ICD-A (407)867-4449

12a. DISTRIBUTION / AVAILABILITY STATEMENT

Unclassified - Unlimited
Subject Category

This publication is available from the NASA Center for AeroSpace Information, (301)621-0390

12b. DISTRIBUTION CODE

13. ABSTRACT *(Maximum 200 words)*

Preliminary results of shearographic inspections of the test panels simulating the Space Shuttle's external tank (ET) spray on foam insulation (SOFI) are presented. Debonding of SOFI may introduce flight debris that may damage the orbiter's thermal protection system (TPS) exposing the orbiter (as well as the ET) to thermal loading. It is estimated that 90 percent of the TPS damage on the orbiter's "belly" results from debonded SOFI during ascent.

A series of test panels were fabricated, with programmed debonds of different geometries and sizes, to determine the sensitivity of shearography as a function of debond size, SOFI thickness, and vacuum excitation. Results show that a Probability of Detection (POD) of 0.95 or better can be expected for debonds with a diameter equal to the SOFI thickness as less than 0.4-psi pressure reduction.

More testing will be required to validate the laser shearography imaging process for certifying its use in nondestructive evaluation (NDE) of Space Shuttle space flight components.

14. SUBJECT TERMS

Laser Shearography, Debonds, Sprayed On Foam Insulation

15. NUMBER OF PAGES

16. PRICE CODE

17. SECURITY CLASSIFICATION OF REPORT	18. SECURITY CLASSIFICATION OF THIS PAGE	19. SECURITY CLASSIFICATION OF ABSTRACT	20. LIMITATION OF ABSTRACT
Unclassified	Unclassified	Unclassified	